

NASA CR-

141612

(NASA-CR-141612) RADIATION EFFECTS CONTROL:
EYES, SKIN Final Report, 1 Oct. 1969 - 31
Dec. 1974 (Texas A&M Univ.) 148 p HC

N75-17081

CSCI 06R

Unclass

G3/52

09693



TEES

TEXAS ENGINEERING EXPERIMENT STATION
TEXAS A & M UNIVERSITY
COLLEGE STATION TEXAS 77843

PRICES SUBJECT TO CHANGE

Reproduced by
NATIONAL TECHNICAL
INFORMATION SERVICE
US Department of Commerce
Springfield, VA. 22151



FINAL REPORT

to

NATIONAL AERONAUTICS AND SPACE ADMINISTRATION

Radiation Effects Control - Eyes, Skin

Contract No. NAS 9-9053

Report Period

October 1, 1969 thru December 31, 1974

Prepared by:

Dan Hightower, D.V.M. and

J.B. Smathers, Ph.D.

Co-Principal Investigators

December 1974

Submitted by:

Texas Engineering Experiment Station

Texas A&M University

College Station, Texas 77843

ACKNOWLEDGEMENTS

During the years this research effort was being conducted, the following personnel were members of the research staff for varying periods of time and contributed to the success of the research effort. Their contribution is gratefully acknowledged.

Mrs. Eva Binford

Mr. George W. Blair

Dr. T.B. Blount

Mrs. Patsy Coalson

Miss Jan Dooley

Dr. Charles Hall

Mr. Nolan Hertel

Dr. J.R. Kyzar

Mr. James Pearce

Mrs. Eileen Piwetz

Dr. Kenneth Routt

Mr. Gary Wood

Dr. E.M. Wright

Mr. Robert Wright

Final Report
to
National Aeronautics and Space Administration

Radiation Effects Control - Eyes, Skin

Contract No. NAS 9-9053

Table of Contents

Section	Page
I. Summary	1
II. Facility	3
III. Dosimetry	6
IV. Biology	53
V. Conclusions	121
Appendix 1	125
Appendix 2	138

FINAL REPORT

October 1, 1969 - December 31, 1974

Radiation Effects Control - Eyes, Skin

Contract No. NAS 9-9053

I. Summary

A study was undertaken to evaluate the possible adverse effects on the lens of the eye and the skin due to exposure to proton radiation during manned space flight.

The following information was considered of prime importance in the evaluation:

1. Relative effects of different proton energies.
2. Relative effects of different irradiation regimes.
3. Relative effects of different radiation doses.
4. Relative latent period.

Consistent with limitations inherent within available facilities and experimental design, every effort was made to simulate actual proton irradiation which might be encountered in space.

The New Zealand White rabbit and Beagle dog were chosen as experimental models.

Proton energies for exposure included 10, 20, 30, 40 and 50 MeV.

Total doses received ranged from 37.5 rad to 2000.0 rad.

Irradiation regimes included single acute exposures, daily fractionated exposures and weekly fractionated exposures.

Animals were exposed and then maintained and examined periodically until data sufficient to meet the objective were obtained.

No significant skin effects were noted.

Ocular effects varied with the varying exposure conditions. However, in cases where induction of lens abnormalities were noted, the abnormalities were minimal in severity. Throughout the investigation, no animal exhibited serious sight impairment.

II. Facility

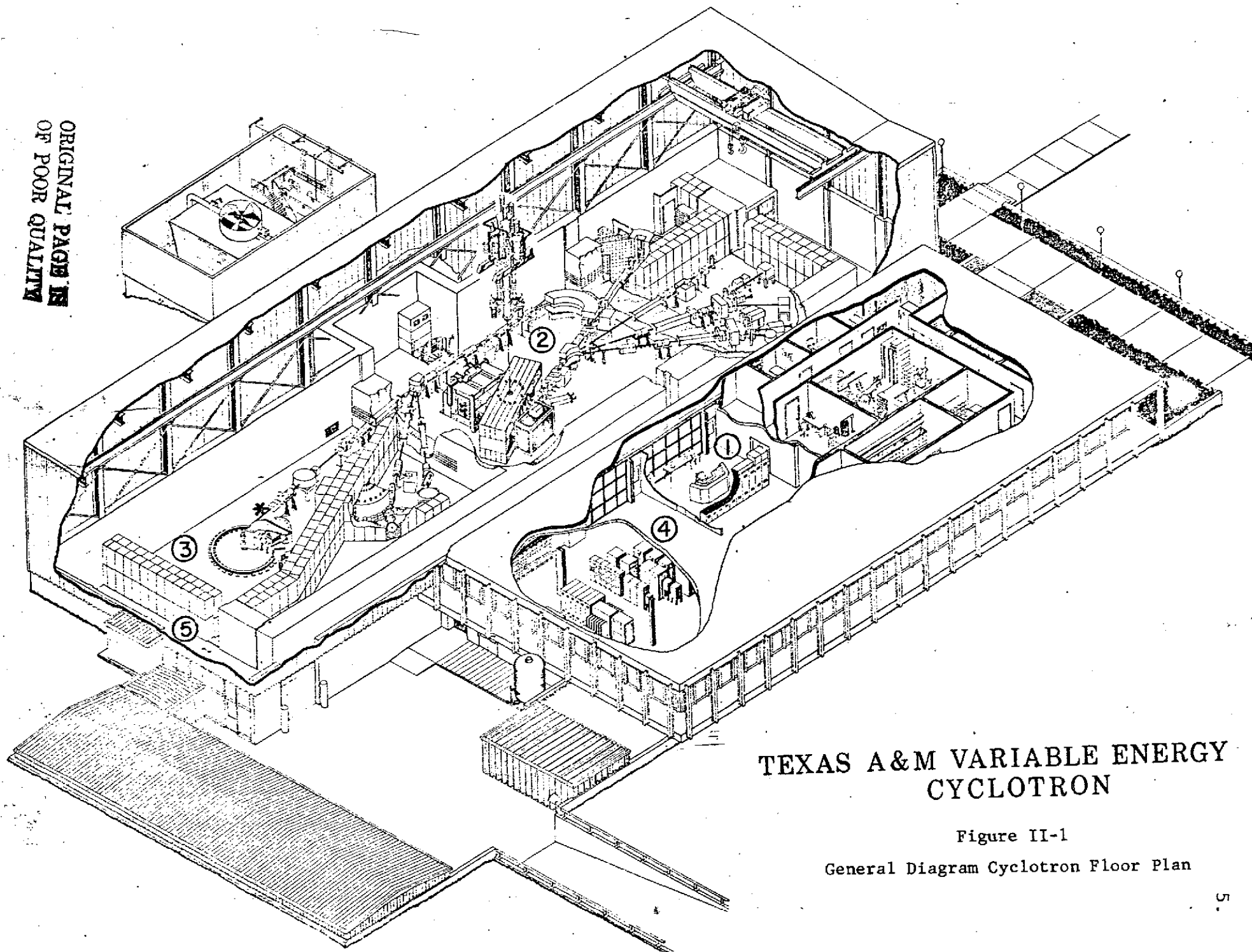
The radiation source used in the research effort was the 88 inch sector focused cyclotron, located at Texas A&M University. The cyclotron has a capability of accelerating protons to 50 MeV, deuterons to 55 MeV and alpha particles to 120 MeV. Within the physical facility there are four irradiation caves, the main cyclotron vault, and associated laboratory areas. The areas of interest to this project are indicated in Figure II-1 with the cyclotron control room indicated by #1, the cyclotron vault by #2, the cave used for the irradiations by #3, the low level counting room, where all dosimetry information was recorded #4, and the staging area for animal preparation outside of the cave area by #5. The star within Cave 3 indicates the position at which the beamline was terminated, the transmission chamber mounted, and the animal irradiations were performed.

The beam is transported from the cyclotron in vacuum through three inch diameter pipe. To bring the beam into Cave 3, the protons were diverted out of the cyclotron along the main beam line, magnetically bent through the 155 degree analyzing magnet, brought down the far wall of the vault area through a switching magnet and into Cave 3. The total distance traveled was in excess of 150 feet. At intervals along the beam line sets of quadrupole magnets are located for focusing the charged particle beam. In addition, sets of slits to restrict the size of the beam and

large carbon blocks, Faraday cups, to totally block the beam are also positioned at several locations.

At the termination of the beam line, a mylar film was used as the vacuum isolation barrier. The incident beam thus passed through the mylar film, the nitrogen gas and polycarbonate film electrodes of the transmission chamber, and several inches of air prior to intercepting the animal being irradiated. The details of the animal setup at this location will be discussed in later sections of this report.

ORIGINAL PAGE IS
OF POOR QUALITY



TEXAS A&M VARIABLE ENERGY CYCLOTRON

Figure II-1

General Diagram Cyclotron Floor Plan

III. Dosimetry

Physical Equipment

The transmission ionization chamber used to monitor the beam during irradiation is illustrated in Figures III-1 and III-2. The chamber is essentially two parallel plate ionization chambers sharing a common central high voltage electrode and having a guard electrode at each extremity. The plate walls are polycarbonate plastic film 2 microns thick with 280 angstroms of aluminum vacuum evaporated on them and the gas medium is dry nitrogen supplied at 0.1 liters per minute. The aluminized conductivity coating is broken in one case by a vertical insulation barrier and in the second ionization chamber by a horizontal insulation barrier of non-aluminized polycarbonate film, thus dividing the two parallel plate chambers into actually four ionization currents - an upper and lower from one chamber and a left and a right from the other chamber. These four signals are then brought out to a beam balance monitor, Figure III-3 which essentially took the signals and summed them (the four of them) to achieve a total signal which was representative of beam intensity. At the same time a difference signal between the left and the right halves of the one ionization chamber was developed and this was illustrative of the degree to which the beam was uncentered - either left or right. An error signal was also developed for the upper and lower ionization chamber indicating out-of-balance in that direction. These two difference signals were minimized by

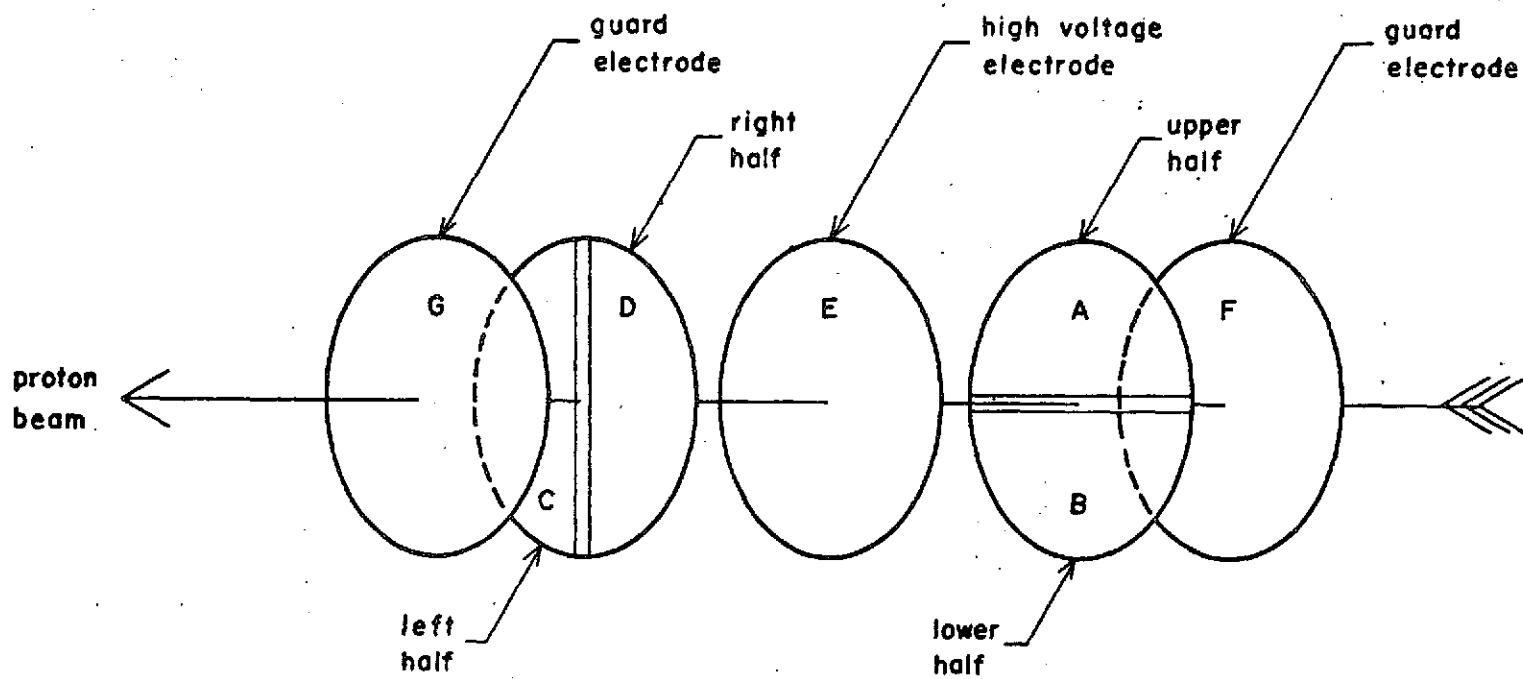


Figure III-1
General Diagram
Transmission Ionization Chamber

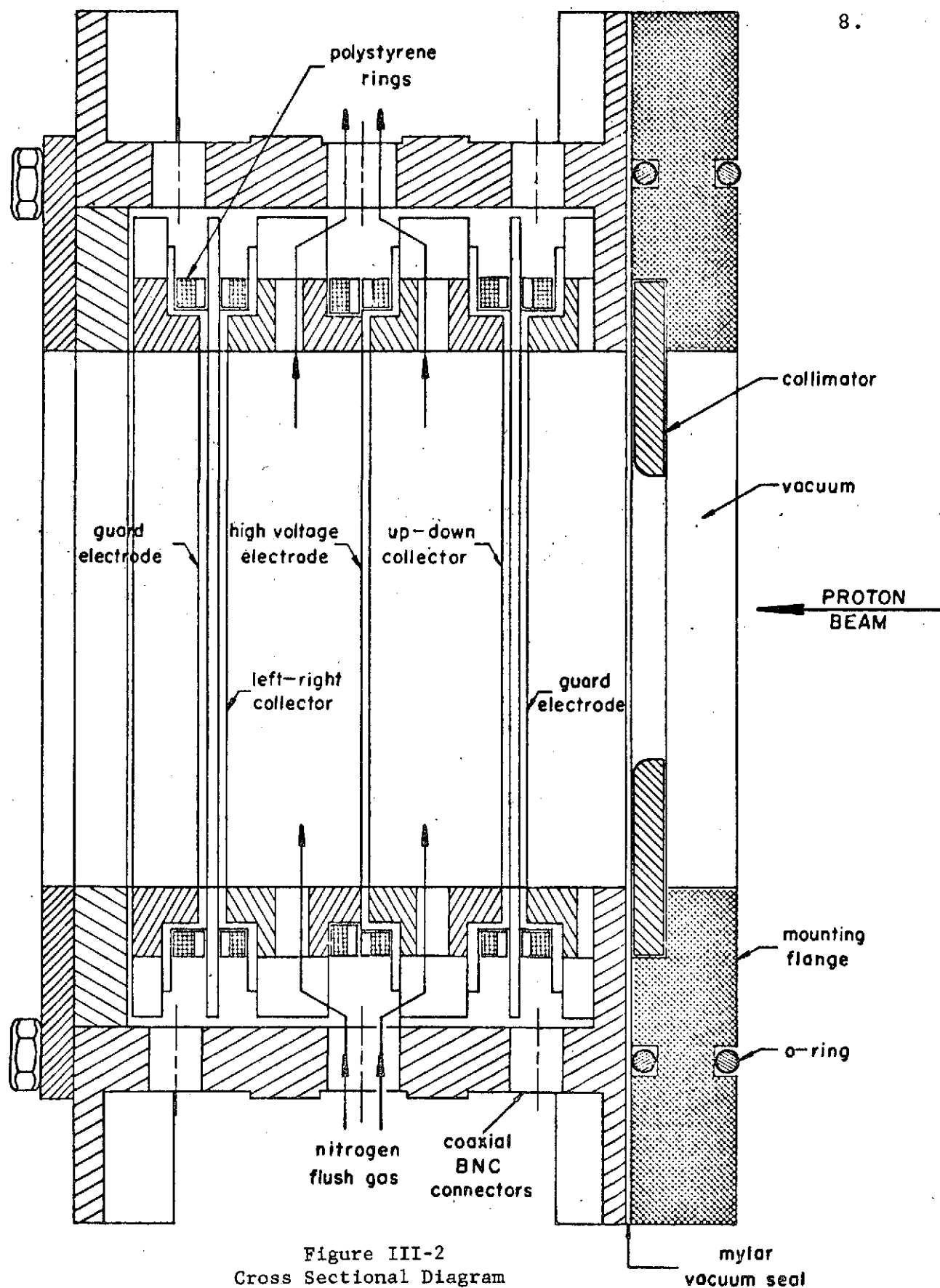


Figure III-2
Cross Sectional Diagram
Transmission Ionization Chamber

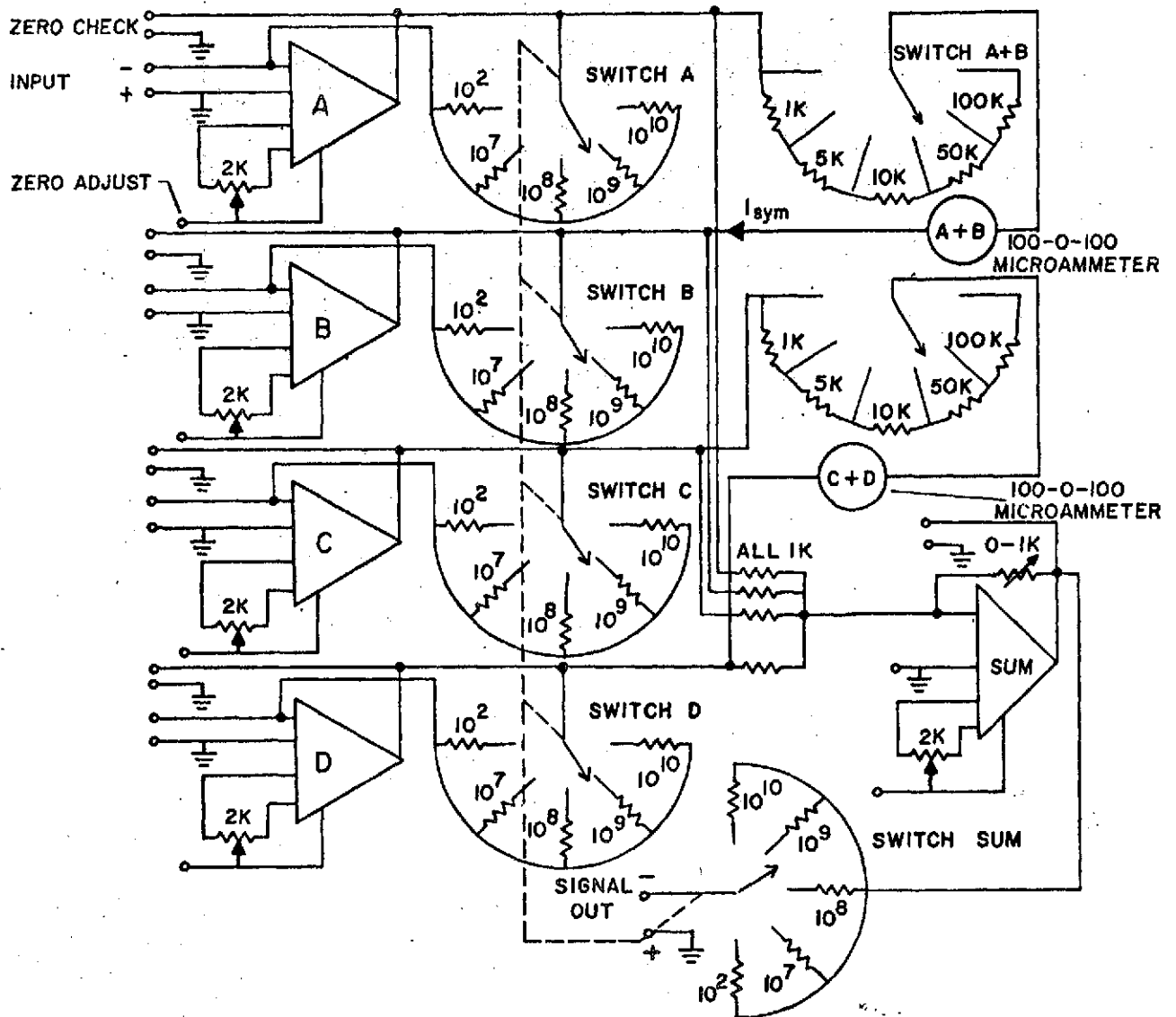


Figure III-3
Circuit Diagram
Transmission Chamber Beam Balance Monitor

magnetically focusing the beam while at the same time maintaining the proper intensity as indicated by the sum of all four signals. Thus, when "balanced" the beam was assumed centered in the beam pipe and having equal intensity in each of the four quadrants. To verify this assumption, every beam was recorded using polaroid film and the uniformity of the image on the exposed film was visually interpreted to indicate the degree of uniformity.

A more quantitative measurement of uniformity was also made using lithium fluoride rods in a tissue-equivalent mosaic holder - as illustrated in Figure III-4. The rods are 1 mm in diameter x 6 mm long and while they have limitations in their use for charged particle dosimetry, when placed in a common plane perpendicular to the proton beam they are excellent for indicating uniformity of the beam throughout that plane.

The absolute calibration of the beam was determined using a tissue equivalent* extrapolation chamber. This chamber also used the very thin aluminized polycarbonate film as an entrance window and is similar in nature to a chamber developed by EG&G and reported in their technical report S-439-R November 1968, Figure III-5. The central electrode is one-half inch in diameter with a guard ring about this and an overall chamber diameter of approximately one and one-half inches. The gas used in the chamber was tissue equivalent gas composed of 64.4% methane, 32.4% CO₂ and 3.2% nitrogen by partial pressure.

*Shonka A-150 Muscle Equivalent Plastic

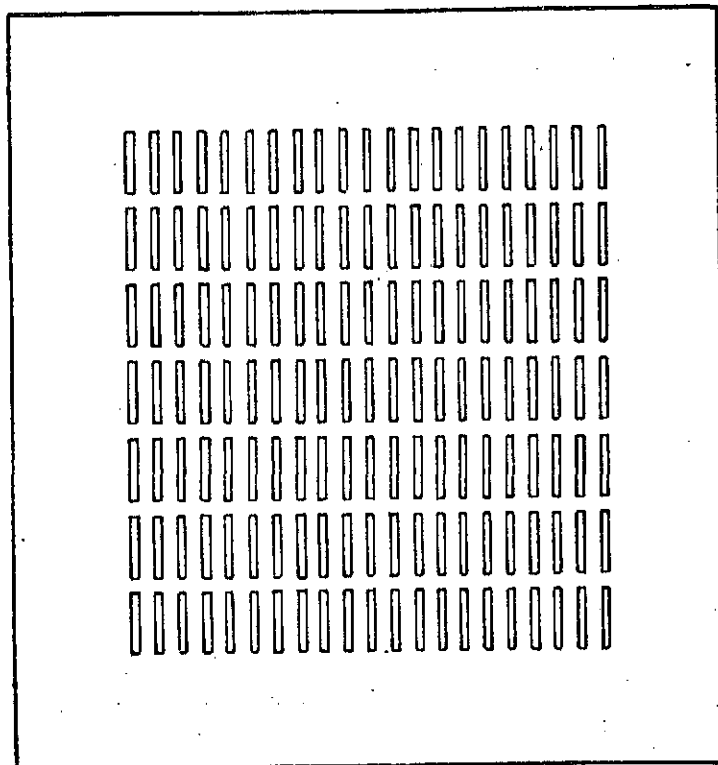
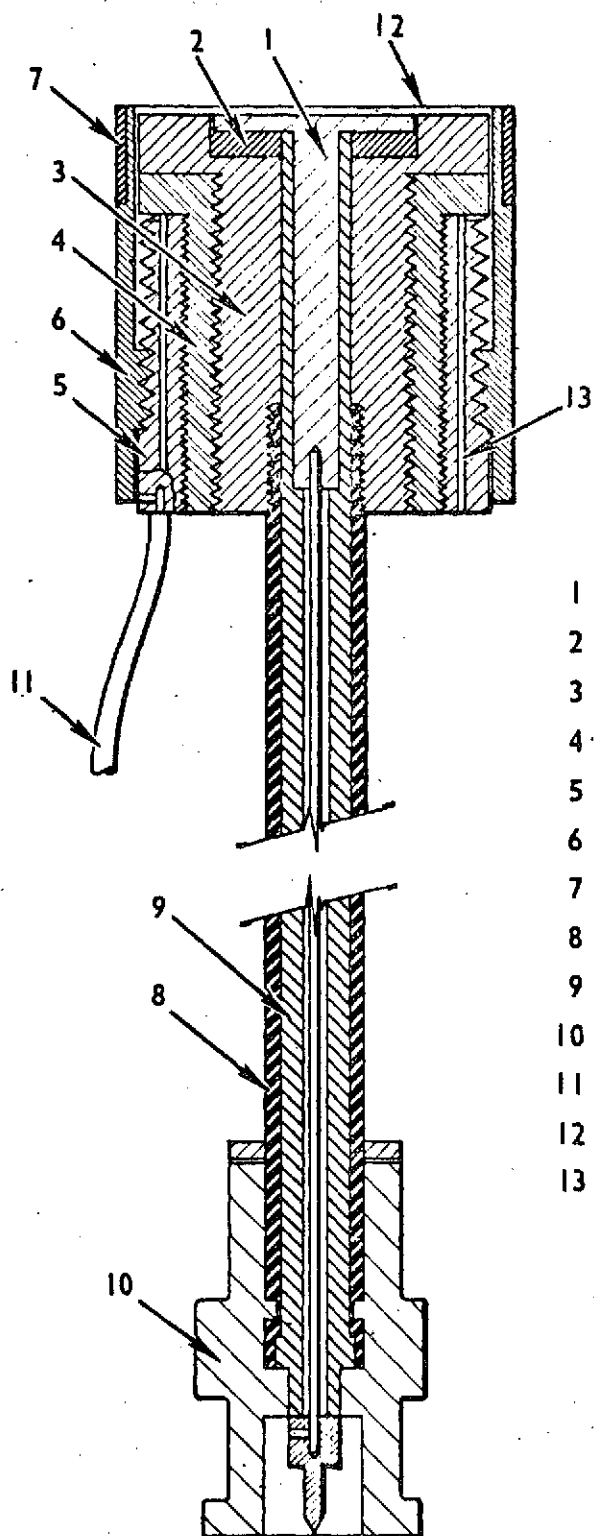


Figure III-4
LiF Rod Mosaic Holder - Tissue
Equivalent Plastic Composition



- 1 - TE PLASTIC ELECTRODE
- 2 - ELECTRODE INSULATOR - POLYETHYLENE
- 3 - TE PLASTIC GUARD RING
- 4 - HIGH VOLTAGE INSULATOR
- 5 - ALUMINUM RING CONNECTOR
- 6 - ALUMINUM VARIABLE SPACING RING
- 7 - ALUMINUM WINDOW RETAINING RING
- 8 - ALUMINUM TUBING CHAMBER STEM
- 9 - POLYSTYRENE SIGNAL INSULATOR
- 10 - UG-260/U CONNECTOR
- 11 - HIGH VOLTAGE WIRE
- 12 - 0.0005" ALUMINIZED MYLAR
- 13 - GAS PORTS

Figure III-5
Tissue Equivalent Extrapolation
Chamber - Cross Sectional View

Total particle fluence was determined by a Faraday cup which was a disc-shaped piece of graphite located at the point at which the animal would be placed and electrically insulated from its surroundings.

A block diagram of the proton spectrometer system is illustrated in Figure III-6. The system is composed of commercially available equipment and was used to obtain the proton spectra as it penetrated through various depths in the tissue equivalent plastic. For the higher energy protons used, the range of the proton exceeded the sensitive thickness of a single detector. For these measurements a series of three detectors were run in parallel into one single preamp and thus into the amplifier system and the rest of the system. This technique maximized the problem of the detector noise but minimized cost in that only one preamplifier and amplifier were required as opposed to three preamplifiers, three amplifiers and a summing amplifier, which would have been required, had a separate amplification system been developed for each detector. The latter technique would have minimized the total system electronic noise but for the energies used in this project, noise was not a problem.

The thermoluminescent readout system used for proton beam uniformity checks was a commercially available TLD readout system and was used in the conventional manner for this project.

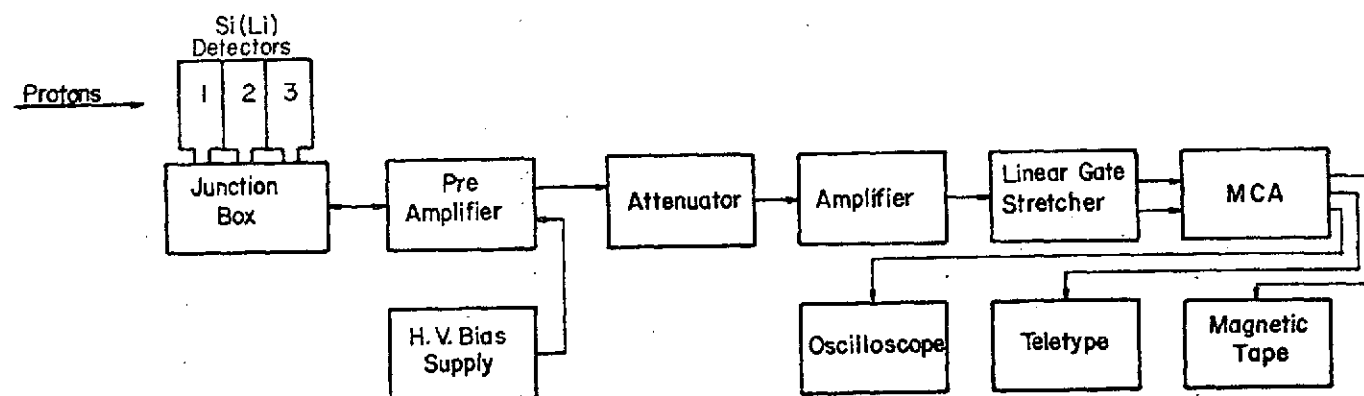


Figure III-6
Proton Spectrometer System

Equipment Characteristics

Prior to animal irradiations the operational characteristics were determined when the equipment was used in detection of proton beams. Saturation curves were first developed for both the transmission chamber and the tissue equivalent chamber. These curves are shown in Figures III-7 and III-8. Based on this data an upper limit of 8×10^{-7} amps was chosen for the maximum current which could be produced with the transmission chamber and not have ion recombination problems. This limit then placed an upper limit on the proton beam intensity and the dose rate which could be achieved. A similar decision was made concerning the extrapolation chamber and this limit correlated well with the limit that had been decided on for the transmission chamber. For the transmission chamber to accurately determine the dose delivered, a linear correlation was required with the Faraday cup and the T.E. extrapolation chamber; which were used for the absolute dosimetry measurements. These correlations are shown in Figures III-9, III-10, III-11. When applicable, the current limits imposed by the saturation curves are indicated. As indicated by the graphs, there is a very good linear correlation between each pair of detectors.

Basic Dosimetry Theory

The absolute dose was determined using the fundamental Bragg Gray cavity theory. The computation of dose was based on the use of equation 1 below:

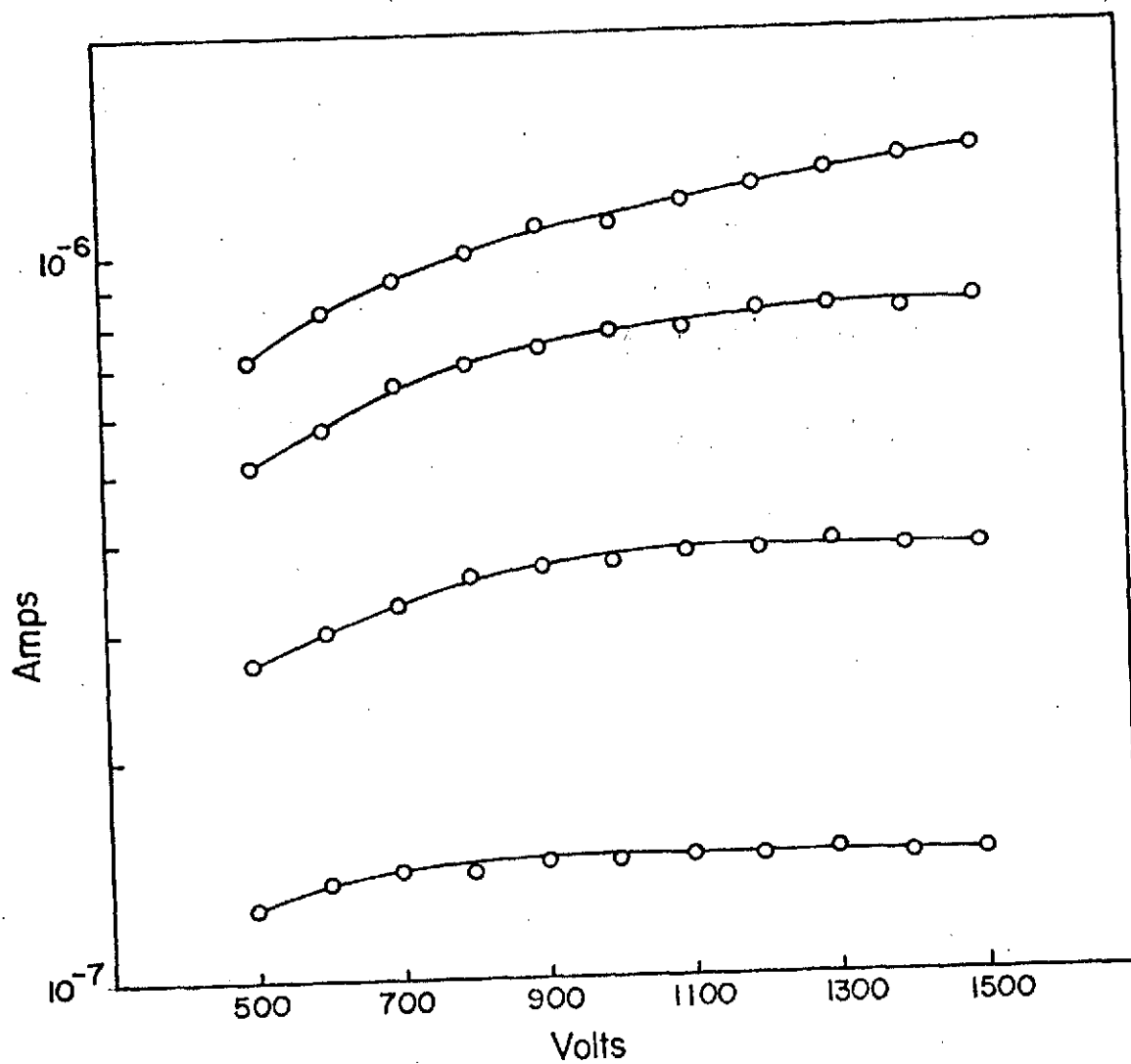


Figure III-7
Ionization Current vs Chamber
Voltage - Transmission Chamber

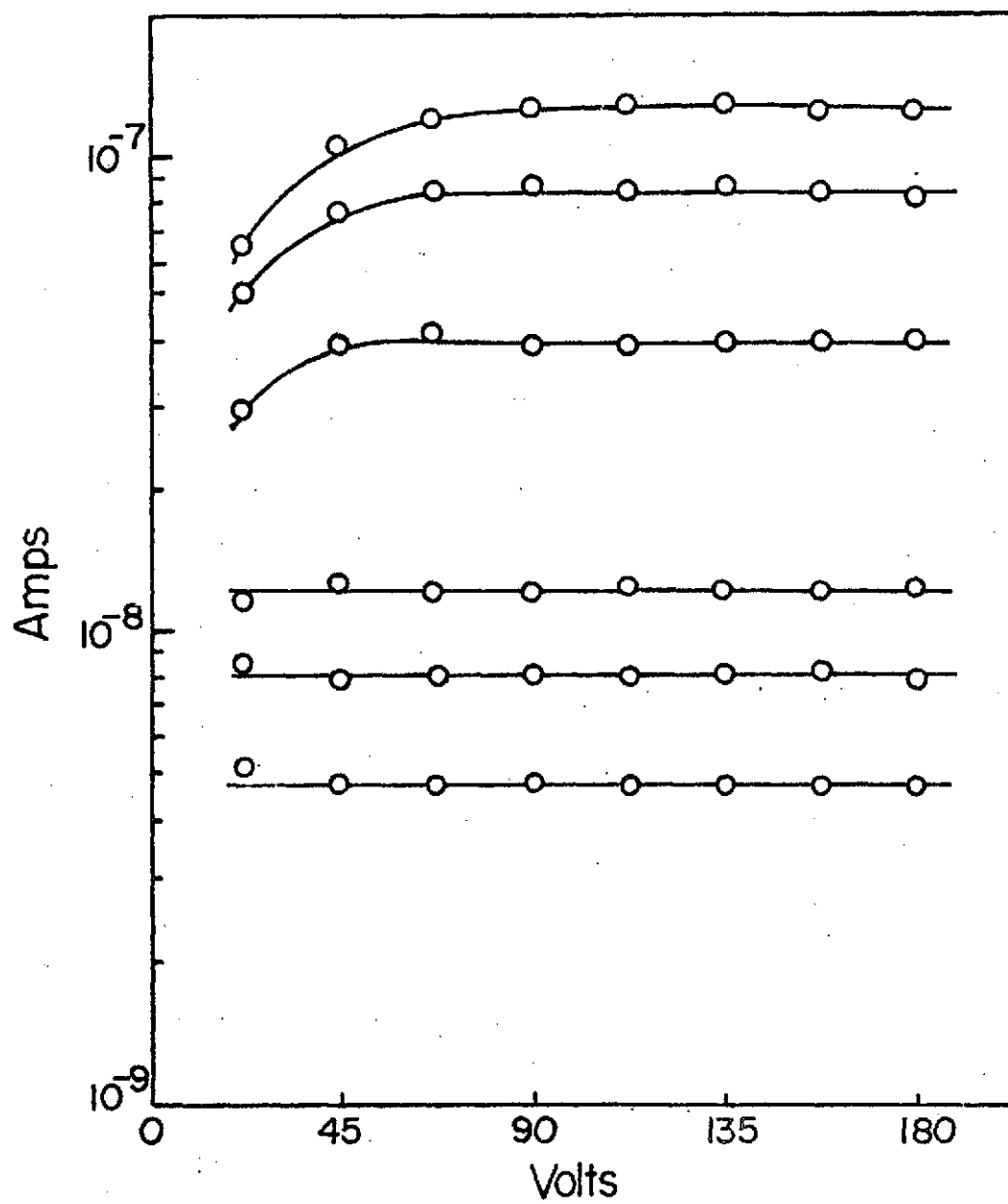


Figure III-8
Ionization Current vs Chamber Voltage -
Tissue Equivalent
Extrapolation Chamber

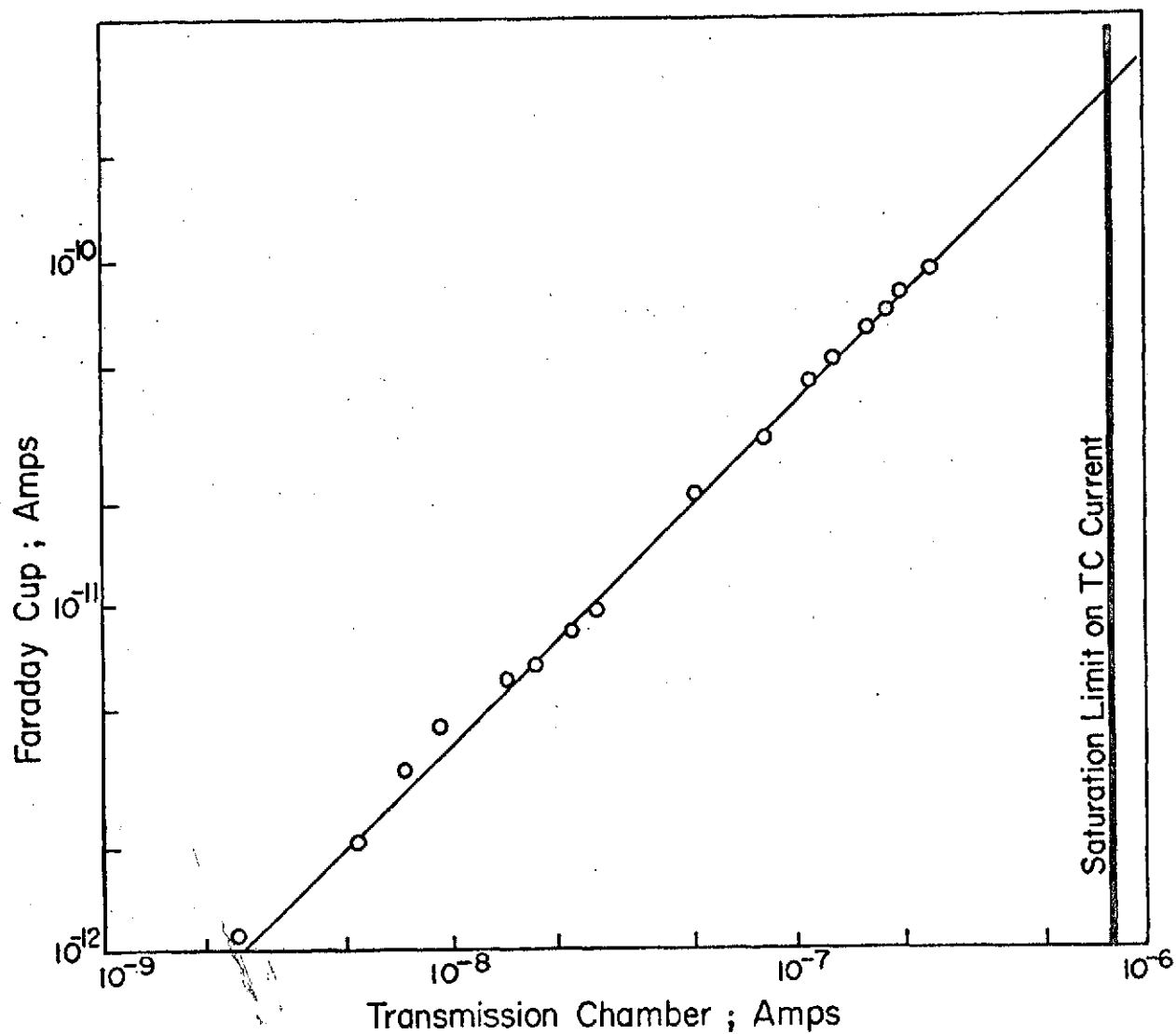


Figure III-9
Transmission Ionization Chamber
Current vs Faraday Cup Current
For 30 MeV Protons

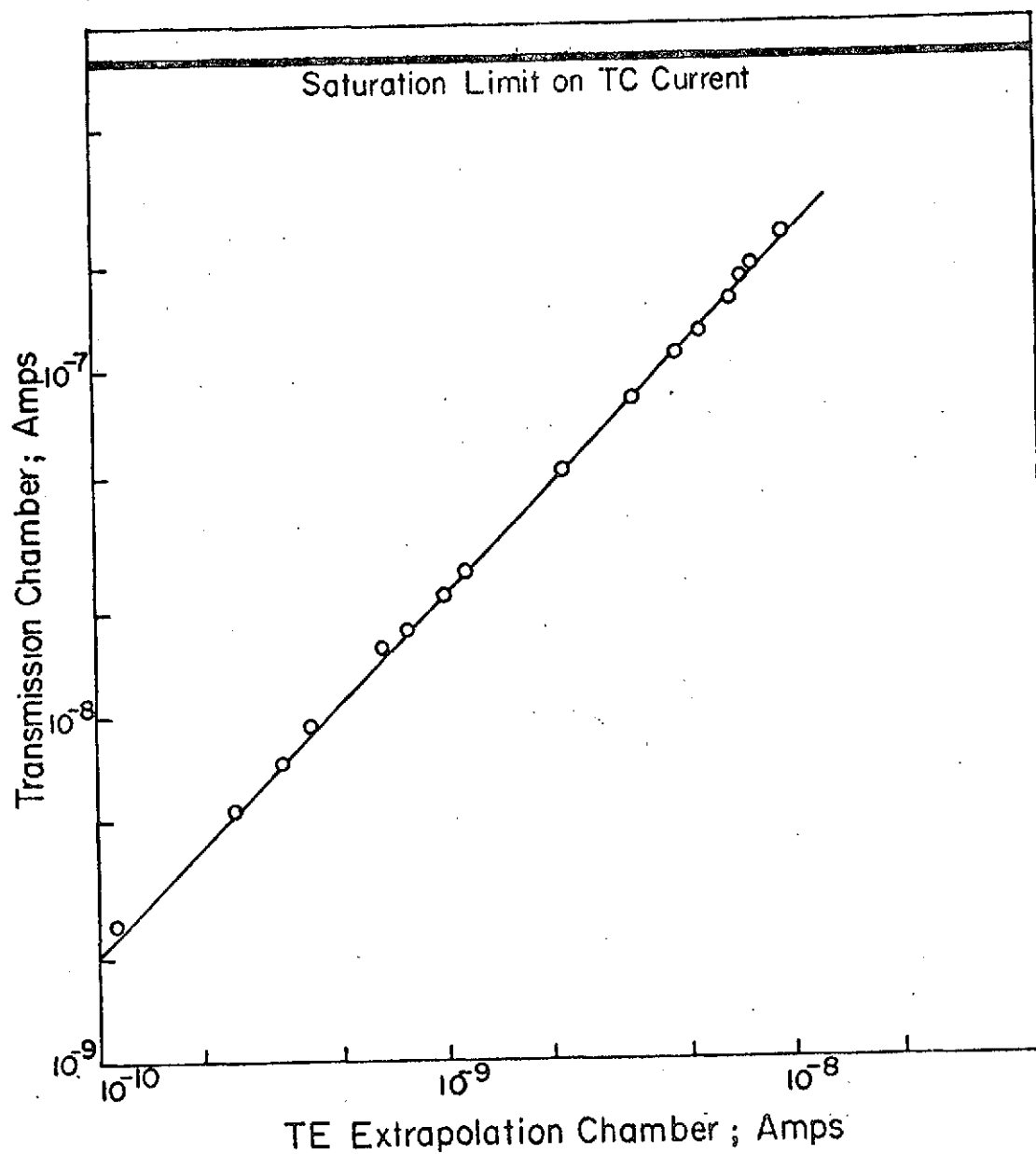


Figure III-10
Tissue Equivalent Ionization Chamber
Current vs Transmission Chamber
Current for 30 MeV Protons

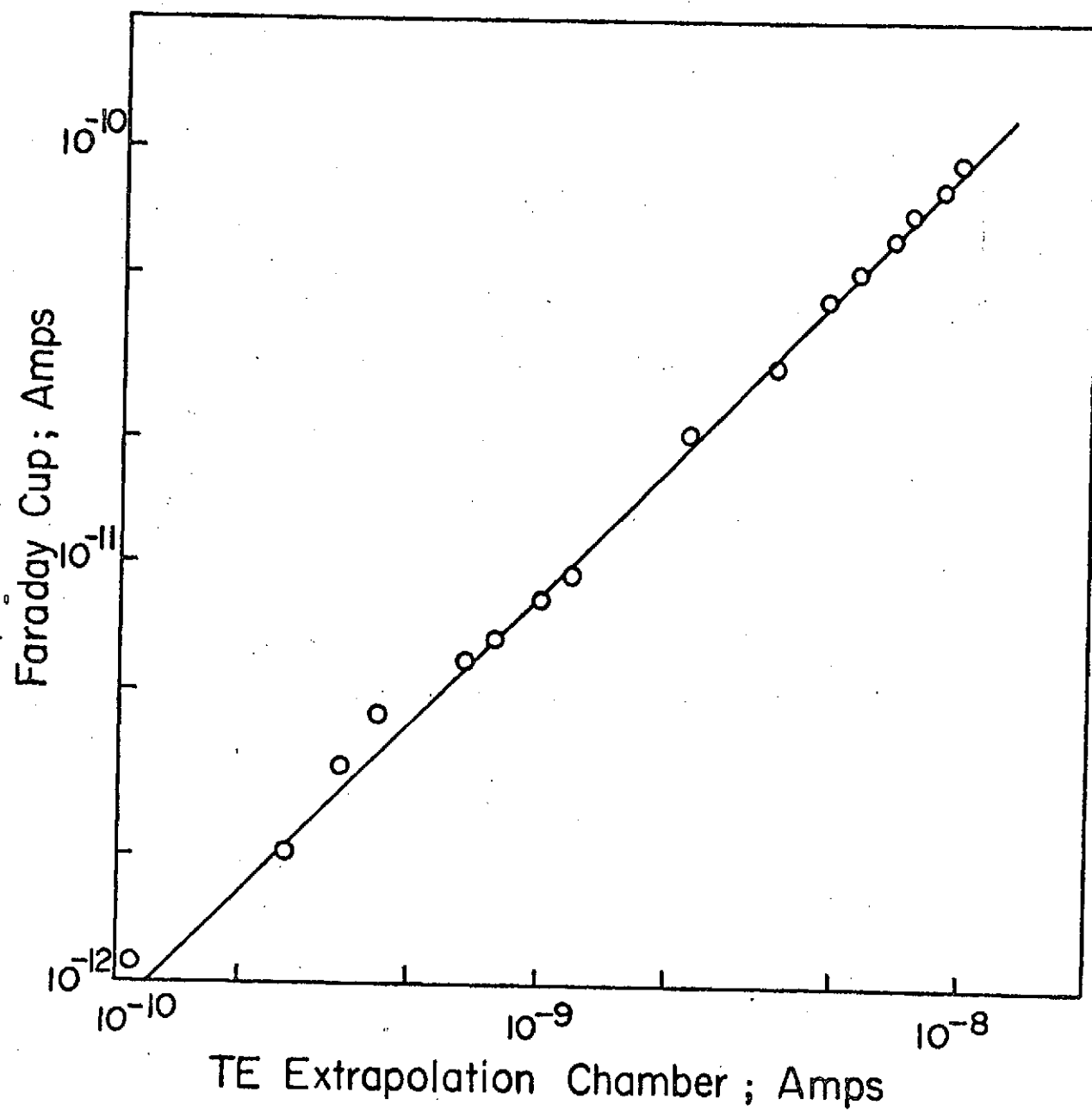


Figure III-11
Tissue Equivalent Ionization Chamber
Current vs Faraday Cup Current for
30 MeV Protons

$$\text{Dose J/Kg} = \frac{\text{Dose Rads}}{100} = \frac{\left[\left(\frac{W}{e} \right) \frac{\text{joules}}{\text{coul}} \right] \left[\frac{\text{wall}}{\text{gas}} \right] \left[Q \text{ coul} \right] \left[\text{TPC} \right]}{\left[M \text{ Kg} \right]} \quad \text{eq 1}$$

where

$$\left[\frac{W}{e} \right] = \text{Joules/coul for formation of ions} = 30.5$$

$$\left[\frac{\text{TE plastic}}{\text{TE gas}} \right] = \text{Stopping power ratio (variable with proton energy)}$$

$$\begin{aligned} [M] &= \text{Kg of gas in sensitive volume of ionization chamber} \\ &= (.3346 \text{ cm}^3) (1.138 \times 10^{-6} \text{ Kg/cm}^3) = 3.8077 \times 10^{-7} \text{ Kg @} \\ &\quad 0^\circ\text{C and 760 mm Hg} \end{aligned}$$

$$[\text{TPC}] = \text{Temperature pressure correction to that existing when chamber was used.}$$

$$[Q] = \text{Charge collected from ion chamber.}$$

The gas used in the ion chamber was a "tissue equivalent" mixture composed of 32.4% CO_2 , 3.2% N_2 , and 64.4% CH_4 by partial pressure. The basic parameters involved in the computation for the various proton energies are listed in Table III-1.

The electrometer used to measure the charge collected was calibrated at the Regional Calibration Laboratory in Houston and is traceable to the National Bureau of Standards. The mass of gas in the sensitive volume of the chamber was determined using the measured volume and an accepted density for tissue equivalent gas. The absolute dose as calculated for each of the cyclotron

TABLE III-1 - Energy Dependent Dosimetric Parameters

Proton Energy MeV	TE Plastic/TE Gas Stopping Power Ratio	W/e (J/C)
10	1.0107	30.5
20	1.0087	30.5
30	1.0084	30.5
40	1.0075	30.5
50	1.0079	30.5

runs was then related to a given reading on the transmission ion chamber. From the previously demonstrated linearity between the two chambers any dose could then be delivered by simply taking the proper ratio of the transmission chamber readings to the given dose in the standard calibration of the day.

The Linear Energy Transfer, LET, of the beam was measured at finite incremental steps and compared to theoretical expression given by equation 2.

$$\frac{dE}{dx} = \frac{4\pi z^2 e^4 NZ}{m v^2} \left[\ln \left(\frac{2 m v^2}{I(1-\beta^2)} \right) - \beta^2 - \sum_i \left(\frac{C_i}{Z} \right) \right] \quad \text{eq 2}$$

with the following symbol definitions:

z = Atomic number of charged particle (1 for proton)

e = Electron charge

N = Atom density of absorber

Z = Average atomic number of absorber atoms

m = Electron rest mass

v = Velocity of charged particle

I = Average excitation energy of the absorber

β = v/c = ratio of charged particle velocity to speed of light

C_i = Shell correction factor

This equation has been programmed to allow computation of either a mean range or for generating dE vs dx versus depth curves for the various energy protons and the materials of interest. The

program is specific in nature in that it does allow incorporation of the absorbing effects of the transmission ionization chamber and the mylar vacuum isolation film in its analysis of the effective energy which reaches the animal. A complete listing of the program is included as Appendix 1.

Beam Spread

Although the beam had been brought some 100 feet through an evacuated pipe and should be at this point and time essentially parallel in nature, once brought into air nuclear scattering occurred and the beam diverged slightly with distance. This effect is illustrated in Figure III-12 for 30 MeV protons. To be sure that this problem did not hamper us in our research, the absolute calibration of the beam for each run was performed at the distance the animals were going to be positioned for their irradiation. Typically this distance was approximately 3 inches from the transmission chamber.

Beam Uniformity and Alignment

Beam uniformity was determined in a "macroscopic" nature using both the Beam Balance Monitor and single sheet polaroid film. For a detailed measurement the LiF rods in the T.E. mosaic holder were used. Initially magnetic focusing was utilized to obtain the spots of desired size, approximately one inch in diameter. The thought behind this being to minimize secondary particle production and beam contamination due to scatter with the beam pipe or collimators. The results of several measurements

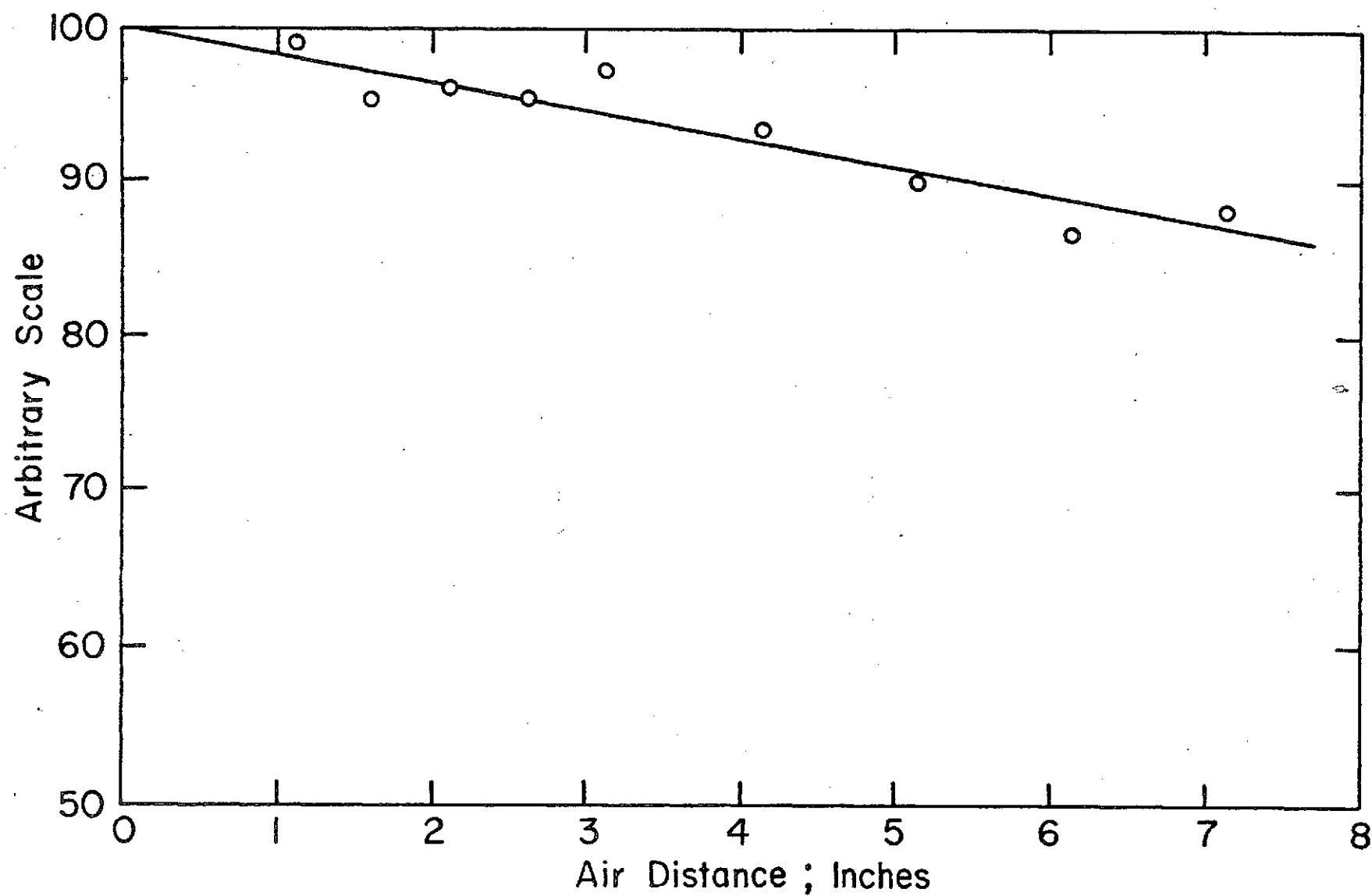


Figure III-12
Proton Dose Rate Variation With
Distance in Air from the Transmission
Chamber

for proton measurements made at two different energies and in depth are shown in Tables III-2 and III-3. Inspection of the tables quickly indicates that throughout the area exposed to the eye there are serious non-uniformities with variations of as much as 40% in some areas. Attempts were made to correct this by various focusing techniques, but with a magnetically focused proton beam, it was not possible to achieve the uniformity we felt was required.

The magnetic focusing of the beam was then abandoned and uniformity was achieved by defocusing the beam till it had a cross sectional area of four to five inches in diameter. Using aluminum collimators the central portion of the beam was selected and passed through the transmission chamber. For the beam obtained in this manner, a series of studies were made to determine if the scattered radiation would pose a problem. It was found that at the energy levels up to 30 MeV, the scattered radiation was minimal. The uniformity of the defocused beam was quite acceptable being plus or minus 5% throughout the whole area of one inch diameter spot, or one and one-half inch spot as the case may be, that was used to irradiate the eye. The same defocused condition was used for the skin irradiations. In this case a two and a half inch diameter circle was used for irradiation and Tables III-4 and III-5 indicate the relative dosage throughout that circle and also illustrate the extent of the beam scattering and enlargement as it passed through air before it was incident

TABLE III-2 - Relative dose distribution at dog eye;
Magnetically Focused Beam

20 MeV Protons - 28 January 1971

Zero Depth

0.989	1.18	0.663	1.07	1.10
0.830	0.884	0.881	1.38	0.999

0.036" Depth

0.656	1.000	1.26	1.28	1.09
1.05	0.570	1.000	0.891	1.20

0.066" Depth

0.988	1.18	0.961	0.728	1.22
0.541	0.714	1.14	1.27	1.11

0.101" Depth

--	0.904	0.932	1.13	1.05
0.867	0.850	--	1.18	1.02

0.115" Depth

1.26	1.09	.681	1.47	1.41
.890	1.14	.536	1.08	1.11

0.130" Depth

0.884	0.796	1.09	1.10	1.25
0.963	1.04	1.08	0.894	1.36

TABLE III-3 - Relative dose distribution at dog eye;
Magnetically Focused Beam

<u>30 MeV Protons - 28 January 1971</u>				
<u>Zero Depth</u>				
0.712	1.281	1.275	0.931	0.854
0.675	0.951	0.881	0.684	0.595
<u>0.032" Depth</u>				
0.673	0.949	1.23	0.782	1.04
0.761	.900	1.05	1.09	.895
<u>0.107" Depth</u>				
0.893	1.17	1.12	1.14	0.860
0.746	1.05	0.796	0.724	0.842
<u>0.148" Depth</u>				
0.971	0.879	1.22	1.10	1.10
0.890	1.19	0.850	0.770	0.963
<u>0.199" Depth</u>				
0.671	1.12	0.963	1.10	0.898
0.853	0.858	1.09	0.864	0.972
<u>0.250" Depth</u>				
0.674	1.37	0.927	0.901	1.00
0.895	0.745	1.12	0.931	0.867
<u>0.276" Depth</u>				
0.397	1.27	1.38	0.629	0.953
0.715	0.925	1.14	0.658	0.853
<u>0.286" Depth</u>				
0.586	1.08	0.912	0.953	1.14
0.808	1.25	1.00	0.811	0.866
<u>0.295" Depth</u>				
0.688	0.984	0.938	1.11	0.703
0.828	1.11	0.859	1.06	0.750

TABLE III-4 - Measured relative dose distribution at dog skin

<u>30 MeV Protons - 13 May 1971</u>						
	.033	.546	.786	.381	.0286	
.168	.923	<u>.889</u>	<u>.832</u>	<u>.830</u>	1.06	.038
	.366	<u>1.07</u>	<u>1.08</u>	<u>1.01</u>	.137	
.877	<u>1.07</u>	<u>1.03</u>	<u>1.11</u>	<u>.926</u>	<u>.984</u>	.438
	.713	<u>.877</u>	<u>.854</u>	<u>1.11</u>	.505	
.569	.996	<u>.745</u>	<u>1.07</u>	<u>.863</u>	1.00	.459
	.0304	.615	.983	.880	.0307	

Readings within 2½" D collimator area.

TABLE III-5 - Measured relative dose distribution at dog skin

<u>30 MeV Protons - 20 May 1971</u>						
	.0505	.551	.961	.140	.035	
.273	1.30	<u>1.21</u>	<u>.933</u>	<u>1.03</u>	.881	.0548
	.327	<u>1.07</u>	<u>1.00</u>	<u>1.07</u>	.0665	
1.10	<u>1.03</u>	<u>1.13</u>	<u>.922</u>	<u>.984</u>	<u>.813</u>	1.07
	.172	<u>1.15</u>	<u>.968</u>	<u>.947</u>	.152	
.172	.993	<u>.801</u>	<u>1.09</u>	<u>1.07</u>	.989	.291
	.0397	1.06	1.09	.903	.0449	

Readings within 2½" D collimator area.

on the animals. The radiation field cut-off is actually closer to a two and three quarter to three inch diameter circle. Again, over this large a spot the uniformity is seen to be plus or minus 15% which is clearly much better than the magnetically focused one inch diameter spot was capable of achieving. To further assist in the alignment of the animals and keep them centered in the spot, two items were used. The first was a series of cross hairs constructed from sewing thread which were positioned such that they were centered in the beam. This was verified with the photographic film analysis of the beam uniformity in that the cross hairs offered sufficient absorption such that they showed in the photograph. The second item was a light located on a removable holder upstream in the evacuated beam line with respect to the transmission chamber. When the light was swung into the center of the beam line, a light beam was transmitted through the intersection of the clear insulating lines that separated the upper and the lower halves and the left and right halves of the two parallel plates in the ion chamber. This light beam was then positioned on central axis and shown directly on the spot that we wished to be irradiated. The coincidence of the light beam with the central axis of the radiation beam was verified by film and proved to be a very convenient method of always properly aligning the eye or the skin in the beam.

Hair Absorption Study

Because of the lack of observable effects on the skin at the dosage used, some concern developed over the amount of energy which the protons were depositing in the hair of the dogs. To evaluate this, hair from four 36 centimeter square areas was removed from a dog and weighed to give a value for the mass per unit area which the proton beam encountered. An average value of 10.8 milligrams per square centimeter plus or minus 17% was obtained. Assuming a chemical composition for the hair of 12.5% water and 87.5% keratin, the energy deposited in such an absorber by incident 30 MeV protons was calculated using the computer code. A total energy loss of .02 MeV was calculated for 30 MeV protons. Based on calculations of the energy loss in passing through the transmission chamber, it is logical to expect slightly larger energy losses for the 10 and 20 MeV instant beams. However, the magnitude of each would still be too small for this absorption to significantly affect the range of the particles in tissue. Thus, the lack of skin effect at the doses which were used in this study cannot be attributed to the fact that the animals were not shaved and thus a large energy absorption occurred in the hair.

Dose Beyond Bragg Peak

Using the computer program representation of the LET distribution, the dose at the Bragg peak and beyond was calculated for the energies 20 through 50 MeV. The results are tabulated in

Table III-6. In essence the results can be summarized by saying the dose drops rapidly with increasing depth to a value of less than 1% of the Bragg peak dose and that any unusual artifacts observed in biological organs located at depths much in excess of the location of the Bragg peak are not due to radiation dosage at that location.

Results

The incremental LET as measured for 10 MeV protons in T.E. plastic is illustrated in Figure III-13. A theoretical computation using the computer program previously described is included as well to indicate the degree with which the two concur. There is some concern as to exactly how high the peak (Bragg peak) truly is. With the experimental techniques used, we were unable to measure doses at thickness increments smaller than 1/1000ths of an inch. It is therefore possible that the actual peak goes slightly higher than that which has been recorded.

There is also a philosophical concern as to what actually is a Rad when one is working with highly ionized charged particles. To be defined accurately, the dose to a given mass would have to be rather uniformly distributed such that one can indeed quote in Joules per kilogram or ergs per gram and have it meaningful. With the very narrow Bragg peaks observed, the given dose rate does not exist for a gram of material but exists only for a very small mass of material. The doses quoted at the Bragg peak are based on this $\Delta E/\Delta X$ ratio and is normalized to what

TABLE III-6 - Dose Beyond Bragg Peak

Proton Energy (MeV)	Depth (cm)	Dose (Bragg Peak = 1.00)
20	0.3510	1.0000
	0.3808	0.0233
	0.4111	0.0015
30	0.7506	1.0000
	0.7650	0.352
	0.7749	0.0019
	0.7980	0.00024
40	1.282	1.0000
	1.292	0.254
	1.438	0.0329
	1.5942	0.0025
50	1.86350	1.0000
	1.9570	0.5920
	1.9940	0.1960
	2.0190	0.0542
	2.106	0.045
	2.3488	0.0020

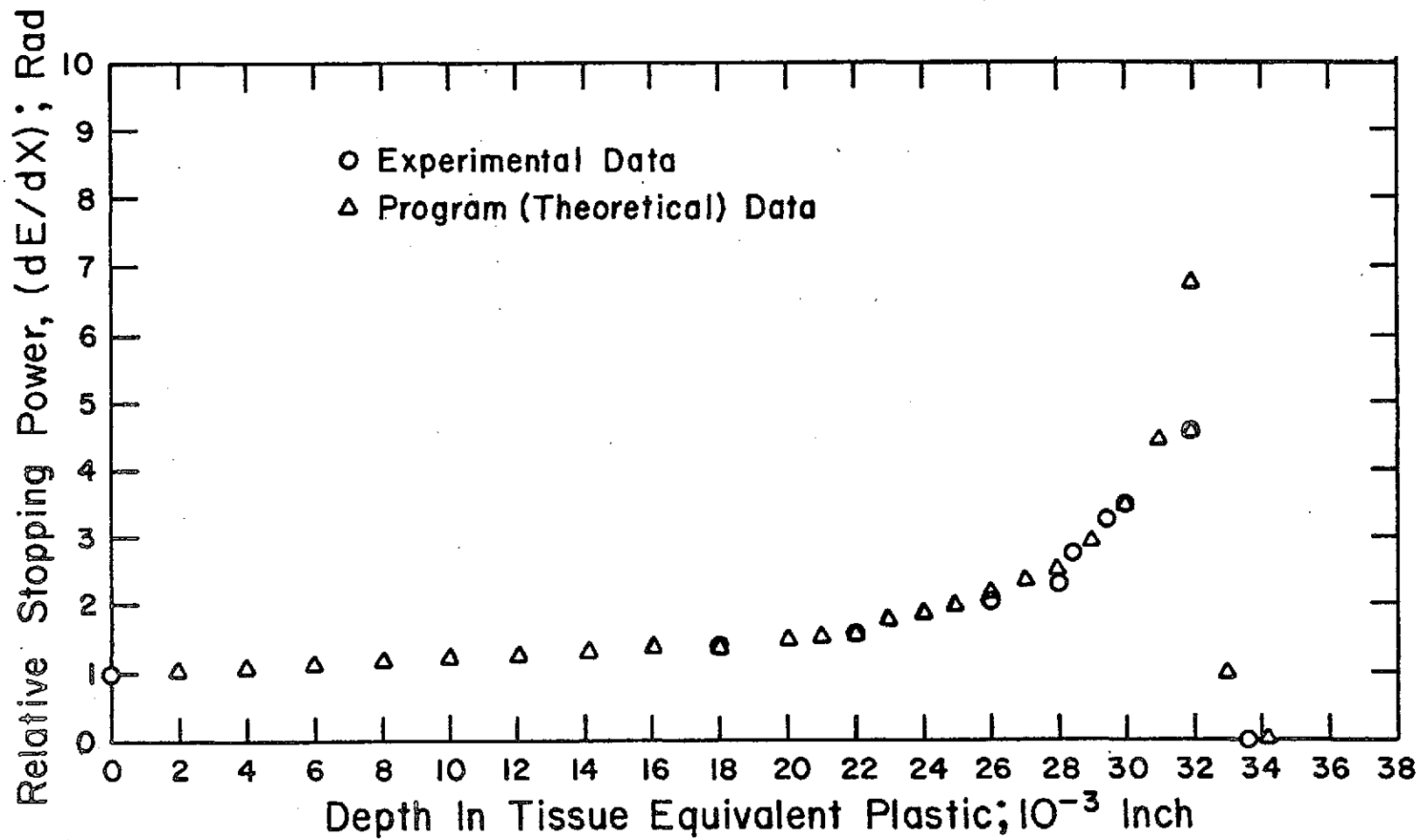


Figure III-13
dE/dx for 10 MeV Protons
in TE Plastic

would have existed for a gram of material. The dose used in all computations has been this Bragg peak dose. Because of the difficulty in accurately measuring the Bragg peak dose, the entrance dose was measured for each calibration and using the determined entrance to peak dose ratios, the equivalent Bragg peak dose was calculated. It must be emphasized that this method of reporting dose was requested by the original contract monitor and was contrary to what the investigators felt to be a more accurate method of reporting dose - namely proton fluence incident on the subject animal.

Proton spectra measured by the lithium silicon spectrometer system is indicated in Figure III-14 for the 10 MeV protons. The only interesting point to note here is that the peaks do broaden as one approaches the lower energies due to energy loss and interaction processes which being statistical in nature tend to spread out the range of energies contained within the proton beam. The values of energy versus depth are plotted in Figure III-15 and, if one extrapolates this back to zero thickness an initial energy leaving the transmission chamber of 8.6 MeV is indicated. This difference from the nominal 10 MeV that is quoted is due in part to energy loss in penetrating through the mylar vacuum barrier, the transmission chamber, the gas gaps within the transmission chamber and to some extent a deviation of the actual energy accelerated on the part of the cyclotron from 10 MeV.

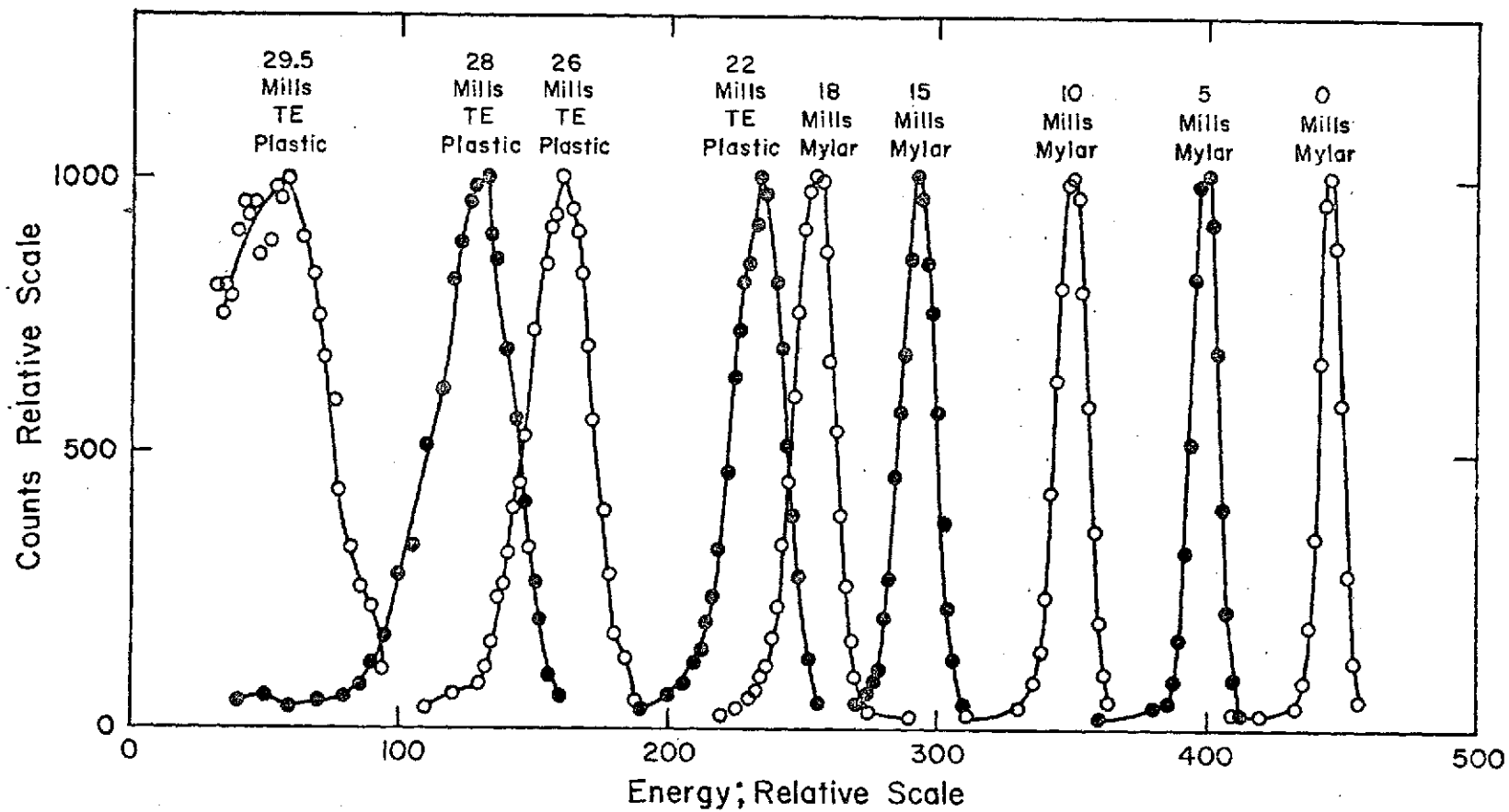


Figure III-14
10 MeV Proton Spectra vs
Depth in TE Plastic

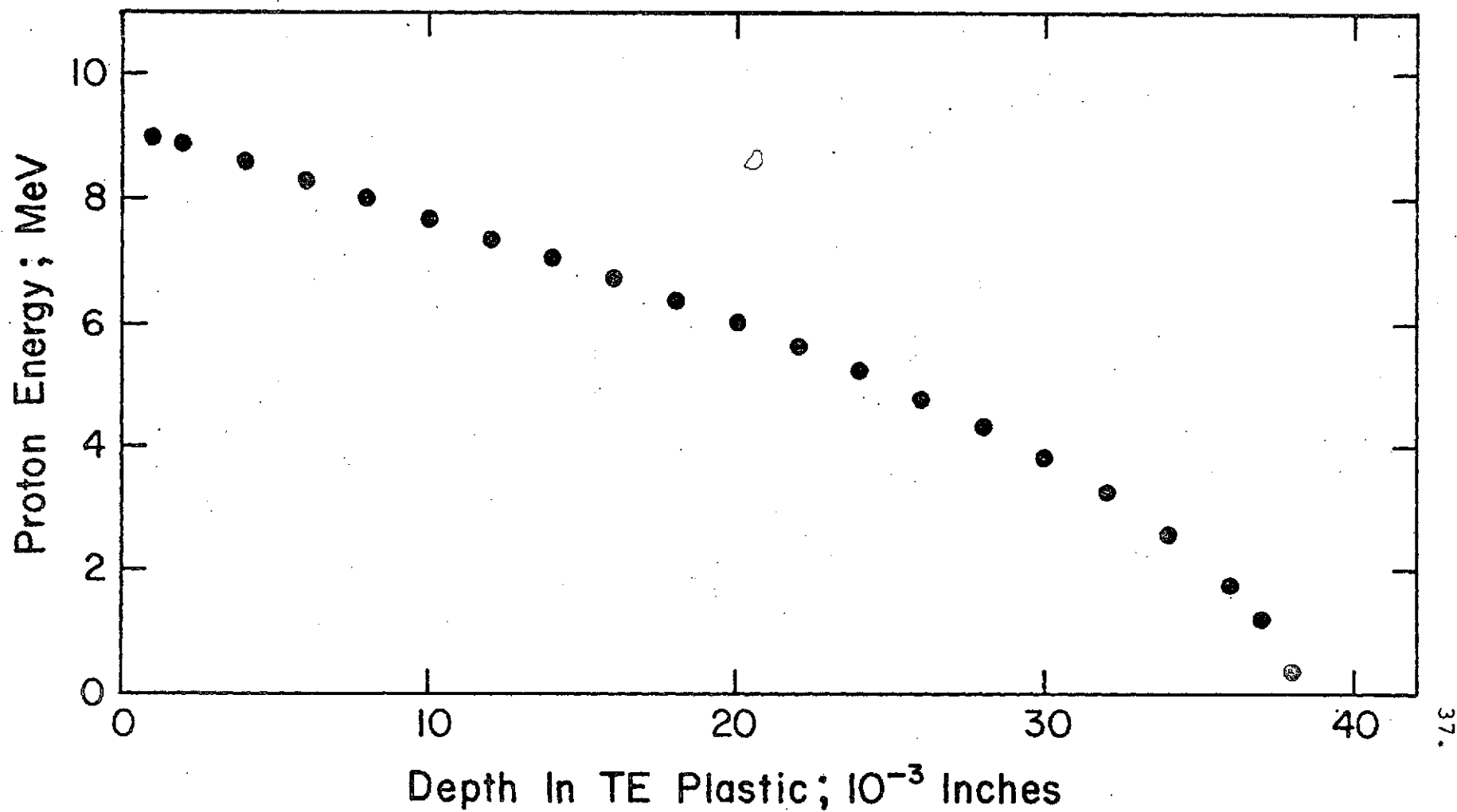


Figure III-15
Measured Proton Energy vs Depth in
TE Plastic - 10 MeV Protons

Similar results are presented in Figures III-16 thru III-18 with a 20 MeV proton spectra. In this case, the energy leaving the transmission chamber was calculated to be 19.07 MeV and the same general comments given for 10 MeV would hold for 20 MeV as well.

For the 30 MeV data presented in Figures III-19 thru III-21, the energy leaving the transmission chamber was determined to be 28.7 MeV. The 40 MeV results are presented in Figures III-22 thru III-24. The energy leaving the transmission chamber was 38.4 MeV and for the 50 MeV data presented in Figures III-25 thru III-27, the energy leaving the transmission chamber was 47.4 MeV. In the latter two cases, the 40 and the 50 MeV data, there is some indication of scattered lower energy protons as part of the original beam prior to any attenuation through tissue equivalent plastic. This is thought to be due in part to scattering off the aluminum walls of the vacuum beam transport system by the beam after it was expanded to allow collimation and transmission of the central inch and half or two and half inches as the case may be for animal exposure. Scattering which occurs up the beam pipe some distance from the transmission chamber can occur and still pass through the hole in the collimator and thus be incident on the animal. This scatter contribution can be minimized by magnetically focusing the beam down to a small diameter but then one is back to the unacceptable conditions discussed earlier of major hot and cold spots within the irradiation area.

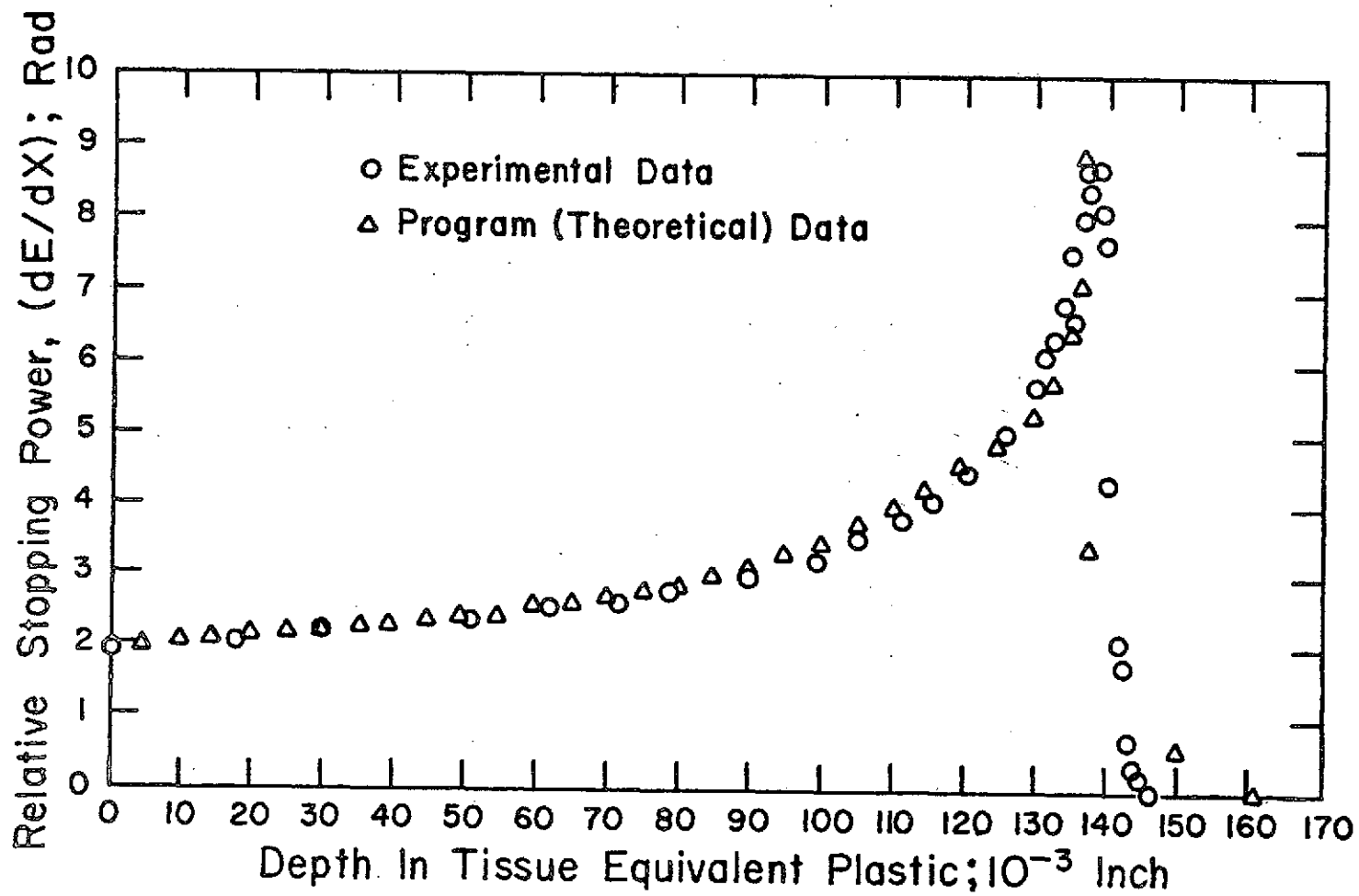


Figure III-16
dE/dx for 20 MeV Protons in
TE Plastic

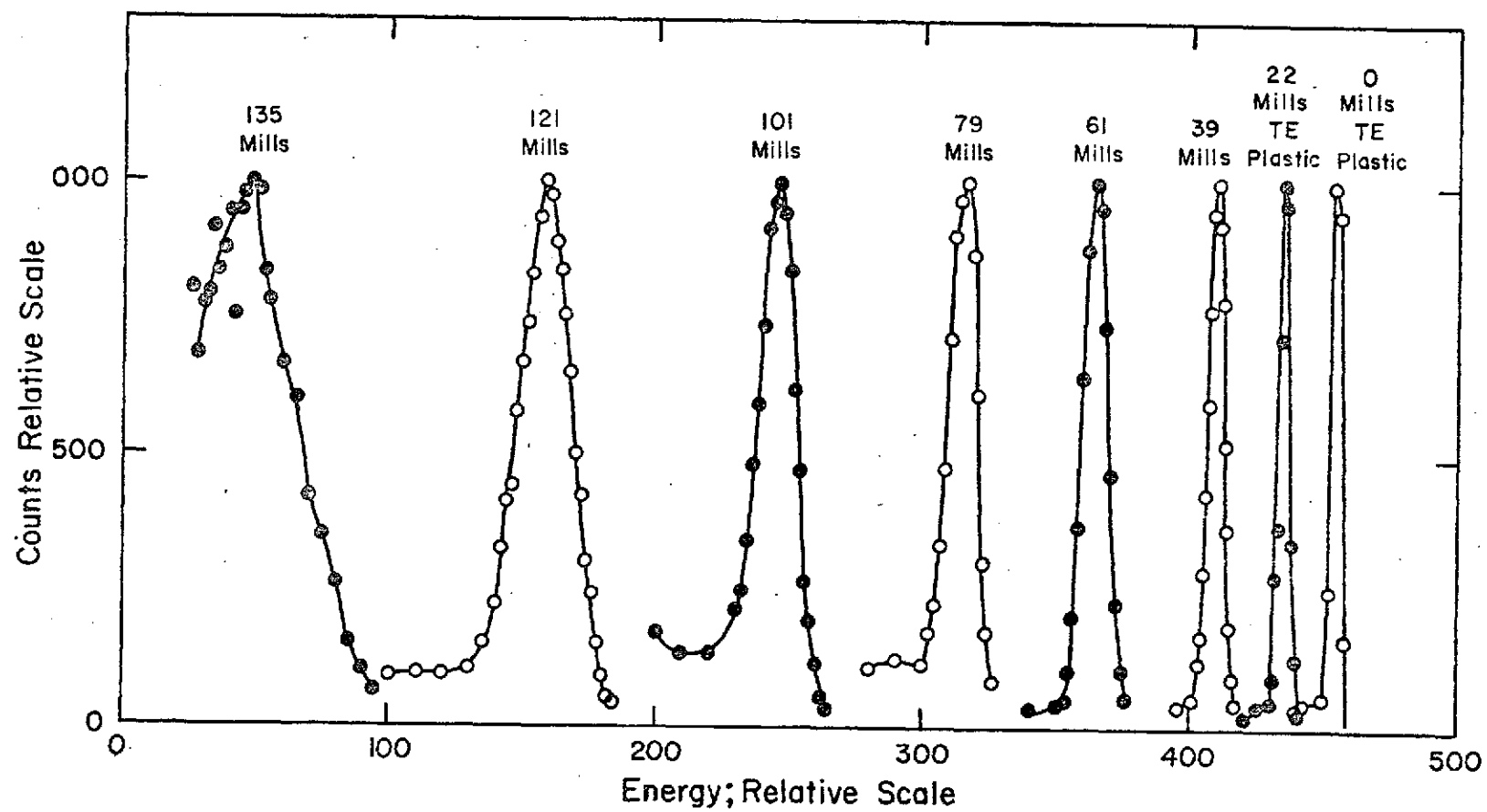


Figure III-17
20 MeV Proton Spectra vs
Depth in TE Plastic

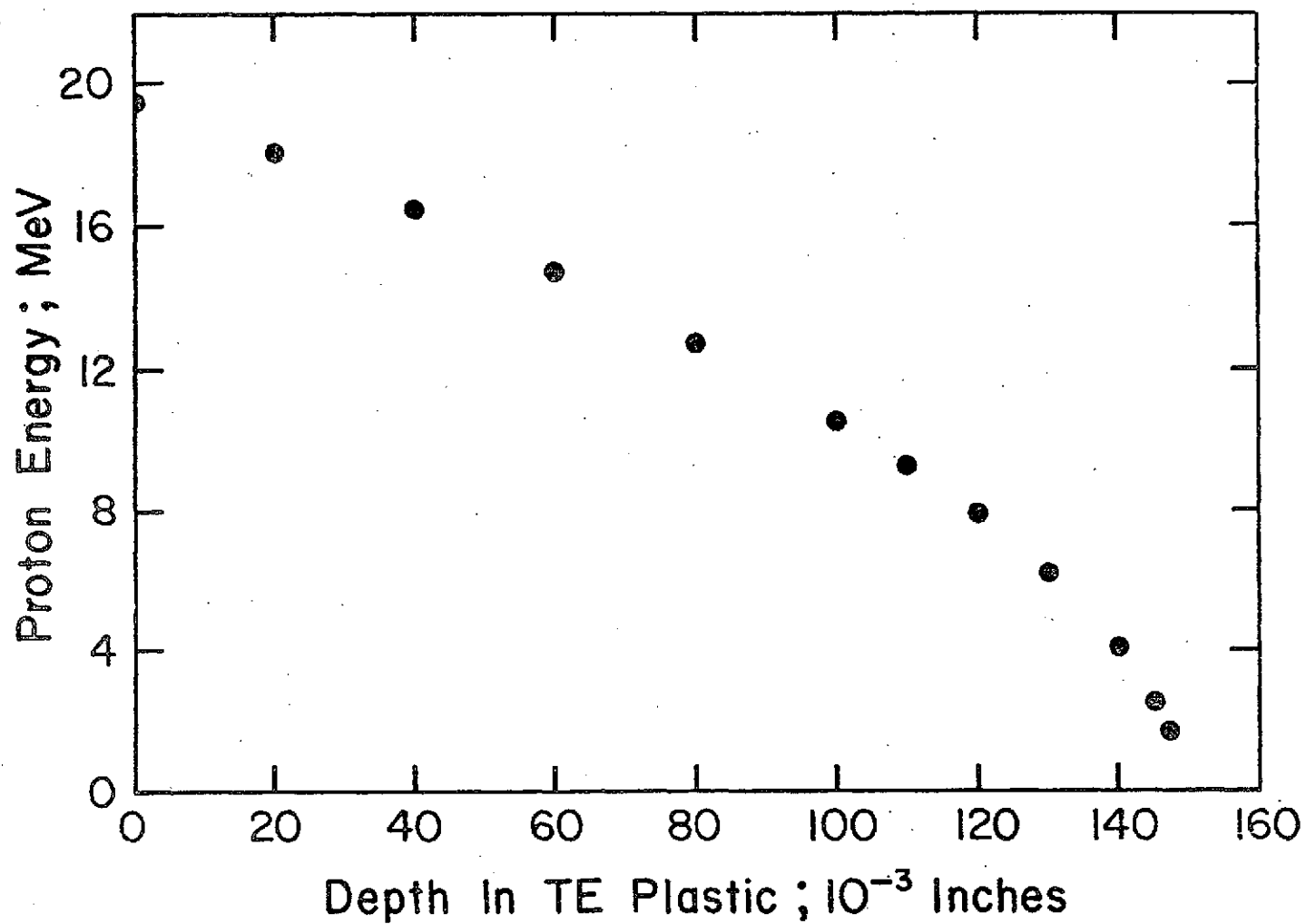


Figure III-18
Measured Energy vs Depth in TE
Plastic - 20 MeV Protons

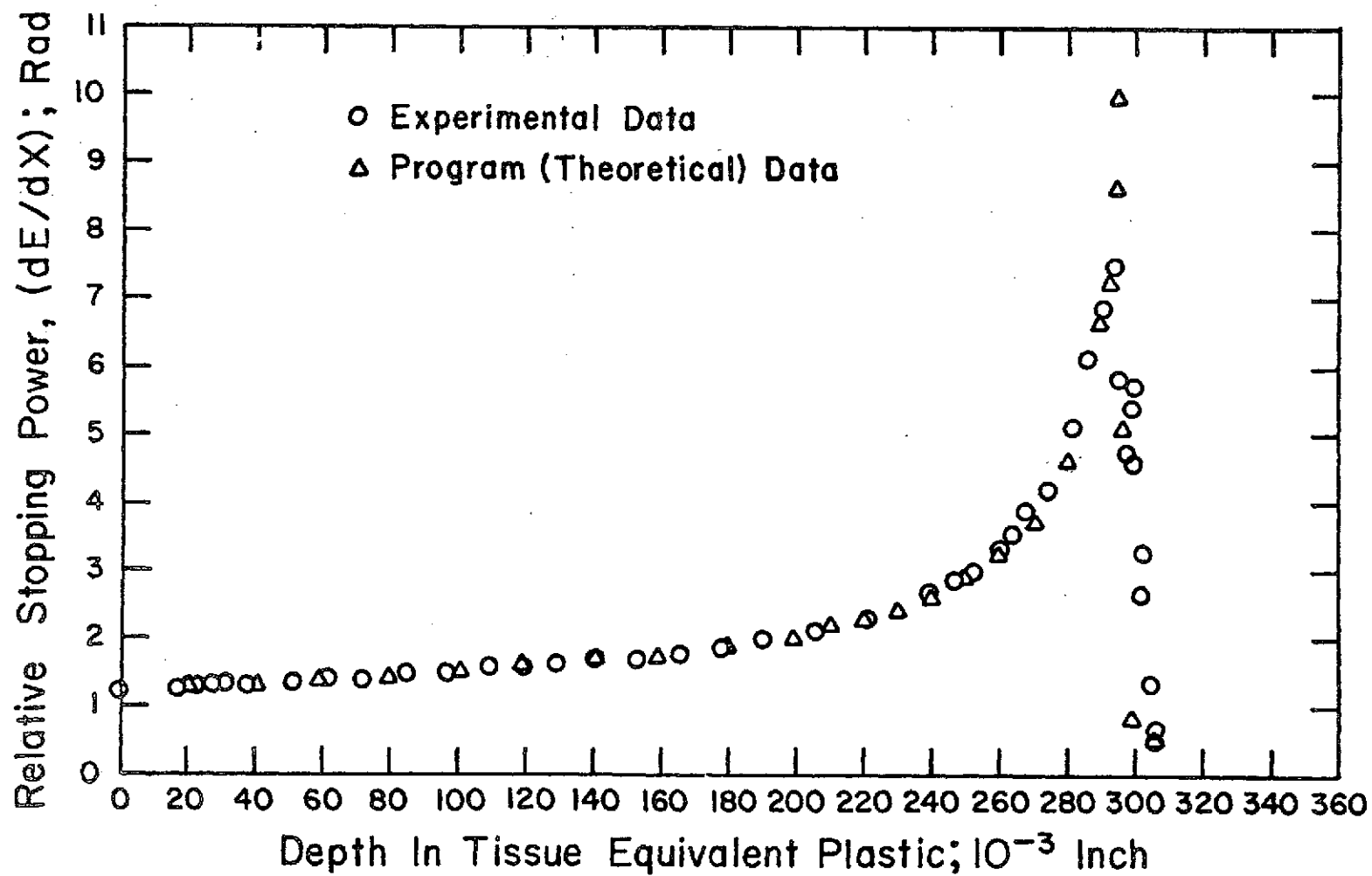


Figure III-19
dE/dx for 30 MeV Protons in
TE Plastic

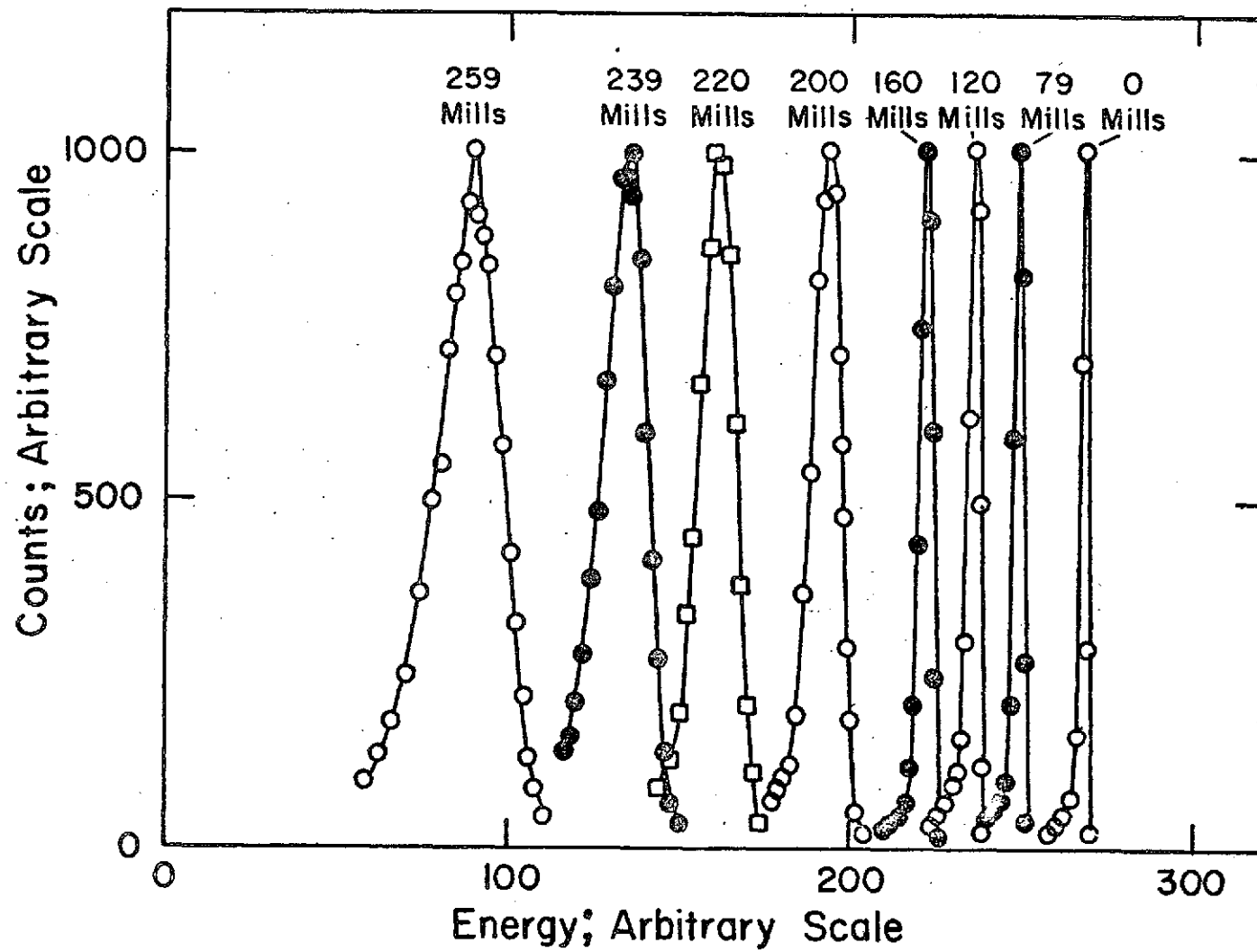


Figure III-20
30 MeV Proton Spectra vs
Depth in TE Plastic

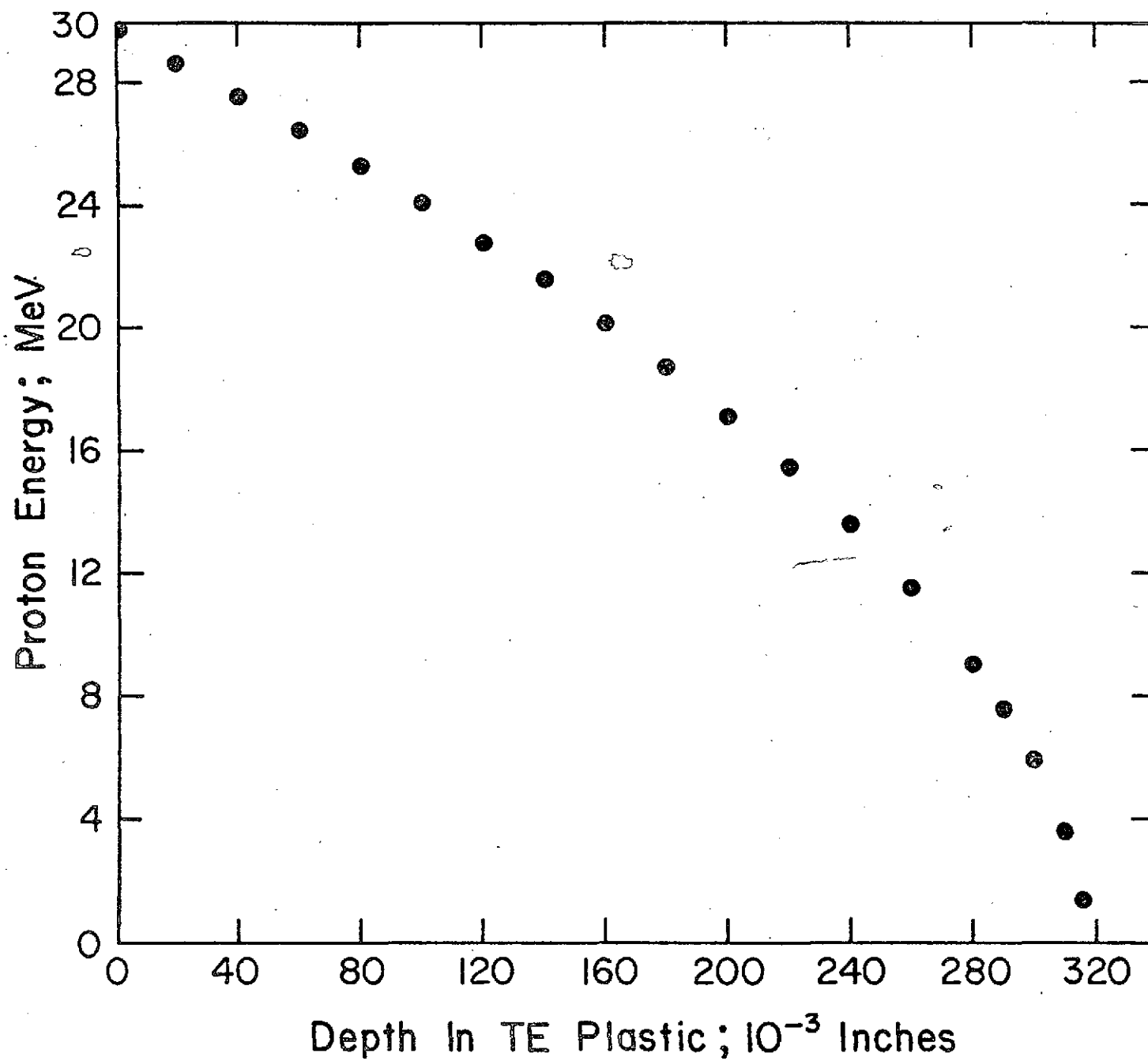


Figure III-21
Measured Energy vs Depth in
TE Plastic - 30 MeV Protons

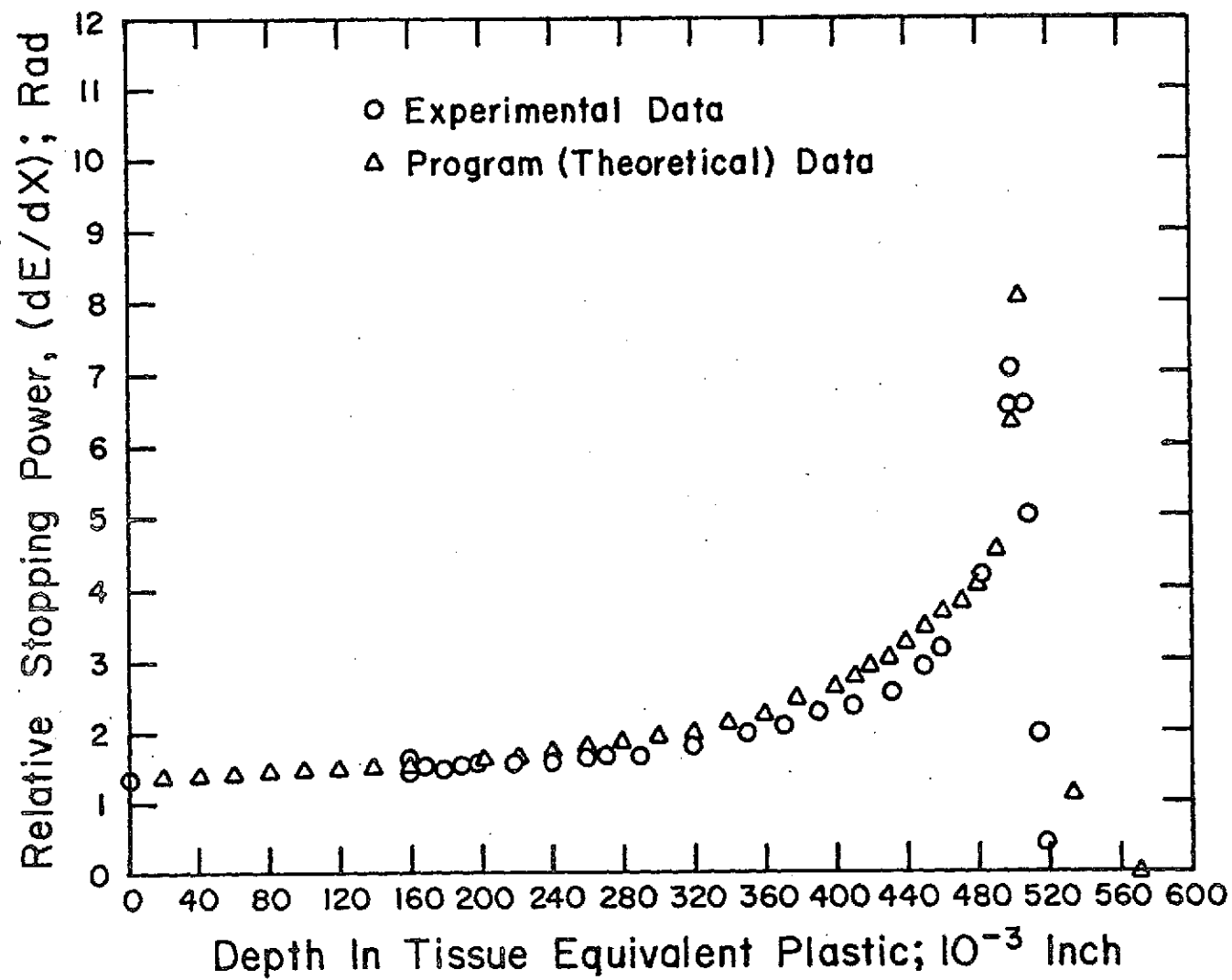


Figure III-22
dE/dx for 40 MeV Protons in
TE Plastic

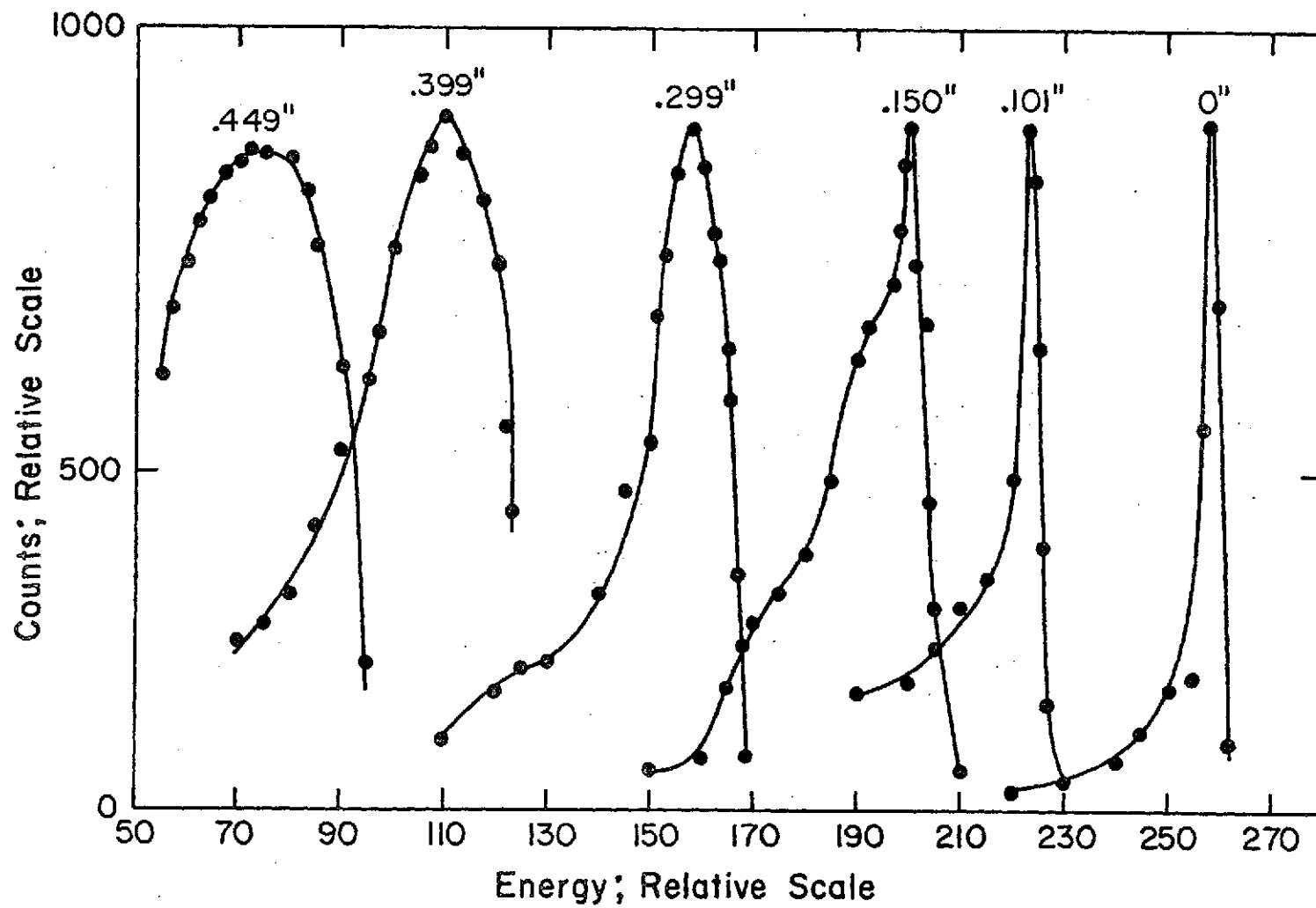


Figure III-23
40 MeV Proton Spectra vs
Depth in TE Plastic

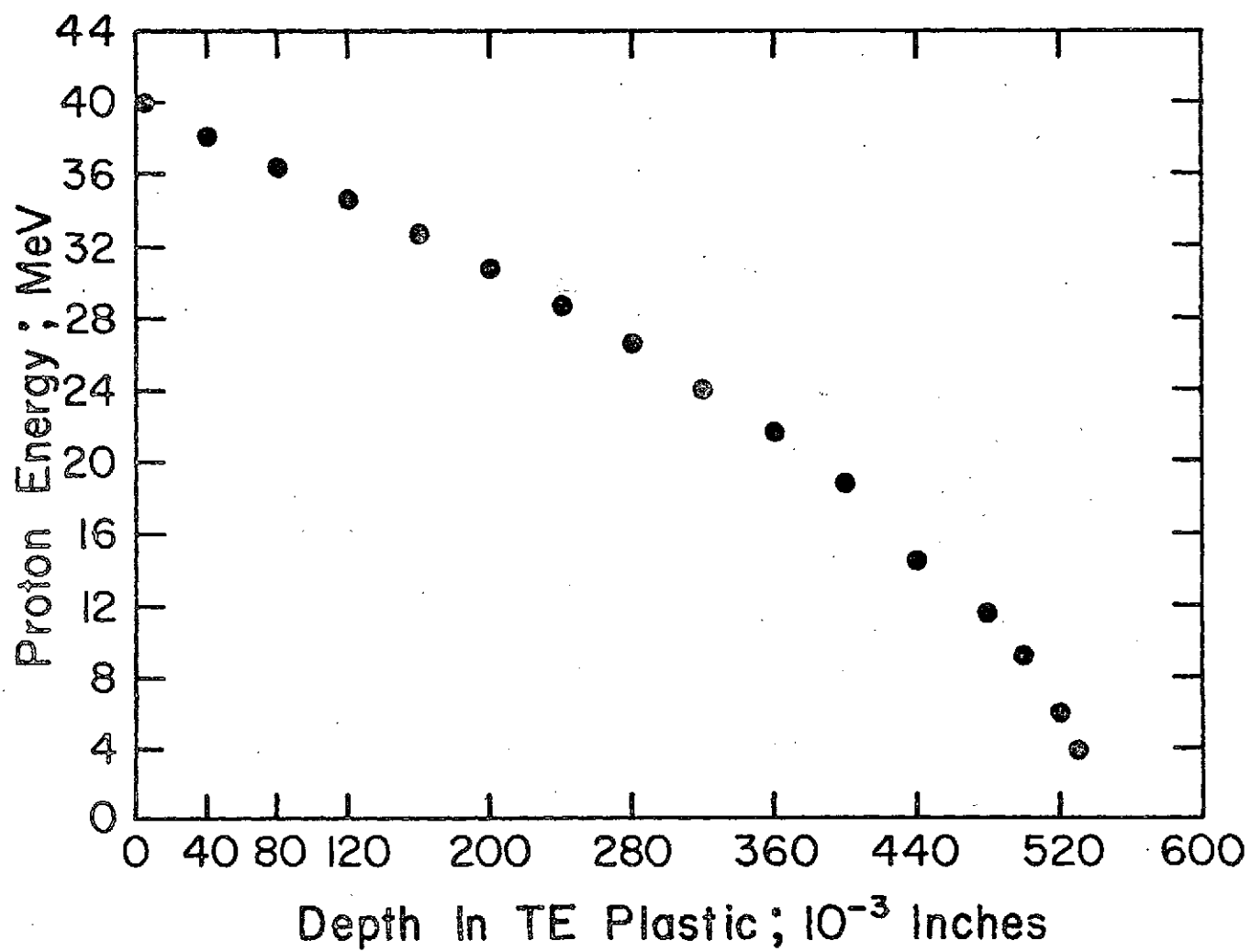


Figure III-24
Measured Energy vs Depth in
TE Plastic - 40 MeV Protons

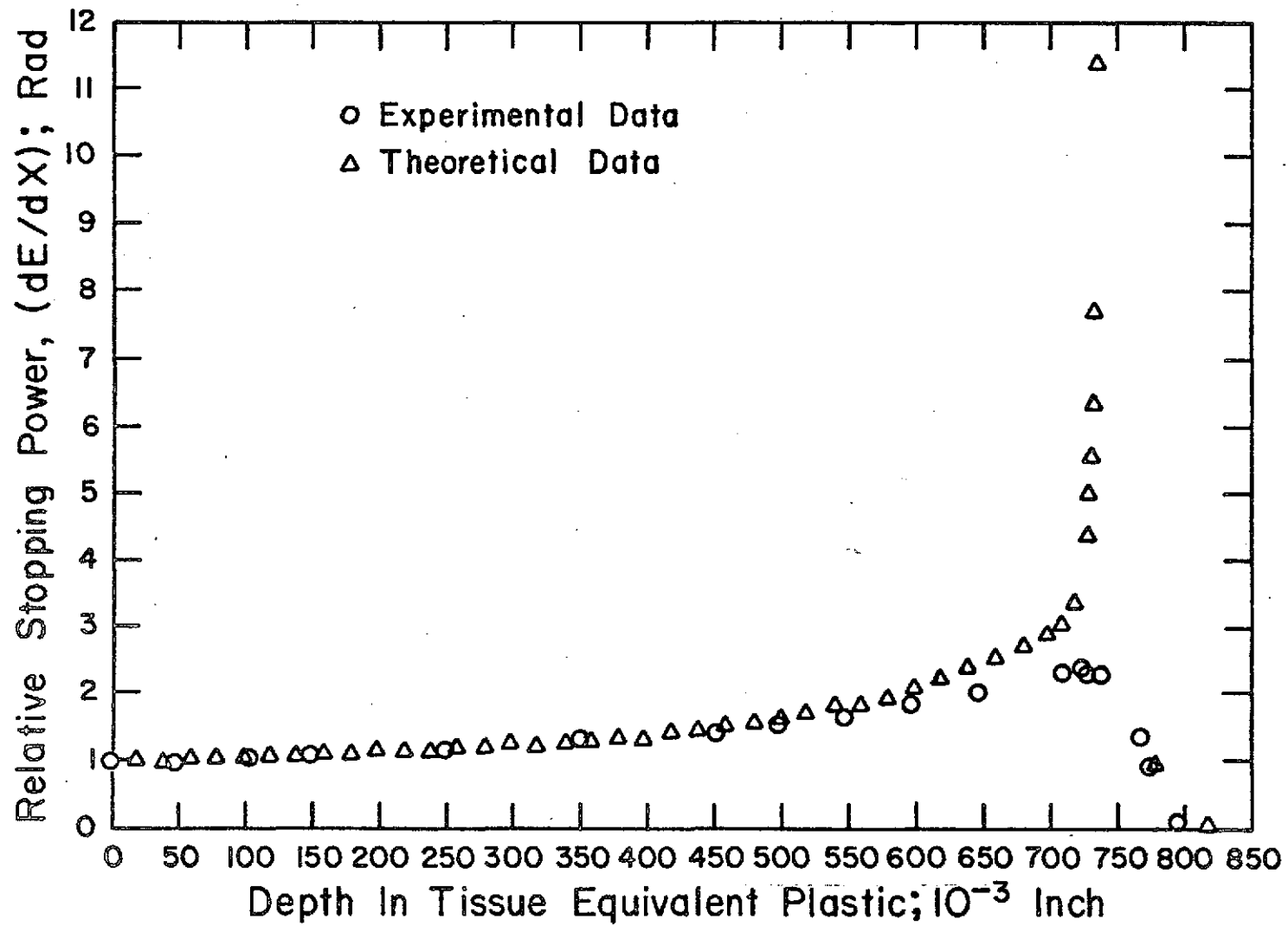


Figure III-25
dE/dx for 50 MeV Protons
in TE Plastic

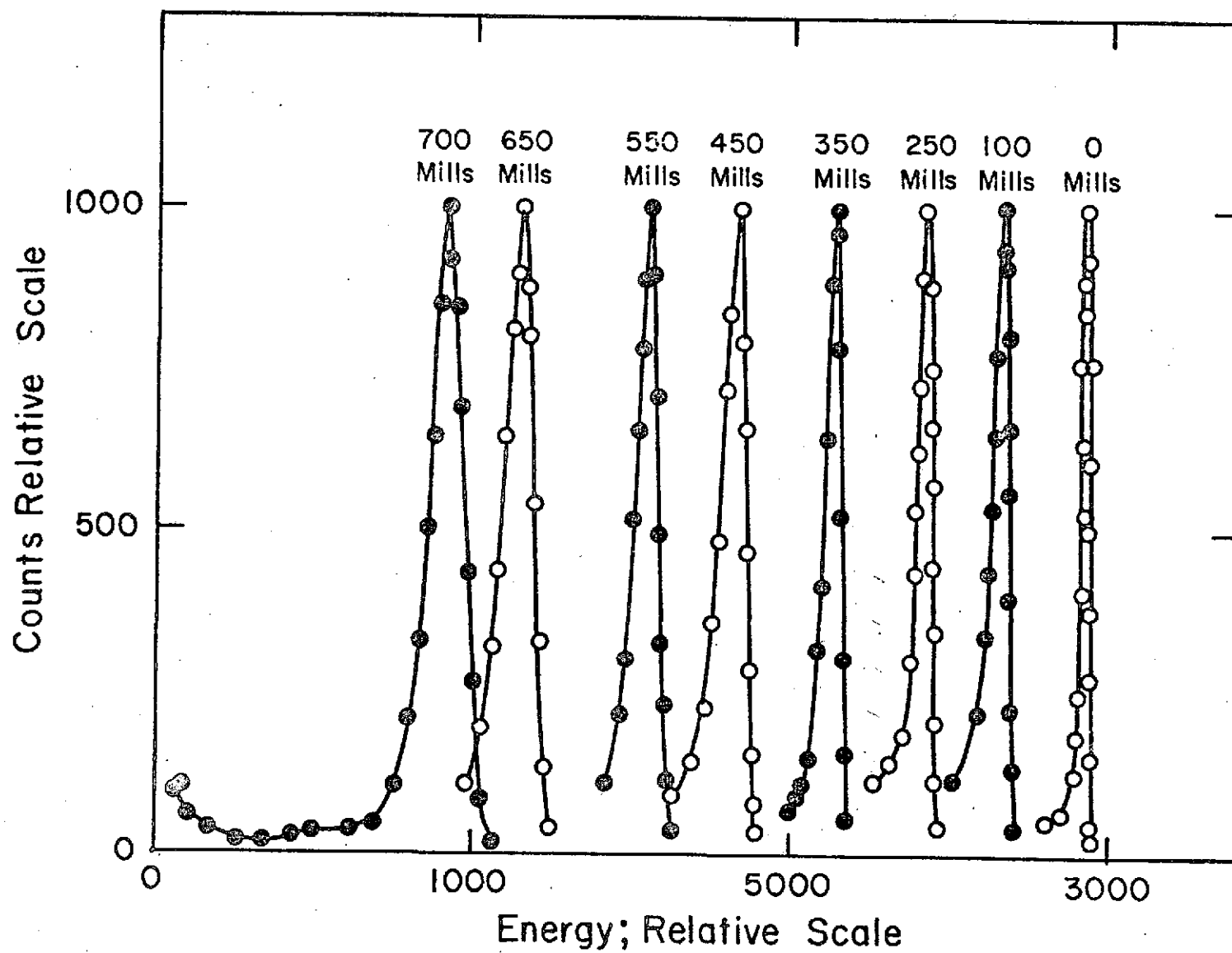


Figure III-26
50 MeV Proton Spectra vs
Depth in TE Plastic

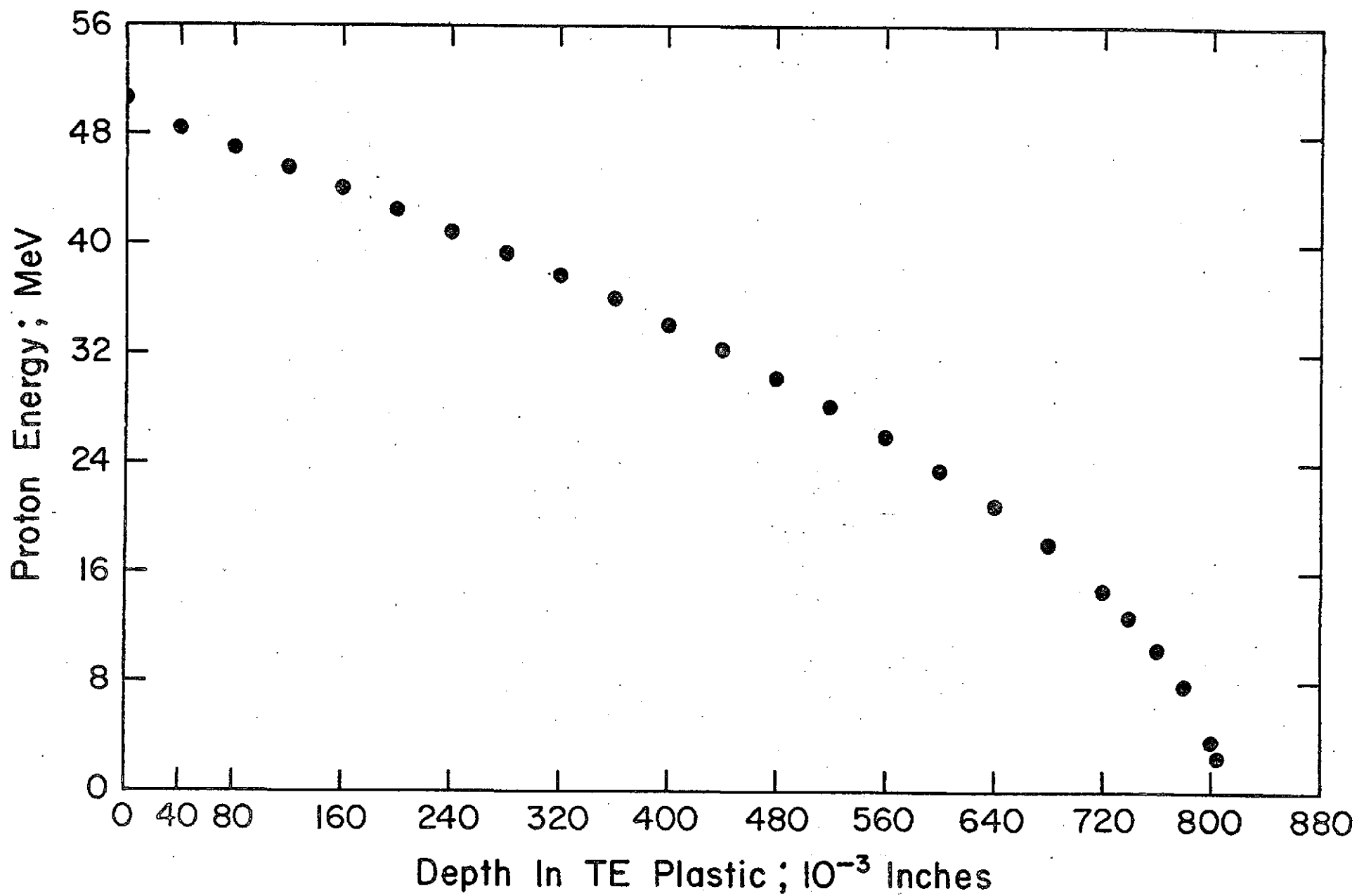


Figure III-27

Measured Energy vs Depth in
TE Plastic - 50 MeV Protons

Because of the energy of the protons one detector was not capable of fully absorbing all of the energy and it took three transmission chambers placed in line to totally absorb the energy. There is a small dead layer to the front and a slightly larger one to the rear of each detector and energy lost in these dead layers is not reflected in pulse put out by the three detectors in parallel. Thus, if one finds a particle that has a very high LET right in the region of a dead layer, there is some loss in the size of the pulse outputed by the detectors for that particular energy or situation. The spectra, therefore, have to be interpreted in their total rather than individual details because only when interpreted in total will these minor artifacts in the data be compensated for and one can get an accurate impression as to what is happening as the beam penetrates with depth. There is also the problem with three detectors that they have to be physically aligned concentrically and parallel to the proton beam. That is not to say that the active detection volumes within each of the three detectors are completely concurrent. The peripheral edges may or may not extend to the same point in all three detectors. Thus, it is possible for particles to deposit energy in the active volume of one detector but deposit energy in the non-active volume in the subsequent detectors. The resultant spectra is thus distorted and the peaks broadened beyond what would actually exist.

Comparison with Other Published Data

During the course of the experiment a paper was published by a group from the Biological Laboratory, University of California, Davis, in which proton dE/dx measurements in Lucite were measured for 20, 35 and 45 MeV protons in Lucite. The measuring technique was to use TLD chips located at various depths in the Lucite and from this to infer that dE/dx at that location. The shapes of the curves were contrary to what we had measured and in trying to determine why the difference between our data and this published data, an analysis was performed of both our technique and their technique for determination of dE/dx with depth. The complete summary of this analysis is included in Appendix 2. It would suffice at this time to state that we feel the technique of measurement using the lithium fluoride chips is quite adequate for determination of the uniformity of the beam at a given depth but due to the physical size of the chips and the rapid variation of dE/dx with position in the phantom, particularly near the Bragg peak, the technique of using the chips is not a valid one and leads to erroneous results. In addition, based on cursory examination of the published spectra, one would also have to conclude that the beam was contaminated with low energy scattered protons similar to problems we had experienced on prior occasions and had to redesign our focusing and exposure techniques to avoid.

IV. Biology

Objective

The objective of this study was to evaluate the possibility of damage to the lenticular structures of the eye and damage to the skin which might be induced due to exposure to protracted low energy proton radiation encountered during manned space flight.

Methods and Materials

The Texas A&M University Variable Energy Cyclotron was utilized as the source of proton radiation.

The irradiations were designed to evaluate the ocular and skin effects of proton radiation with respect to relative effects of different proton energies, different proton doses, different irradiation regimes, and latent period for induction of tissue damage.

In keeping with the objective, it would have been desirable to perform irradiations utilizing a spectrum of proton energies similar to that encountered in space. As it was beyond present capability to duplicate such a spectrum and, in addition, difficult to interpret results obtained from an energy spectrum, discrete, monoenergetic protons were indicated. The energies selected were 10, 20, 30, 40 and 50 MeV as these energies were within the range of energies of interest in space exploration.

Total doses received ranged from 37.5 rad to 2000.0 rad. Selected doses were based on those necessary to induce lens

environment. Also considered were its ophthalmological characteristics lending well to examination, its relative ease of handling and restraint for both irradiation and examination purposes, and its proven susceptibility to development of radiation cataracts (reported to be a greater susceptibility than man). Lastly, previous radiation cataract studies utilizing the rabbit gave this animal some advantage for accurate evaluation of collected data. Females were used to maintain one sex throughout the colony thereby avoiding any possibility of breeding during periods in which animals were held in group cages.

Rabbits were housed in individual rabbit cages in a vivarium. Each cage was 46 cm x 46 cm x 76 cm with food containers located at one end and water nipples installed high enough to require standing located at the other end. This arrangement forced some degree of mild exercise.

Cage pans were steam cleaned daily and provided with litter. Individual cages were cleaned on a regular basis. Occasionally, during transport to the irradiation facility and holding immediately prior to exposure, animals were held in group cages. Such transport was in an enclosed air-conditioned van designed specifically for animal transportation.

Food and water were provided ad libitum.

Animal holding rooms within the vivarium were equipped with an air conditioning system which provided a mixture of fresh and recirculated air. Temperature of the rooms was maintained at

opacities from exposures to other types of radiation, i.e., primarily neutrons. Since these dosages were in the range predicted to be encountered on a space journey, they were satisfactory for the skin studies also.

Irradiation regimes for both ocular and skin studies included total dose administered as a single irradiation, total dose divided into five daily equal irradiations, and total dose divided into five weekly equal irradiations.

Again, in keeping with the objective to simulate space travel conditions, chronic or low dose rate irradiation would have been desirable. Cyclotron produced chronic irradiations were not feasible. Thus, chronic irradiation was approximated by fractionating the total dose. Acute studies necessitated the use of the single irradiation.

Experimental Animals and Animal Maintenance: Initially the experimental model for this investigation was female rabbits of the New Zealand White, breed. These were obtained as immature 1.5 to 2 kg animals from a reliable supplier. Rabbits were examined, including ophthalmic examination, upon arrival to insure they were healthy and free of ocular defects prior to experimentation. The animals were held for a 30-day quarantine period preceding onset of experimentation. During this period each animal was tattooed in both ears for identification purposes.

The rabbit was used because of its size, constitution, availability and proven adaptability to a laboratory colony

approximately 22° C. In addition, a slight positive pressure was held in the rooms to aid in avoiding contamination from the outside environment.

As a preventive measure, rabbits were treated against ear mites at 30-day intervals by topical application of an insecticide containing rotenone as the active ingredient.

As the study progressed, AKC registered quality Beagle dogs, both male and female, were included as an additional experimental model. This was done to provide an animal model with a longer life span than the rabbit, this, in that respect, more closely correlating results with man. Also considered was the reported finding that the dog exhibits a somewhat lower susceptibility to radiation induced cataracts than man. Therefore, it was believed that the choice of experimental models had bracketed the supposed response of man.

The Beagle was chosen over other canine breeds for much the same reasons as the rabbit was chosen, i.e., size, constitution, availability, proven adaptability to colony surroundings, relative predictable good temperament, and abundance of previously reported biological parameters and data.

The dogs were obtained from reputable commercial kennels as 16 to 20 week old puppies. Initial routine canine immunizations, deworming and identification tattooing had been administered at the kennels prior to shipment. As with the rabbits, dogs were examined upon arrival to insure health and freedom from pre-

existing ocular or skin defects prior to introduction into the experimental program. A quarantine period of at least 30 days was also provided for the dogs.

Dogs were housed in outdoor runs 2.4 m x 6 m. Runs were constructed on a concrete slab with chain link fencing. Located at the rear of every run was a completely enclosed shelter 1.5 m x 2.4 m. The entire front and roof of the enclosure could be opened to allow ventilation and cooling during warm weather.

Individual runs were provided with two self-feeders and a self-waterer. Two feeders were necessary to prevent undue fighting between dominant animals and more submissive run mates vying for control of a single feeder. Wooden pallets were supplied in each run to provide dogs an occasional alternative surface upon which to rest.

Each run contained five animals of the same sex. The arrangement of sexes precluded the possibility of breeding and pregnancy.

Runs were cleaned daily. Food and water were provided to the dogs ad libitum.

Immunizations against canine distemper, hepatitis, leptospirosis and rabies were administered at recommended intervals. Deworming drugs and other routine medications were administered to the dogs as indicated to maintain good health.

Irradiation Procedure: Throughout the irradiation procedures, animals were randomly divided into the various groups. Randomizing

was accomplished through the use of a table of random numbers and the identification numbers tattooed in each animal's ears.

For the initial exposures, rabbits were divided into three major groups of approximately 75 animals each. These major groups received exposure to 10 MeV protons, 20 MeV protons and 30 MeV protons respectively. Each major energy group was further divided into three subgroups of approximately 25 animals each. One subgroup received a single acute irradiation; one fractionated into five weekly equal irradiations; and one into 5 daily equal irradiations. Additionally, each subgroup contained five dosage subdivisions of five animals each. These dosage subdivisions were composed of animals exposed to total doses of 37.5, 75.0, 150.0, 300.0 and 600.0 rad respectively. All major groups, subgroups and subdivisions received their respective exposures to both the eyes and a target area of the skin. An appropriate group of control rabbits was maintained.

During exposure the rabbit was restrained in a modified squeeze box leaving the eye and the skin target area (on the midline just anterior to the point of the shoulders) clear of any obstruction to the radiation beam. Irradiations were always done to the eye of the rabbit first, then to the skin target of the same animal. No eyelid retracting device was necessary to insure that the eye remained open during irradiation. The target, eye or skin, was "aimed" at a crosshair apparatus placed at the end of the beam transporting tube, the center of which was in exact

alignment with the center of the radiation beam itself. This alignment was determined prior to exposure by photographing the radiation beam as it passed through the crosshairs. Initially a beam with a nominal diameter of 2 cm was utilized.

Throughout irradiation the animal was observed visually via a closed-circuit television monitor to be certain no excessive movement interfered with the radiation beam striking the target.

After evaluating early data obtained from the original rabbit irradiations, a group of rabbits totalling 58 animals was irradiated with single exposure at the 30 MeV energy. This group was divided into five subdivisions, each containing ten animals and receiving approximately 150.0 rad, 300.0 rad, 600.0 rad, 900.0 rad, and 1200.0 rad respectively. A sixth group of eight animals received approximately 1500.0 rad. Irradiations were done to the eye first on the entire group using a 2 cm diameter beam. Skin irradiations were then done using a 5 cm diameter beam.

This was followed by two additional 30 MeV energy groups of about 50 rabbits each. One group was irradiated with five daily equal fractions; one to five weekly equal fractions. Each was subdivided into 37.5, 75.0, 150.0, 300.0, 600.0, 900.0 and 1200.0 rad dosage subdivisions. Another group of about 50 rabbits was irradiated with a single acute irradiation to 20 MeV protons. This group was subdivided into dosage subdivisions identical to the two 30 MeV groups.

As trends in data obtained from rabbit irradiations were developed, dogs were added to the protocol.

Initially, a group of 100 dogs was used, the entire group being irradiated with 30 MeV protons. Fifty dogs received a single acute irradiation and 50 received five weekly equal irradiations. Dosage subdivisions for the ocular exposures were 62.5, 125.0, 250.0, 500.0 and 1000.0 rad, each containing ten animals. Dosage subdivisions for skin irradiations were 1000, 1200, 1400, 1600 and 2000 rad, each containing ten animals. Both the single and the fractionated groups contained these total dose subdivisions. An appropriate group of control dogs was maintained.

The irradiation procedure for dogs was much the same as that followed for the rabbits. Irradiation was accomplished utilizing a combination of chemical and physical restraint. Chemical restraint consisted of a combination sedation/anesthesia produced by an intramuscular injection of a synthetic narcotic plus phenothiazine-type tranquilizer 10 to 20 minutes prior to irradiation. Physical restraint consisted of a sling apparatus and sand bag weights to properly position the dog and prevent movement. Eyelid retractors were necessary for ocular exposures in the dogs. Bilateral eye irradiations were performed on each dog followed by irradiation of two skin patches, one on the forequarter and one on the hindquarter. Again, the crosshair aiming apparatus and closed-circuit television were used.

After evaluating results obtained from initial dog irradiations, two additional groups of dogs were included. These two groups received radiation to the eyes only and none to the skin

as sufficient data had been gleaned from all previous skin irradiations to permit the formation of a definite conclusion regarding proton radiation effects on the skin. Each of these two groups was composed of twenty dogs. One group of twenty was exposed to a single ocular irradiation of 40 MeV protons, ten exposed to a total dose of 125.0 rad and ten 1000.0 rad. The remaining group of twenty was exposed to a single ocular irradiation of 50 MeV protons with identical total dose subdivisions.

These final irradiations concluded all animal exposures for the contract.

Examination Procedures

Immediately following irradiation, animals were examined weekly. It became apparent that weekly intervals were a greater frequency of examination than necessary and thereafter rabbits were examined every 30 days while dogs were examined every 60 days.

Skin evaluation was largely by objective means, mainly by gross observation. More elaborate evaluating techniques such as biopsy and microscopic evaluation, skin conductivity tests or skin secretion evaluation were never indicated by the results noted grossly.

The ophthalmic examinations were performed in a darkened room using both direct and indirect ophthalmoscopes and a slit lamp. Eyes were dilated for examination using 1% atropine solution. At the time of examination, the examiner had no knowledge

of the radiation energy, radiation dose, or prior finding for the various animals. No unusual restraints were necessary for examination purposes in either rabbits or dogs.

Lens opacities were scored according to the following system:

- 0 - No opacity
- + - Barely detectable opacity
- ++ - Easily detectable, but not a sight impairing opacity
- +++ - Sight impairing, but not sufficient to result in blindness
- ++++ - Animal blind due to lens opacity

While admittedly this was a subjective method of scoring opacities, there appeared to be no satisfactory objective alternative.

For the purpose of reporting data in a more interpretative method, a numerical system of grading based on the four-plus scoring was developed. A numerical value representing degree of lens opacities for any given group was obtained simply by dividing the total number of plus signs assigned to that group of animals by the total number of eyes in the group. Thus, the maximum possible degree of lens change was a numerical value of 400 indicating every eye in that group was determined to be four-plus (totally blind). If every eye in a group were determined to be a two-plus, the numerical value for that group would have been 200.

Photography was attempted in an endeavor to document changes found within the lens. However, for a variety of reasons

photographic results proved to be far from satisfactory and this method of verifying findings was abandoned.

Animals were maintained and examined periodically until data sufficient to meet the objectives were obtained. In the rabbits this period was approximately 450 days post irradiation. In the dogs, this period varied from approximately 700 days to about 1400 days.

Results

With regard to skin effects, no animal, rabbit or dog, subjected to irradiation ever exhibited any truly significant skin alteration throughout the entire study. No epilation, no erythema, no edema and no ulceration were ever observed. This held true even after initial doses and beam diameters were markedly increased in later irradiations.

The complete experimental design for irradiation of the eyes is illustrated in Tables 1 thru 3. With respect to ocular effects, the initial groups of rabbits were considered to be a pilot study to suggest the optimum way to proceed with further study. Data obtained from these groups are illustrated in Figures 1 thru 25.

Figure 1 shows the control data for all 3 groups.

Figures 2, 3 and 4 show the results of 30 MeV proton radiations delivered in single, daily, and weekly exposures, respectively. It is to be noted that in all instances doses of 600 and 300 rad are greater than control values. Furthermore, the

TABLE 1: Exposure Schedule For Initial Rabbit Eye Studies

TABLE 1A:

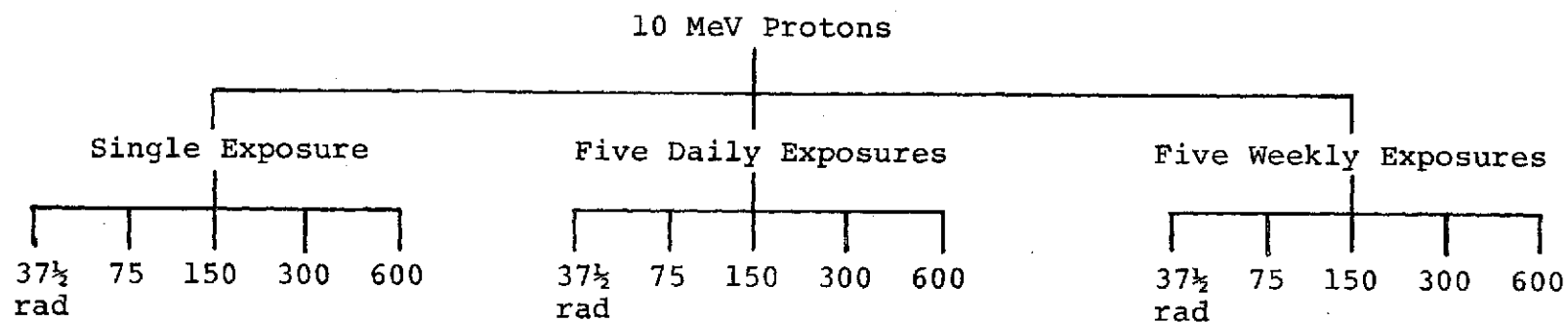


TABLE 1B:

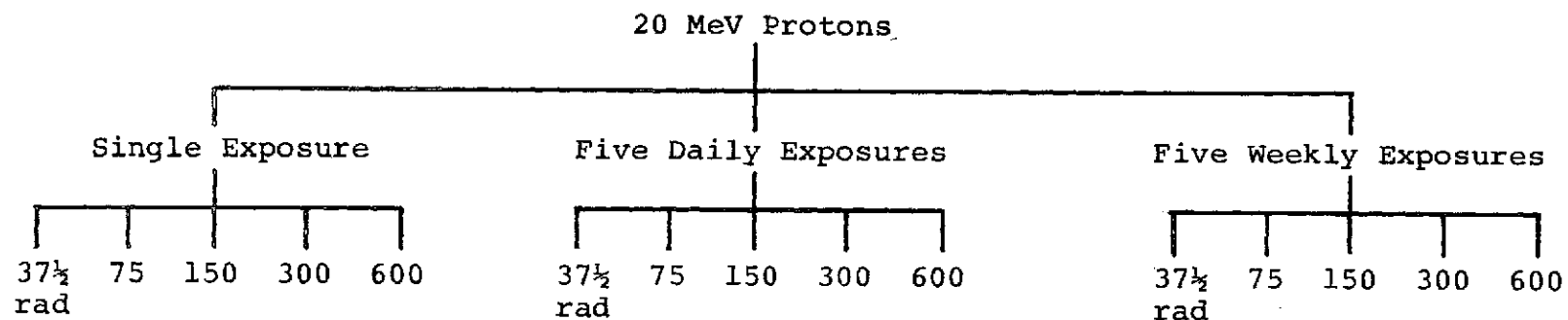


TABLE 1: Continued

TABLE 1C:

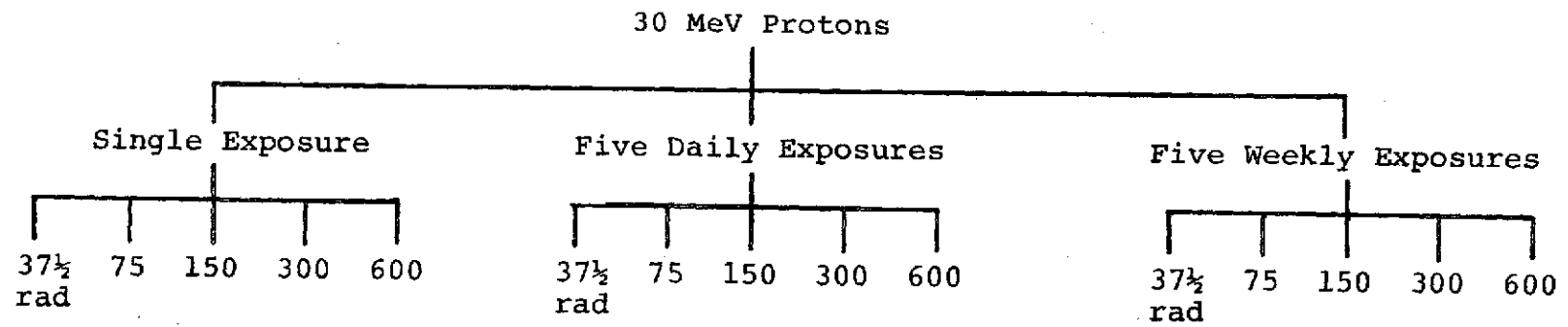


TABLE 2: Exposure Schedule For Subsequent Rabbit Eye Studies

TABLE 2A:

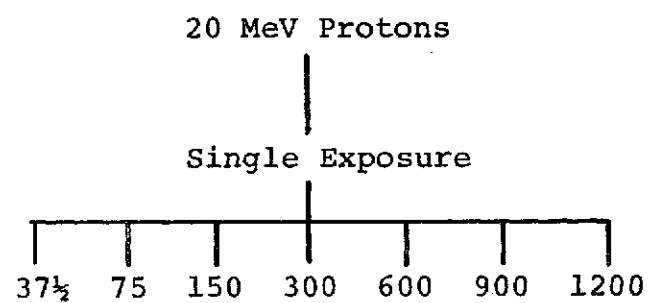


TABLE 2: Continued

TABLE 2B:

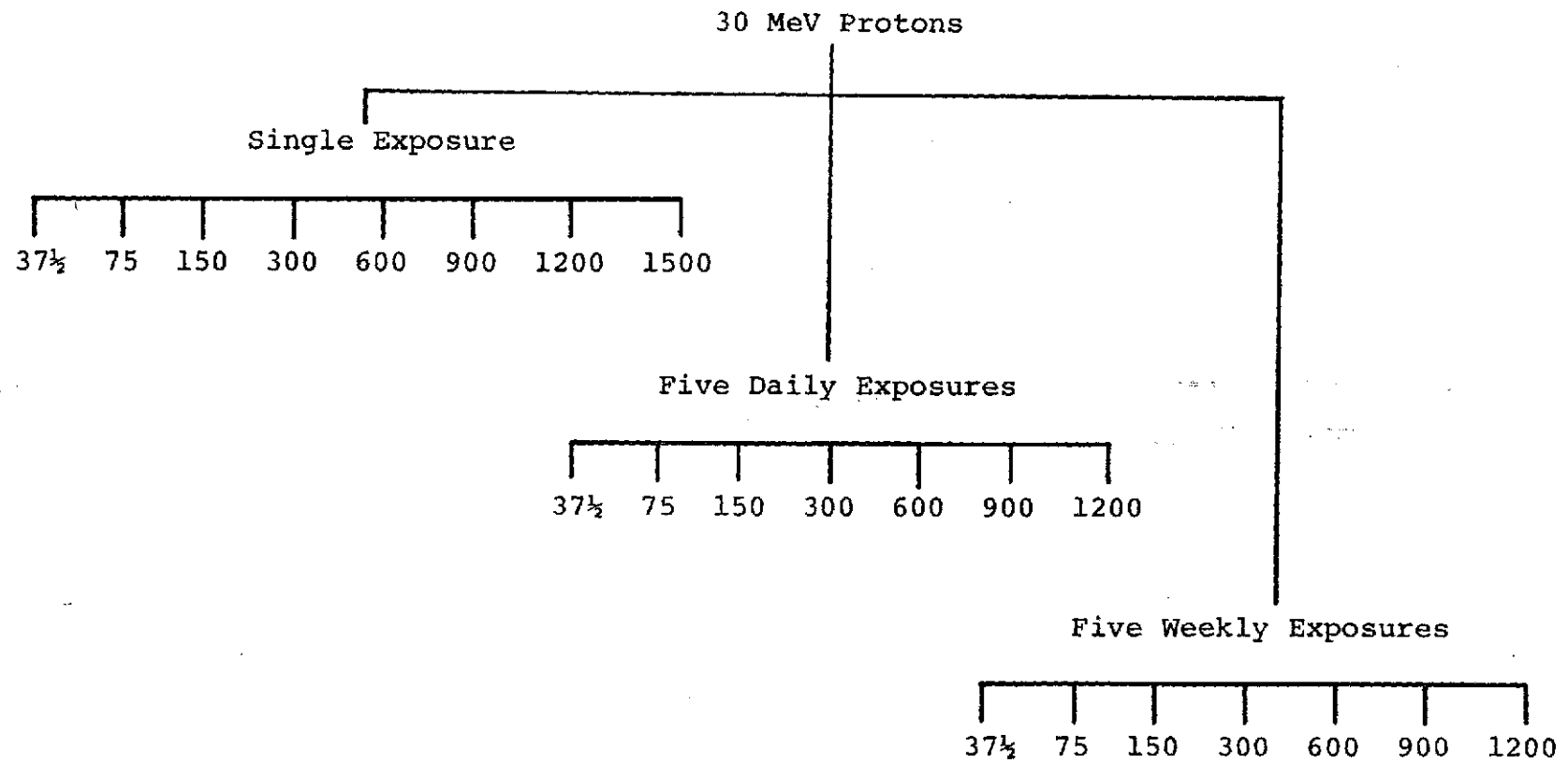


TABLE 3A: Exposure Schedule For Dog Eye Studies

TABLE 3A:

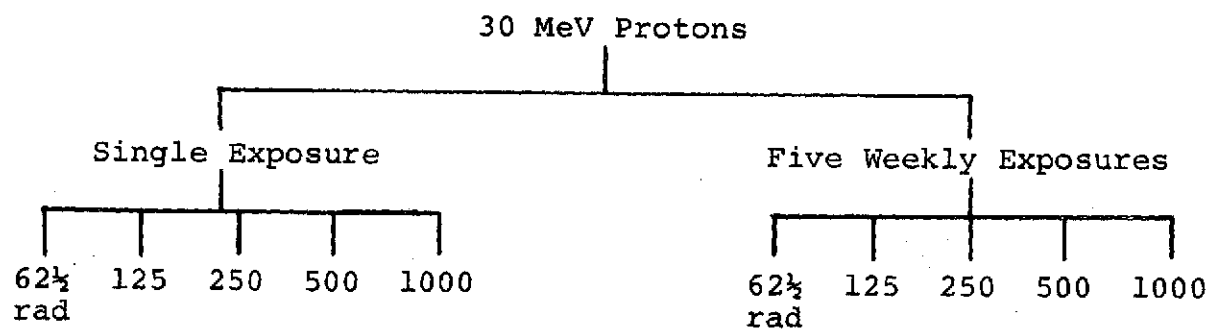


TABLE 3B:

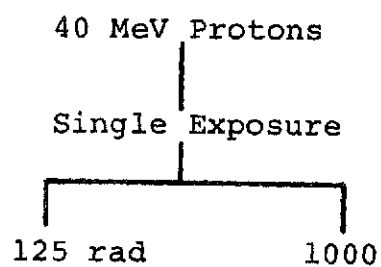


TABLE 3C:

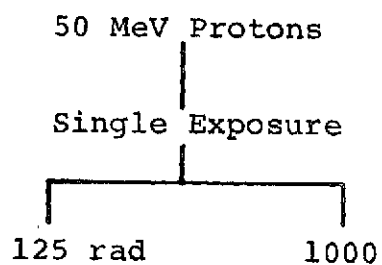


Figure 1

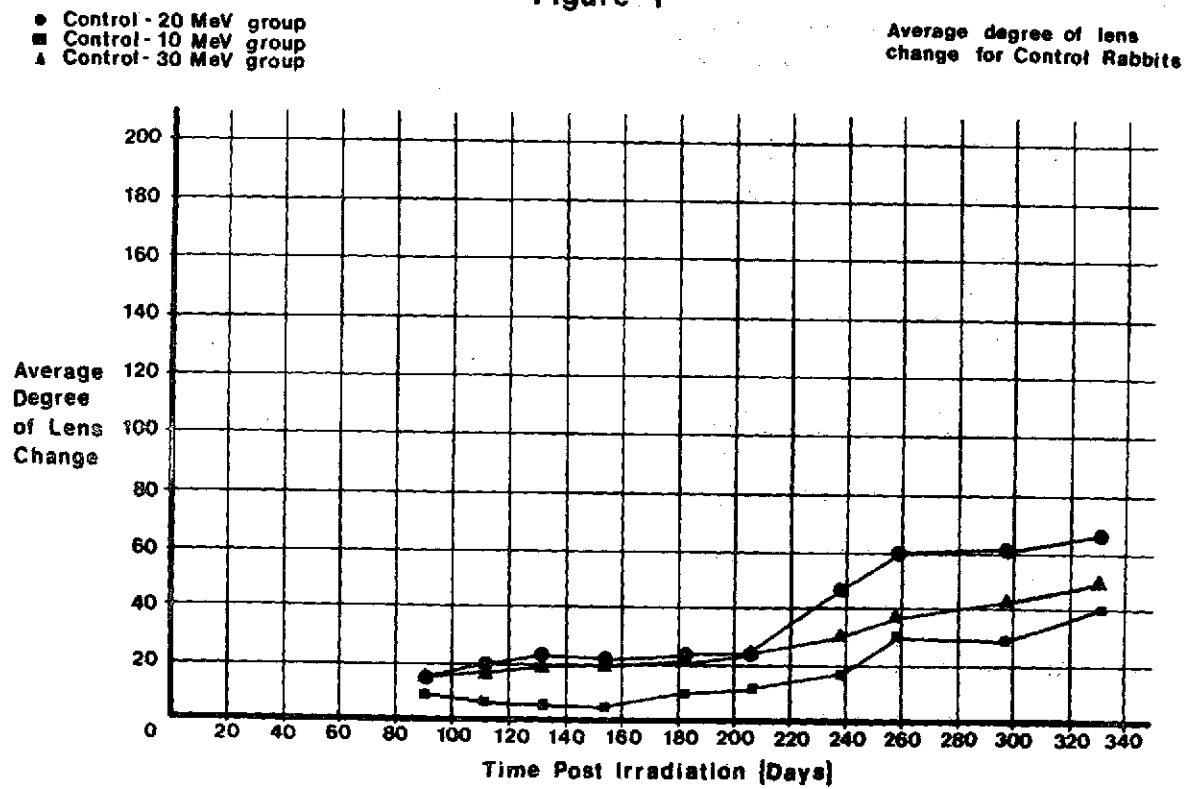


Figure 2

- Controls
- 37.5 rad.
- ◆ 75.0 rad.
- ▲ 150.0 rad.
- ★ 300.0 rad.
- ⊙ 600.0 rad.

Average degree of lens change
for rabbits receiving 30 MeV
protons in a single irradiation

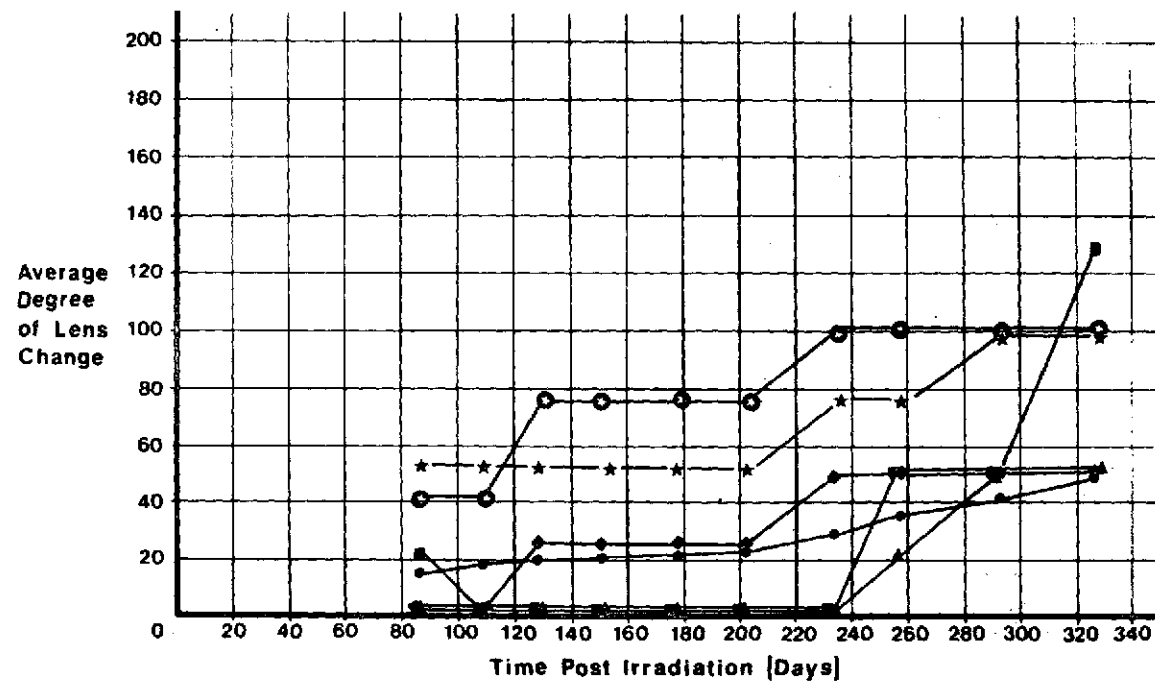


Figure 3

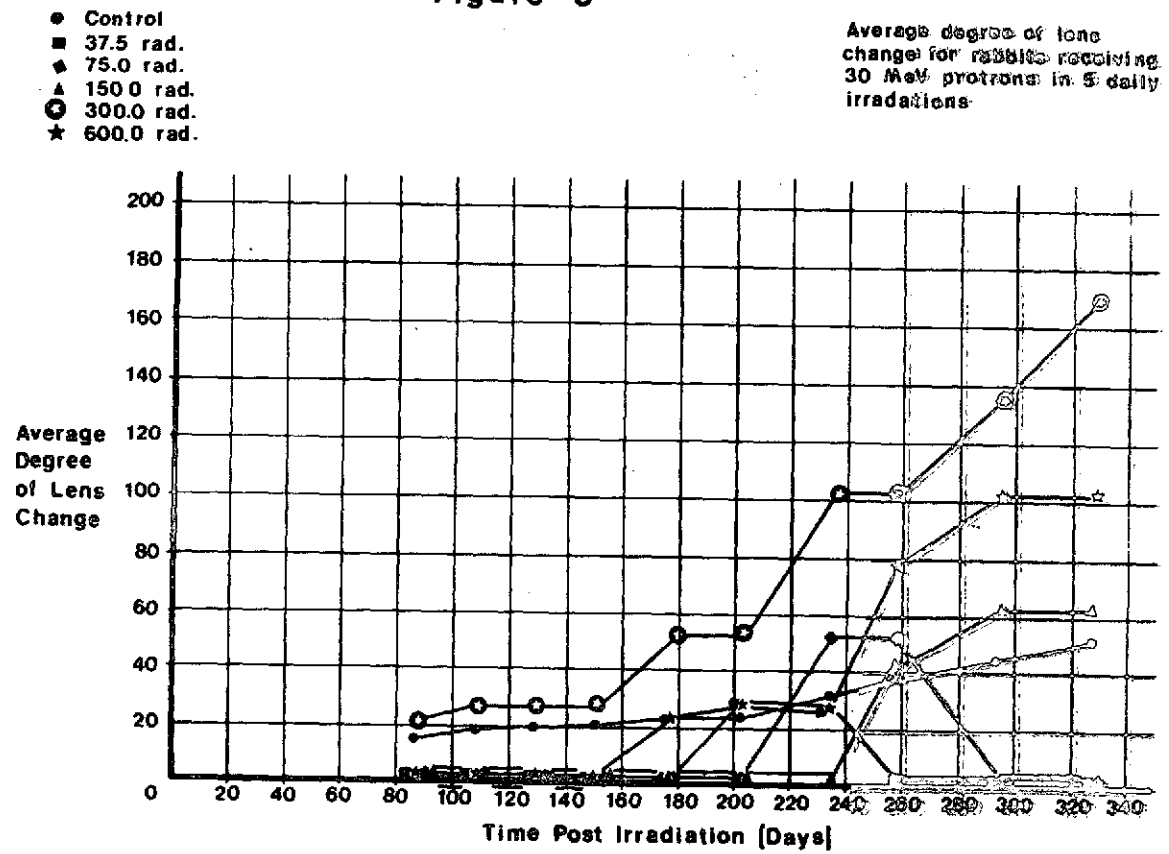
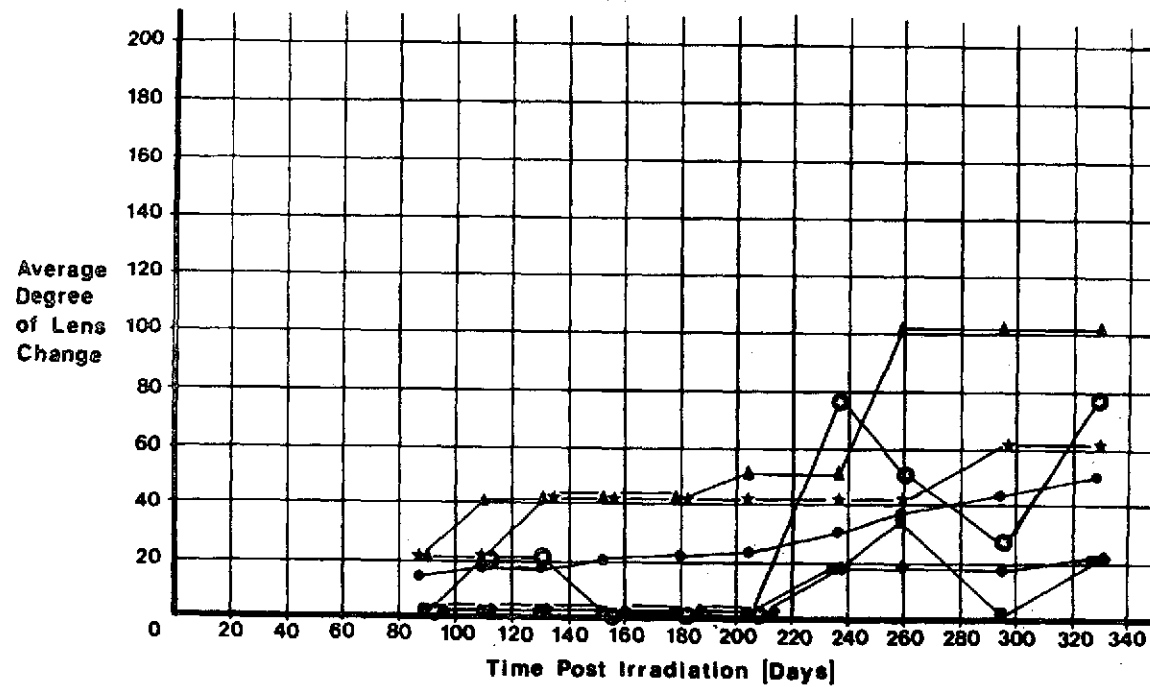


Figure 4

- Controls
- 37.5 rad.
- ◆ 75.0 rad.
- ▲ 150.0 rad.
- ⊙ 300.0 rad.
- ★ 600.0 rad.

Average degree of lens
change for rabbits
receiving 30 MeV_e protons
in 5 weekly irradiations



150 rad dose was greater than control values for daily and weekly irradiations.

Figures 5, 6 and 7 show the results of 20 MeV proton radiations delivered in single, daily, and weekly exposures, respectively. It is to be noted again that in all instances of doses of 600 and 300 rad are greater than control values. Of particular interest is the fact that all doses except 150 rad were above control values for animals exposed weekly.

Figures 8, 9, 10, 11 and 12 show the results of 30 MeV protons delivered in single, daily, and weekly exposures at a single total dose. These data also reflect the greater effects for higher doses.

Figures 13, 14, 15, 16 and 17 show the results of 20 MeV protons delivered in single, daily, and weekly exposures at a single total dose. It was believed that two things were suggested by this data. First, the relative magnitude of effect is greater at 20 MeV than at 30 MeV. Second, at least at the lower doses, protracted irradiation, i.e., daily and weekly, is more effective in causing lens changes.

Figures 18, 19 and 20 show the results of 10 MeV protons delivered in single, daily, and weekly exposures at the three highest single total doses. It was believed that there was no difference from control values for 10 MeV protons.

Figures 21, 22, 23, 24 and 25 show the results obtained by combining single, daily, and weekly irradiation data for each

Figure 5

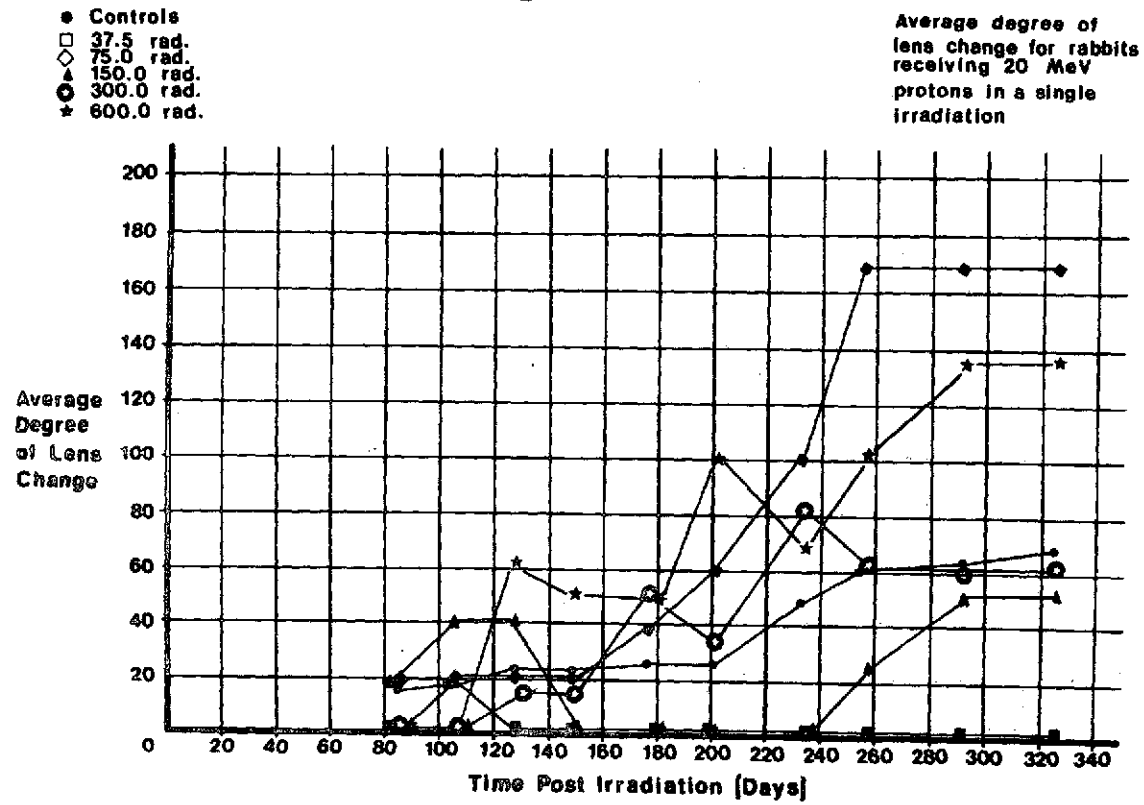


Figure 6

Average degree of lens
change for rabbits receiving
20 MeV protons in 5 daily
irradiations

- Controls
- 37.5 rad.
- ◆ 75.0 rad.
- ▲ 150.0 rad.
- ⊙ 300.0 rad.
- ★ 600.0 rad.

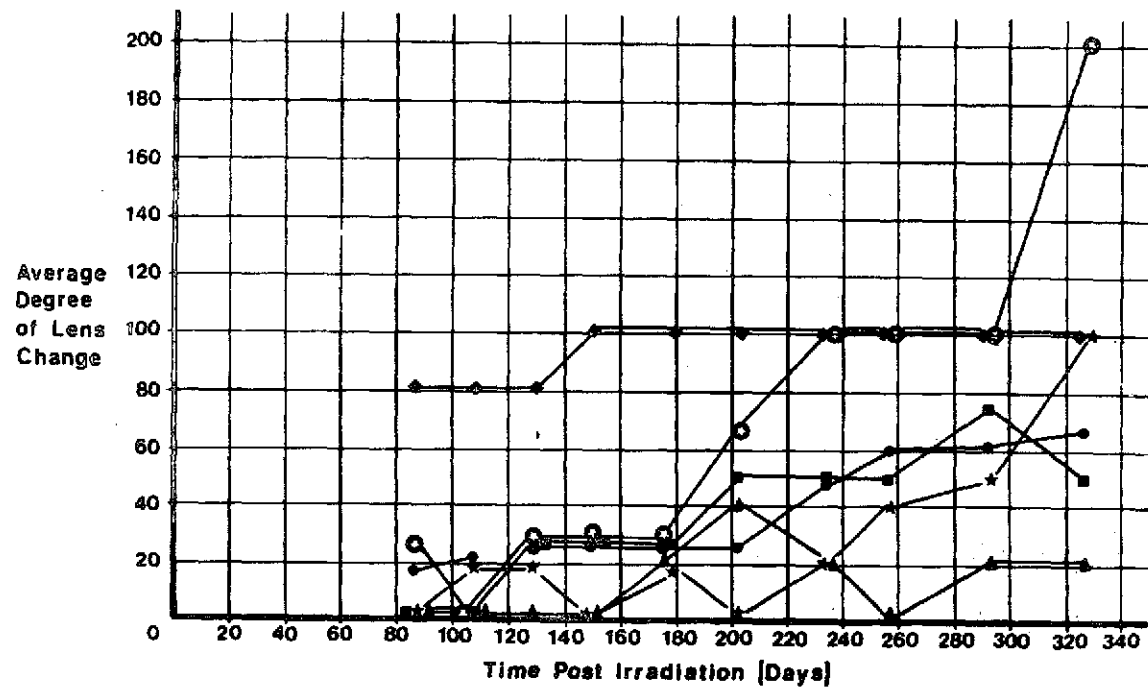


Figure 7

- Controls
- 37.5 rad.
- ◆ 75.0 rad.
- ▲ 150.0 rad.
- ⊙ 300.0 rad.
- ★ 600.0 rad.

Average degree of lens
change for rabbits
receiving 20 MeV protons
in 5 weekly irradiations

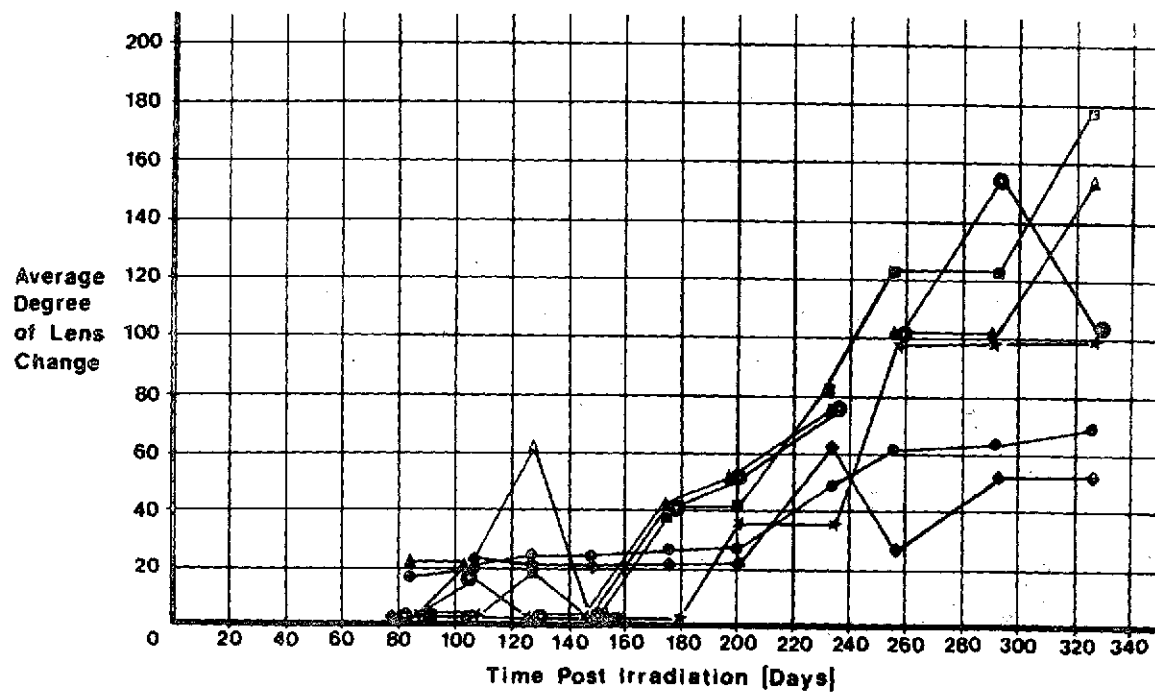


Figure 8

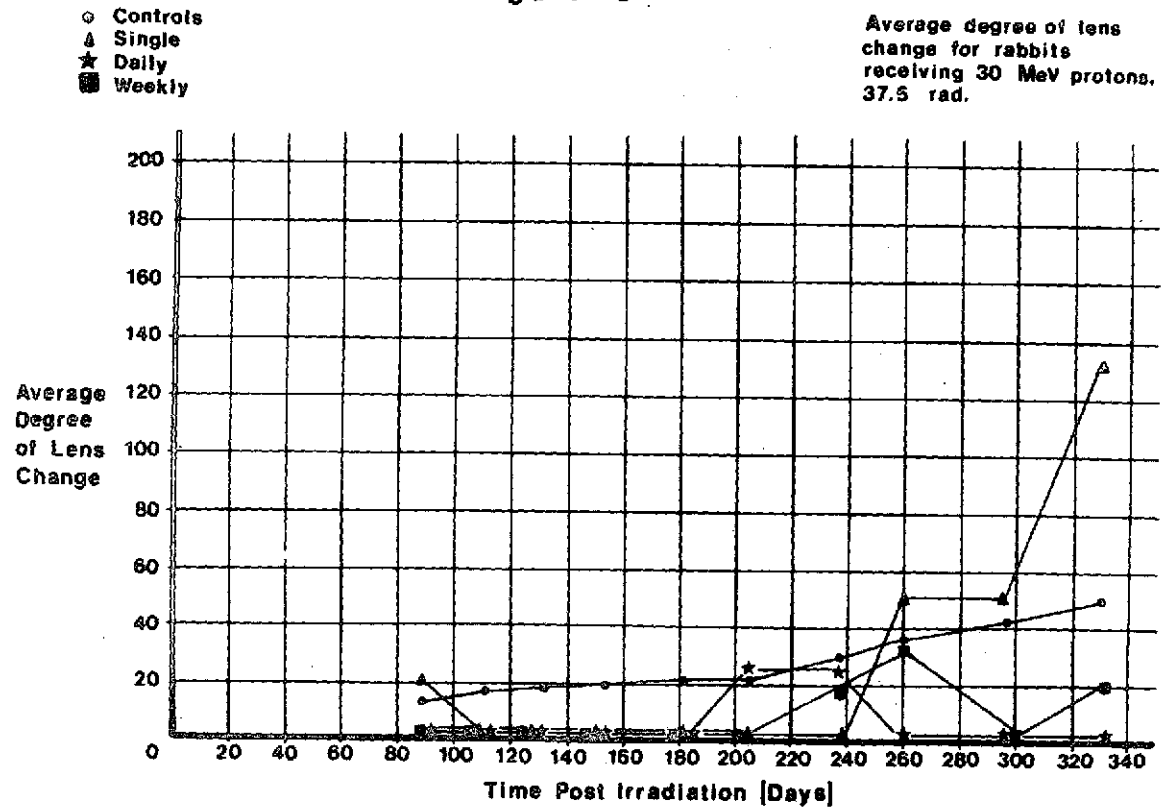


Figure 9

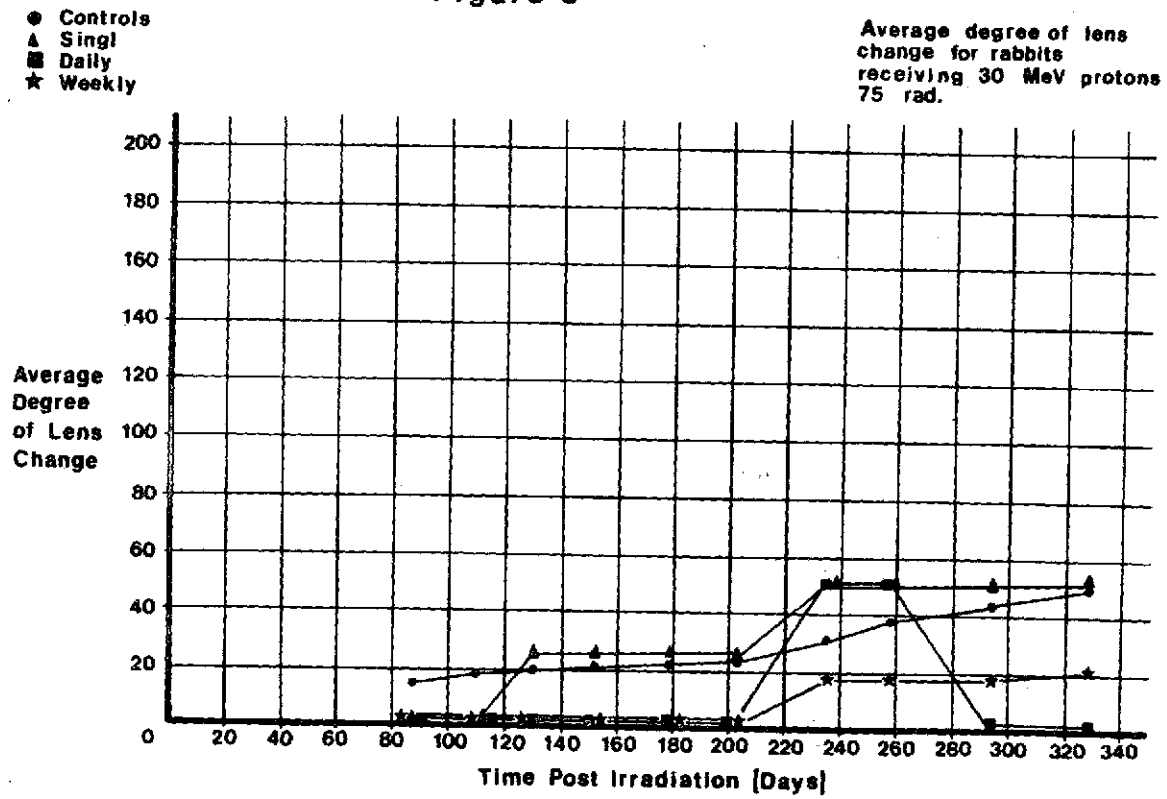


Figure 10

● Control
▲ Single
■ Daily
★ Weekly

Average degree of lens change for rabbits receiving 30 MeV protons, 150 rad.

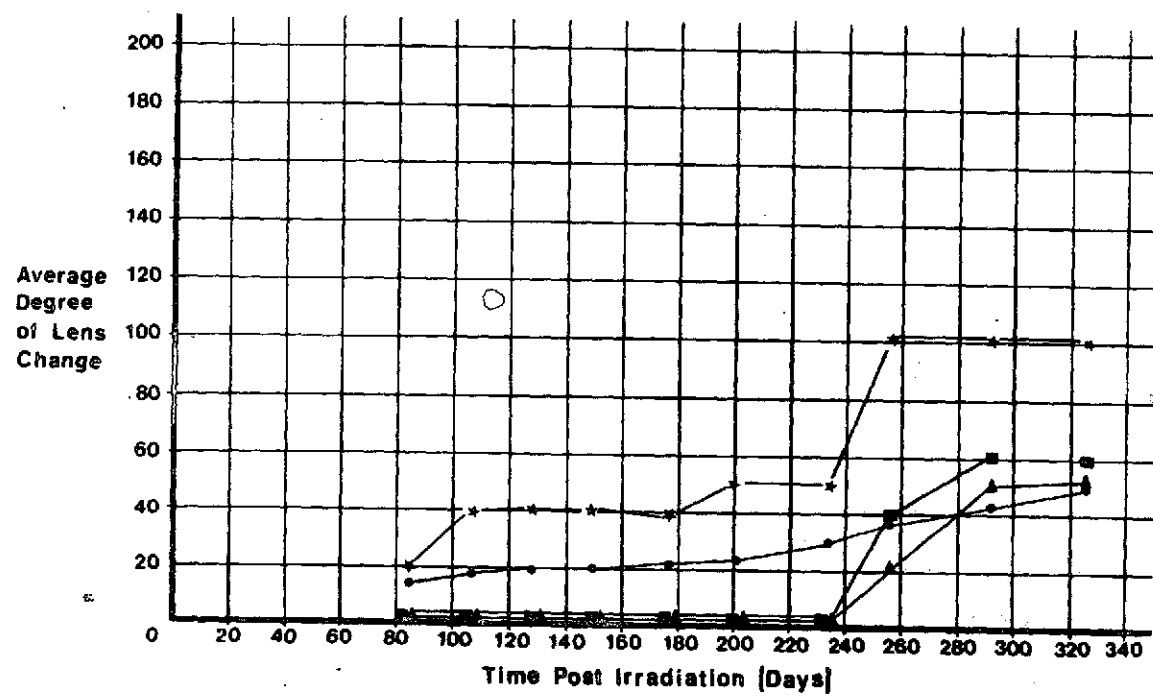


Figure 11

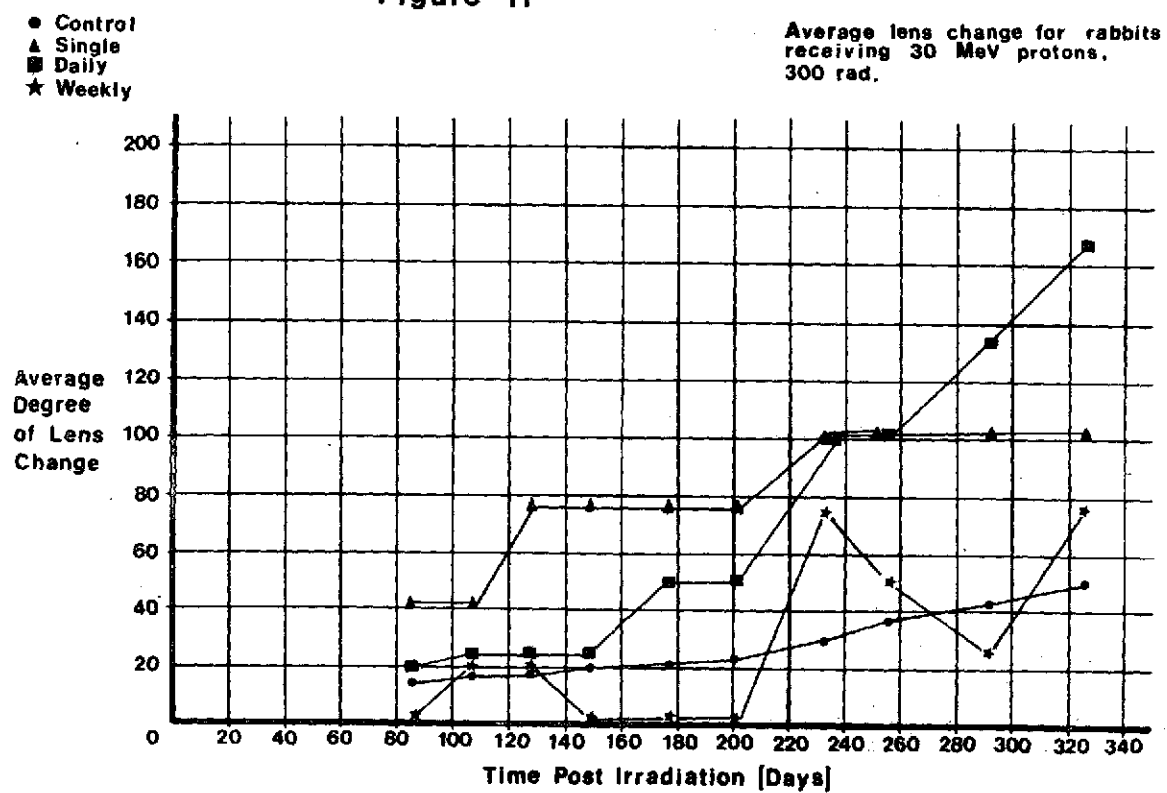


Figure 12

● Control
▲ Single
■ Daily
★ Weekly

Average degree of lens change for
rabbits receiving 30 MeV protons,
600 rad.

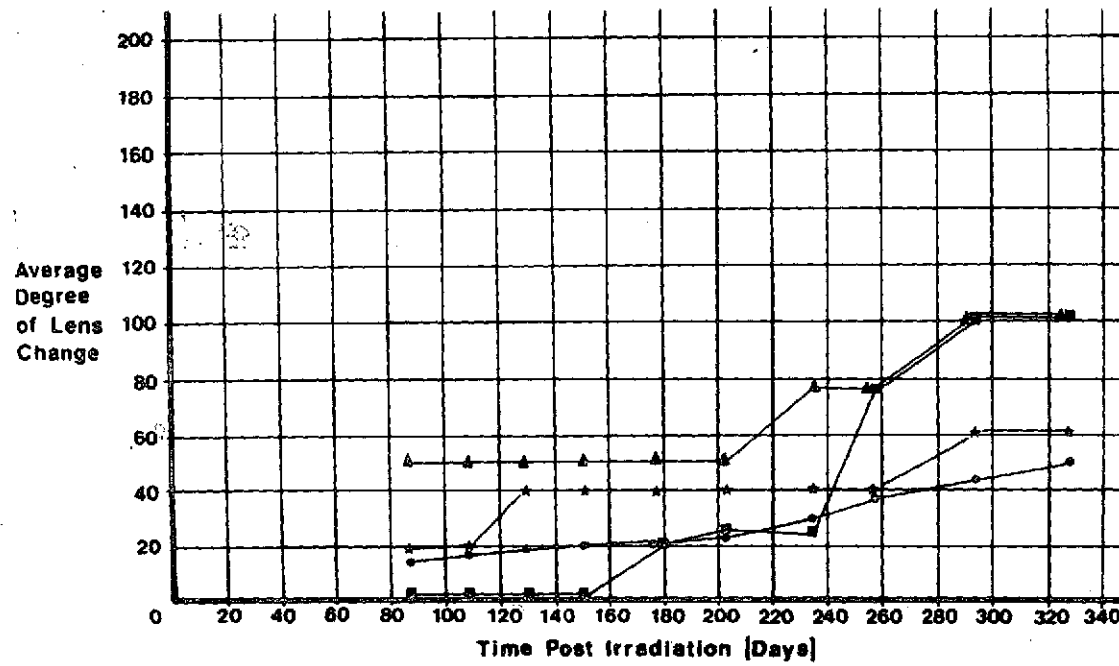


Figure 13

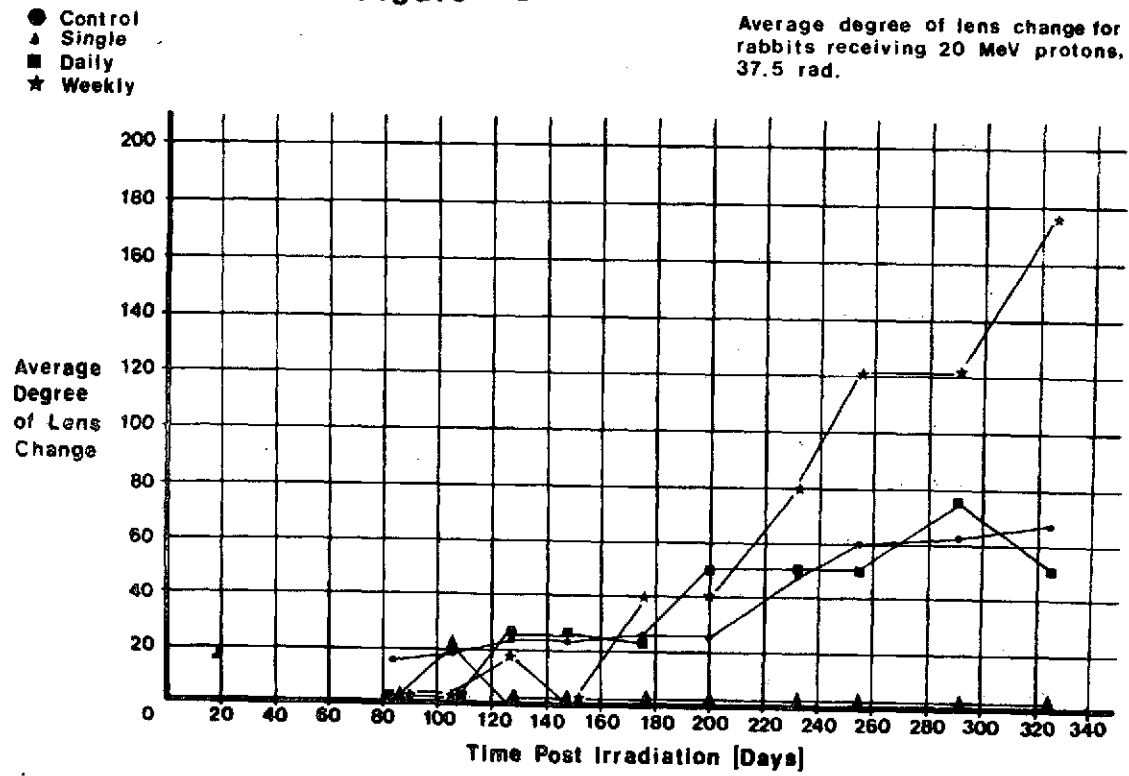


Figure 14

● Control
▲ Single
■ Daily
★ Weekly

Average degree of lens change for rabbits receiving 20 MeV protons, 75 rad.

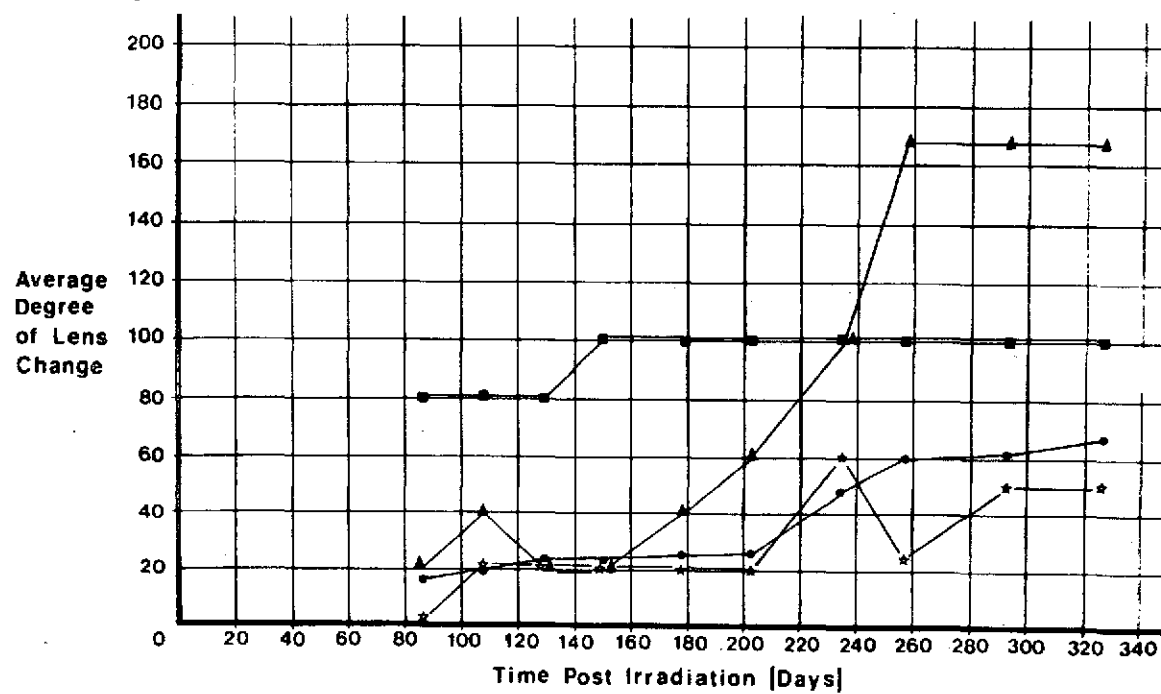


Figure 15

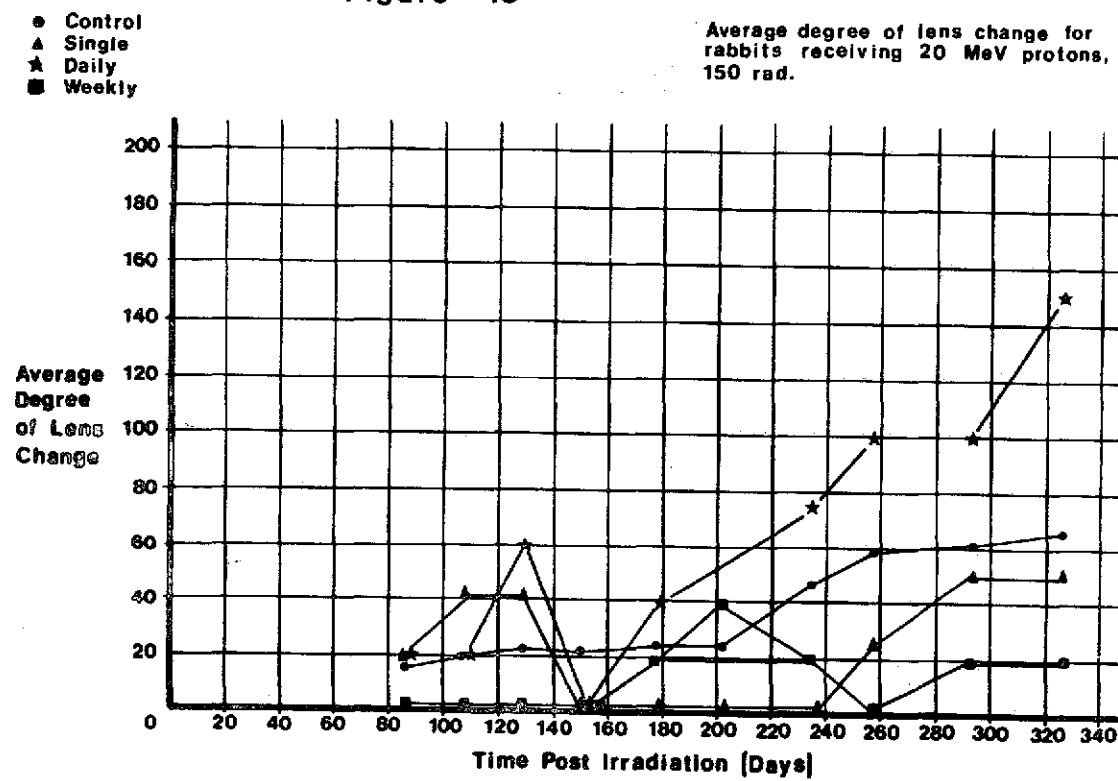


Figure 16

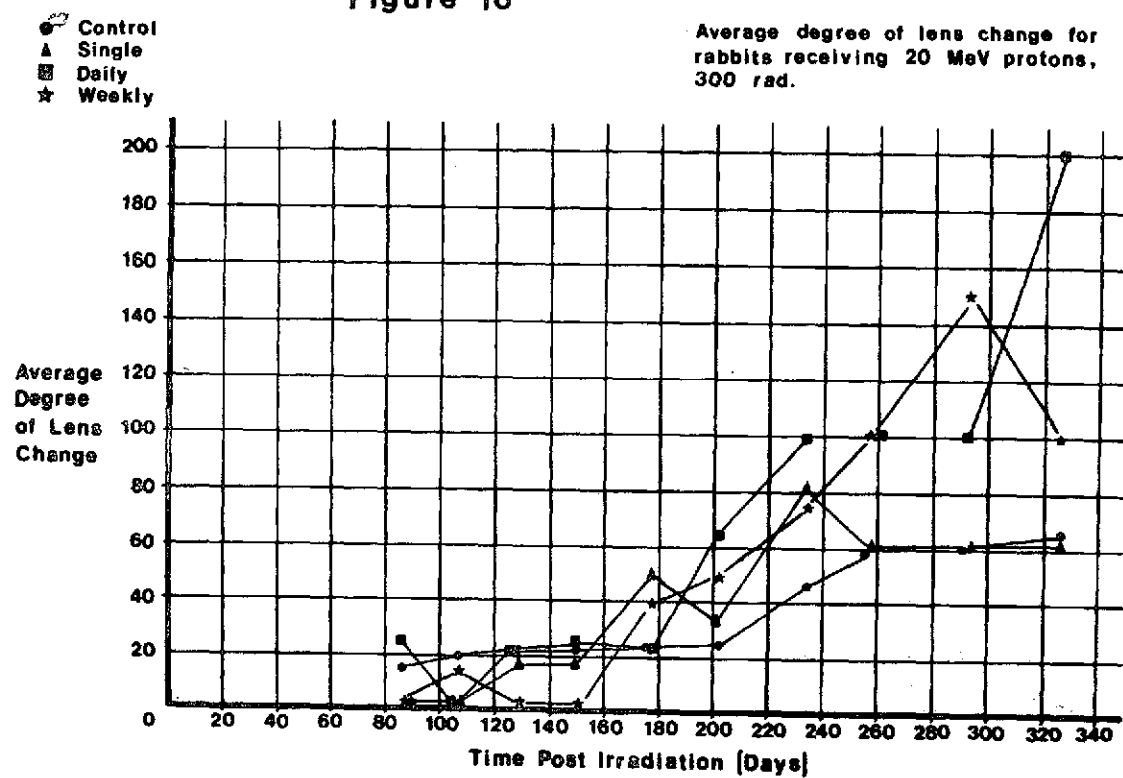


Figure 17

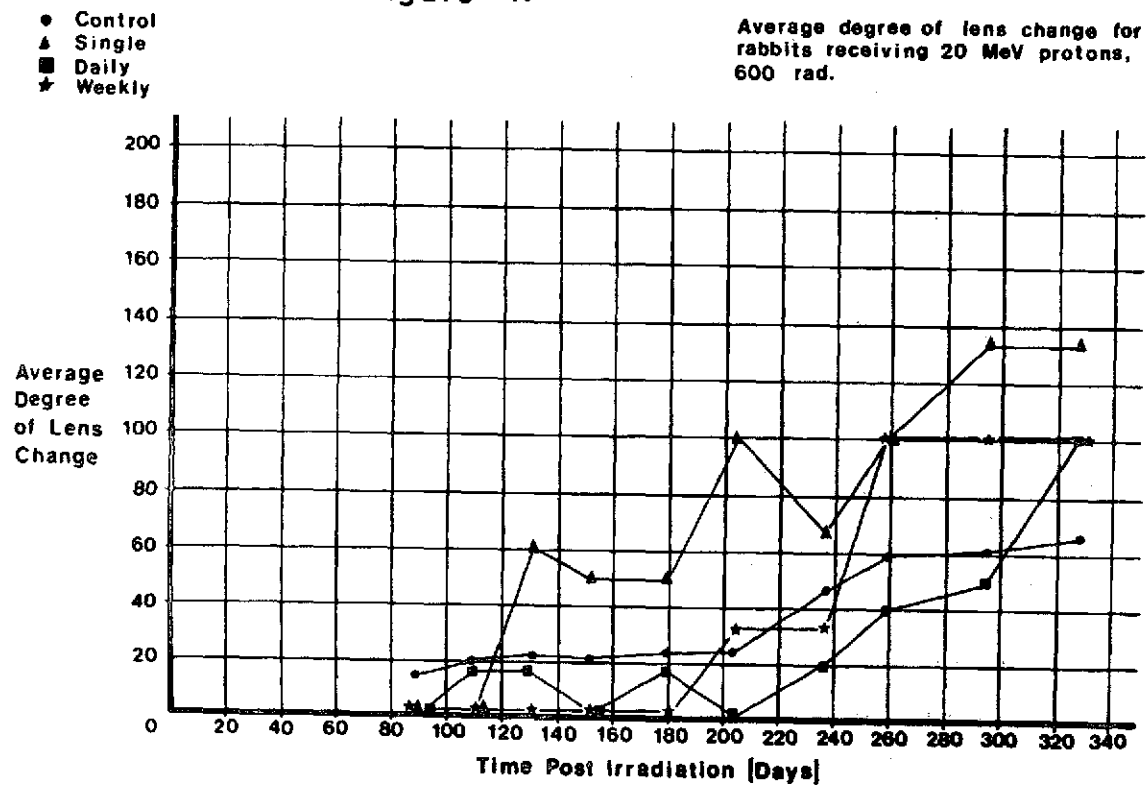


Figure 18

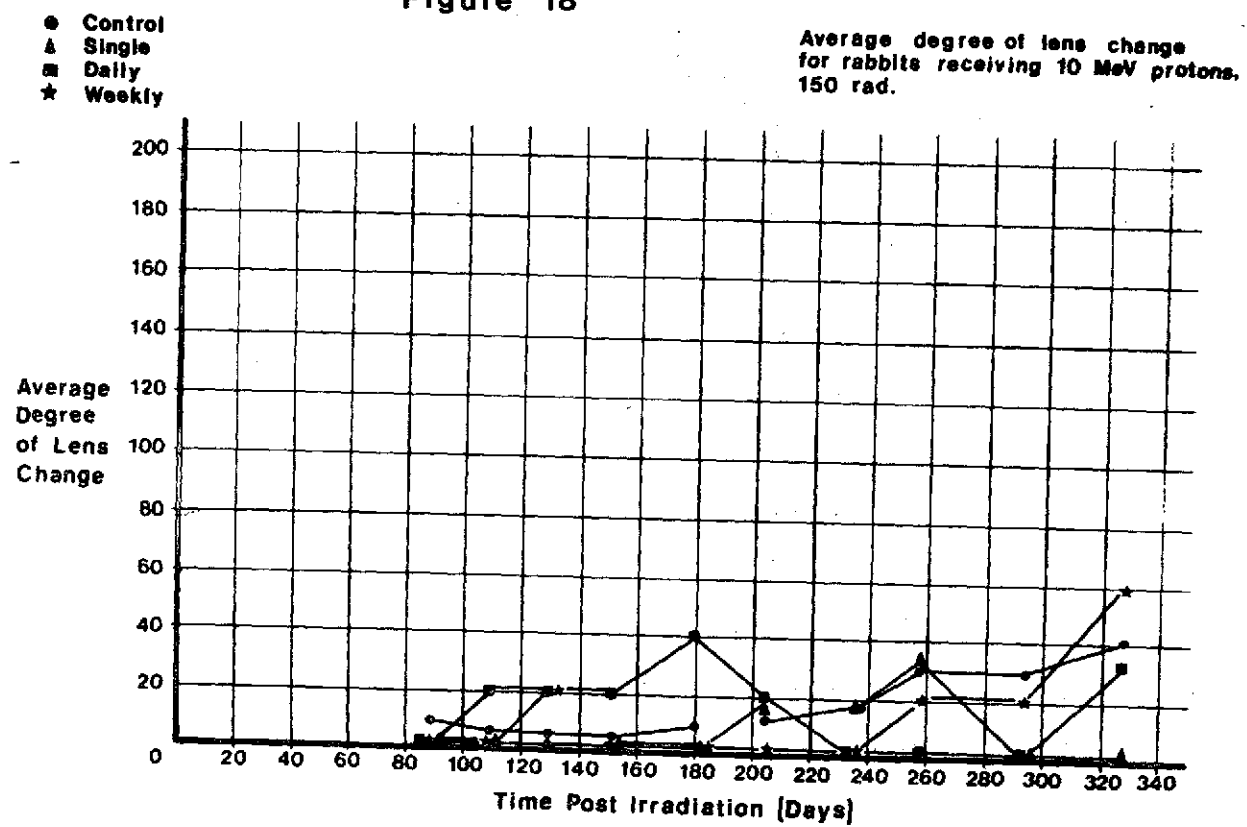


Figure 19

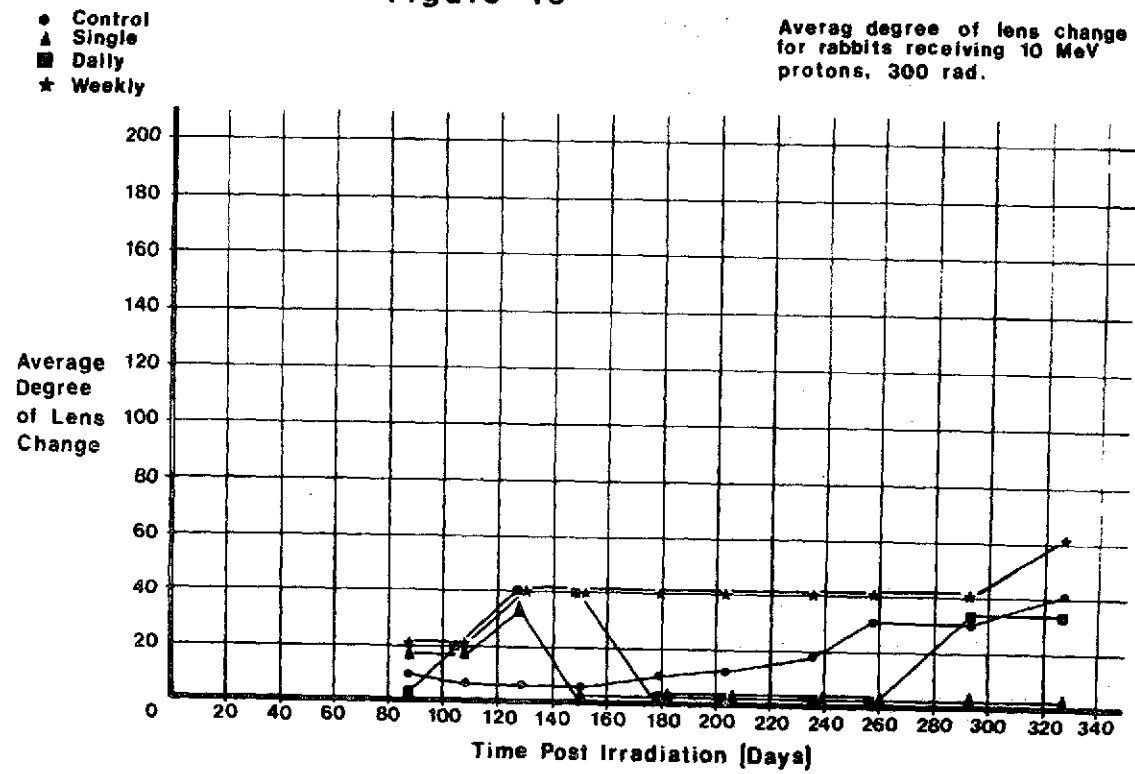


Figure 20

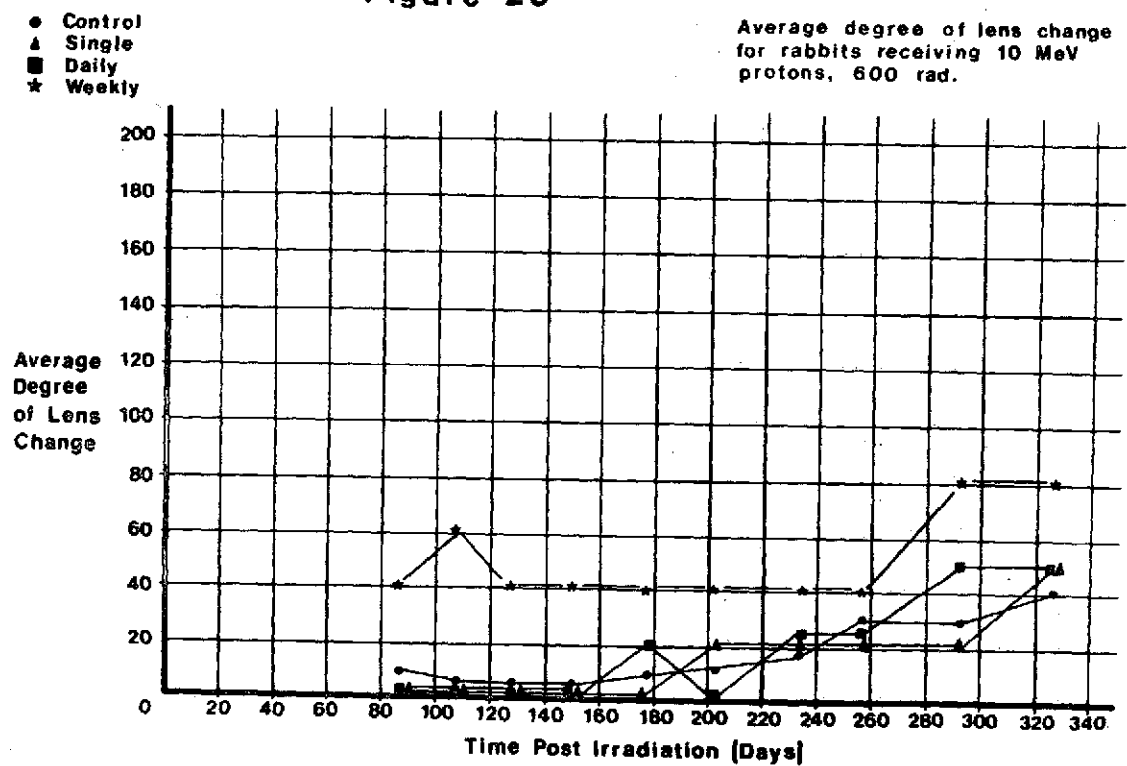


Figure 21

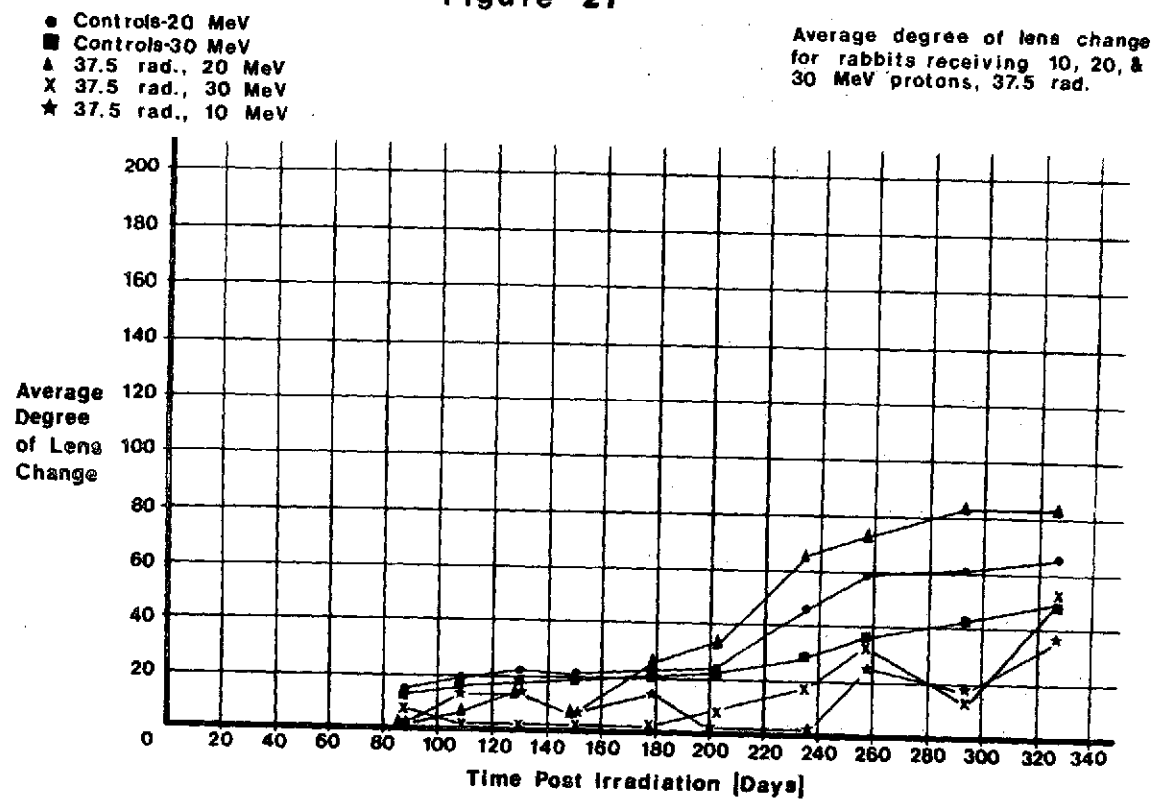


Figure 22

- Controls-20 MeV
- ▲ Controls-30 MeV
- 75 rad., 20 MeV
- X 75 rad., 30 MeV
- ★ 75 rad., 10 MeV

Average degree of lens change
for rabbits receiving 10, 20, &
30 MeV protons, 75 rad.

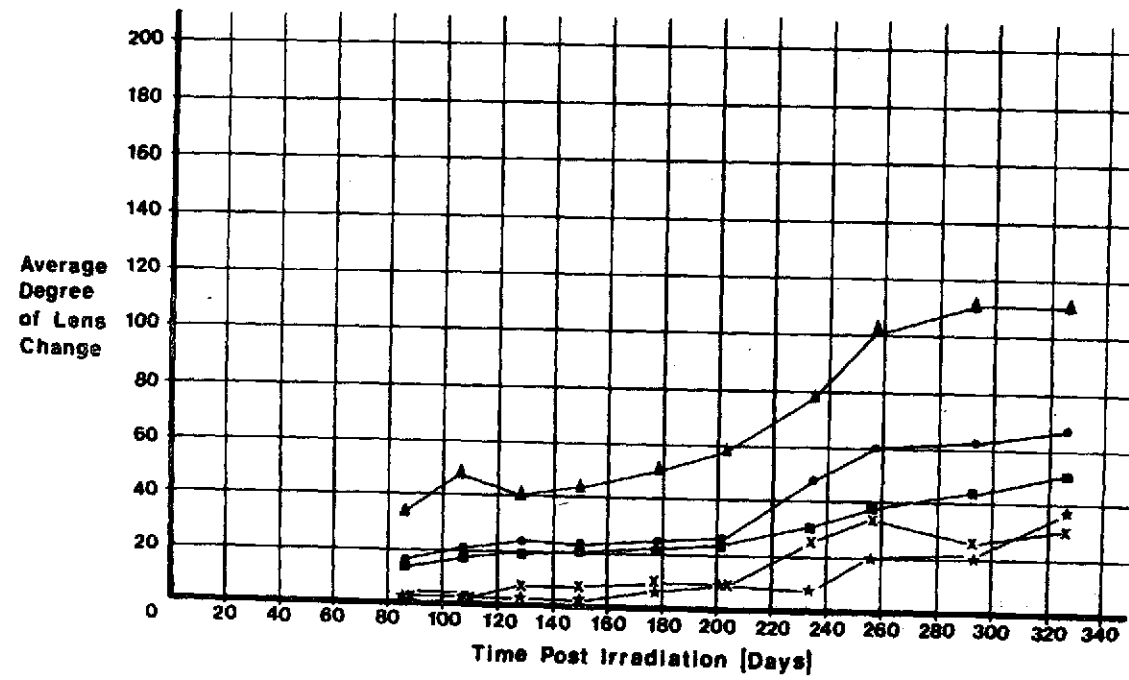


Figure 23

● Controls-20 MeV
 ■ Controls-30 MeV
 ▲ 150 rad., 20 MeV
 X 150 rad., 30 MeV
 ☆ 150 rad., 10 MeV

Average degree of lens change
 for rabbits receiving 10, 20, &
 30 MeV protons, 150 rad.

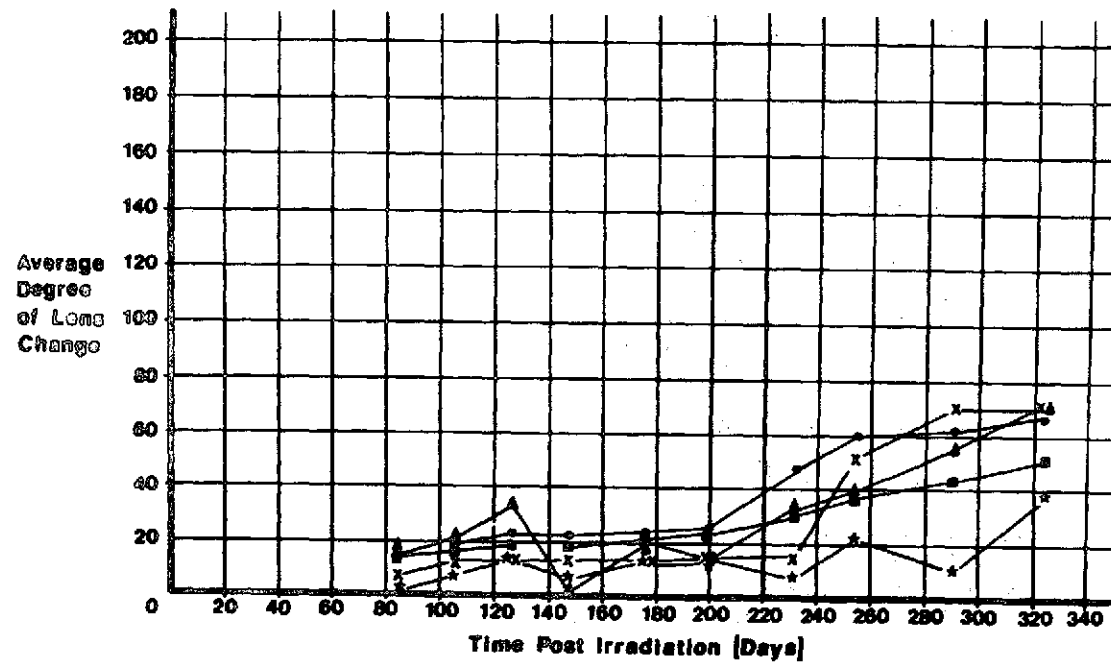


Figure 24

● Controls-20 MeV
 ■ Controls-30 MeV
 ▲ 300 rad., 20 MeV
 X 300 rad., 30 MeV
 ☆ 300 rad., 10 MeV

Average degree of lens change
 for rabbits receiving 10, 20, &
 30 MeV protons, 300 rad.

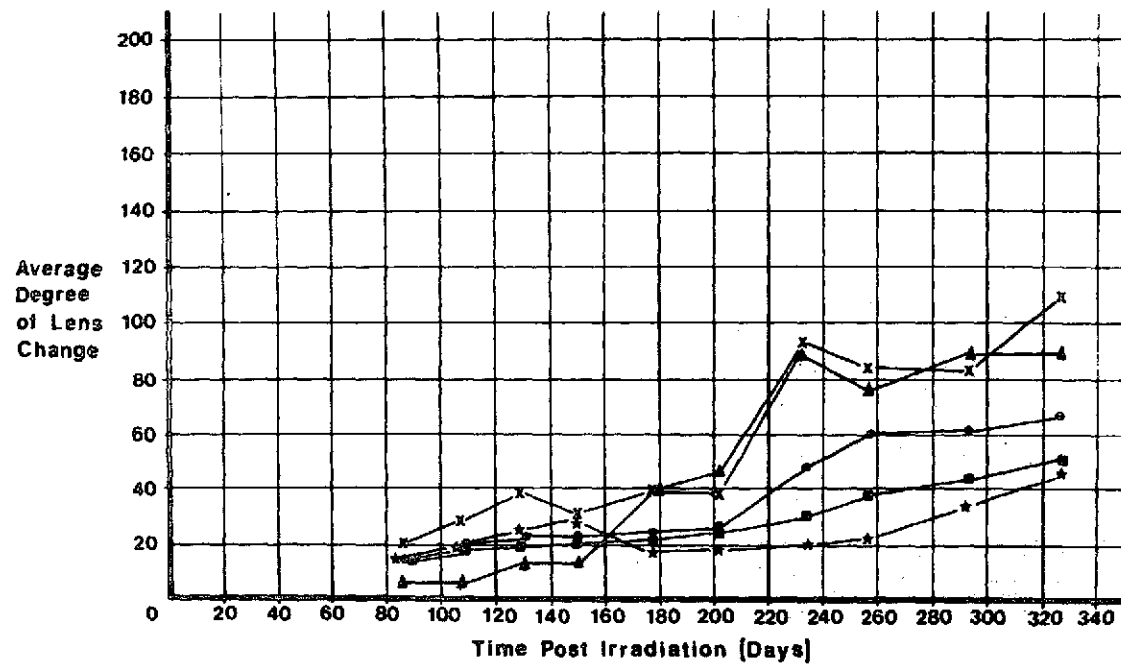
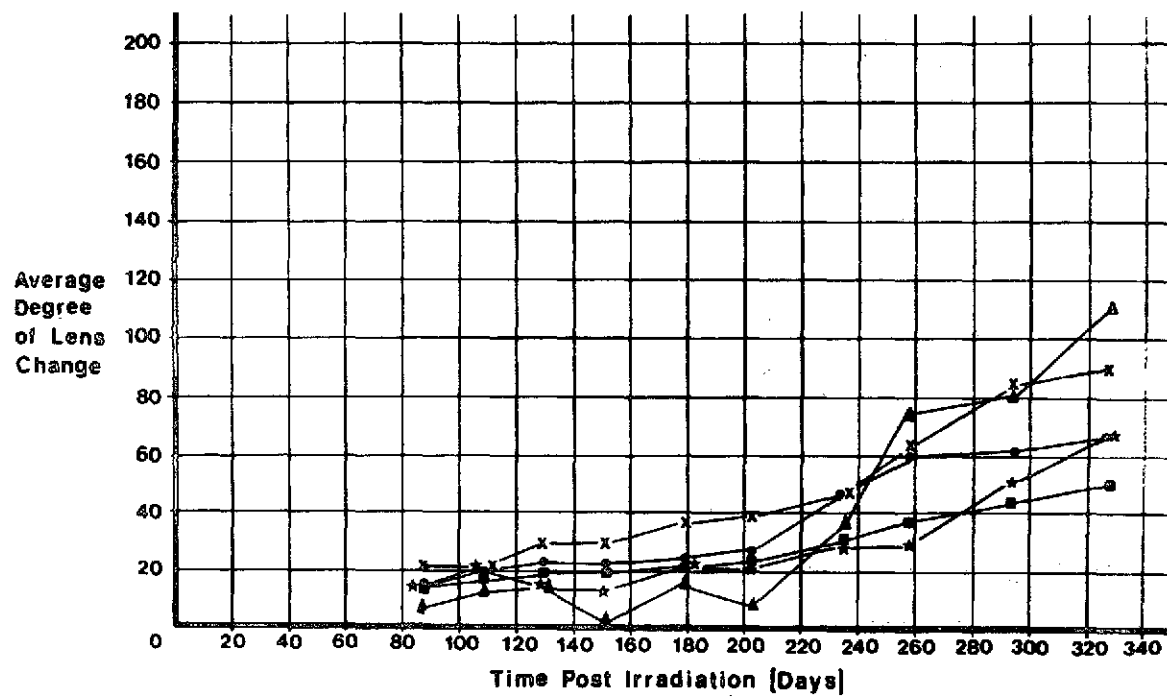


Figure 25

- Controls-20 MeV
- Controls-30 MeV
- ▲ 600 rad., 20 MeV
- X 600 rad., 30 MeV
- ★ 600 rad., 10 MeV

Average degree of lens change
for rabbits receiving 10, 20,
& 30 MeV, 600 rad.



energy and each dose. These graphs more or less summarize the data in all graphs previously presented.

While this initial data would not withstand statistical analysis, it was considered that it did provide some definite information regarding the ocular effects of proton irradiation.

First, it was felt that the data indicated no effect from 10 MeV protons, and that the effects from 20 MeV protons were greater in the rabbit than 30 MeV. This was readily explained in the rabbit. The Bragg peak occurred at the following approximate depths in the eye:

10 MeV - 0.76 mm

20 MeV - 3.5 mm

30 MeV - 7.6 mm

These depths indicated that the Bragg peak, or peak ionization, occurred respectively in the anterior chamber, lens, and vitreous humor of the rabbit eye. Thus, a greater effect at 20 MeV would be expected.

Second, it was more difficult from the data to determine an absolute difference in the effects of the different exposure regimes. Even so, it was felt the data suggested a greater effect when the irradiations were protracted. It was also felt that weekly exposures may have been more effective than daily, particularly at the lower doses.

Third, there was little doubt that the data suggested a greater effect at the higher doses used.

Lastly, the data suggested that a latent period was observed. While the relationship between dose and latent period could not be determined, it was believed that the latent period at the higher doses was between 150 and 200 days.

The above data provided the information required to proceed with the study.

Figures 26 thru 29 illustrate data obtained in subsequent rabbit exposures.

Figure 26 exhibits data obtained from rabbits exposed to a single acute irradiation of 20 MeV protons in total doses ranging from 37.5 rad to 1200.0 rad. Every dosage subdivision within this group exhibited lens abnormalities greater than control throughout the post exposure period of study. This difference became less with increasing time post exposure presumably because of an increasing degree of lens abnormalities in control eyes due to normal aging processes. A dose dependent response was not noted.

Figures 27, 28 and 29 illustrate data obtained from rabbits exposed to 30 MeV protons in a single irradiation, five daily fractions and five weekly fractions respectively. All three groups showed a greater degree of lens abnormalities in exposed eyes than in control eyes. Again, this difference became less with advancing age in the animals. There was no really significant difference in overall degree of lens changes between the single and fractionated exposure groups. Also no really apparent

Figure 26

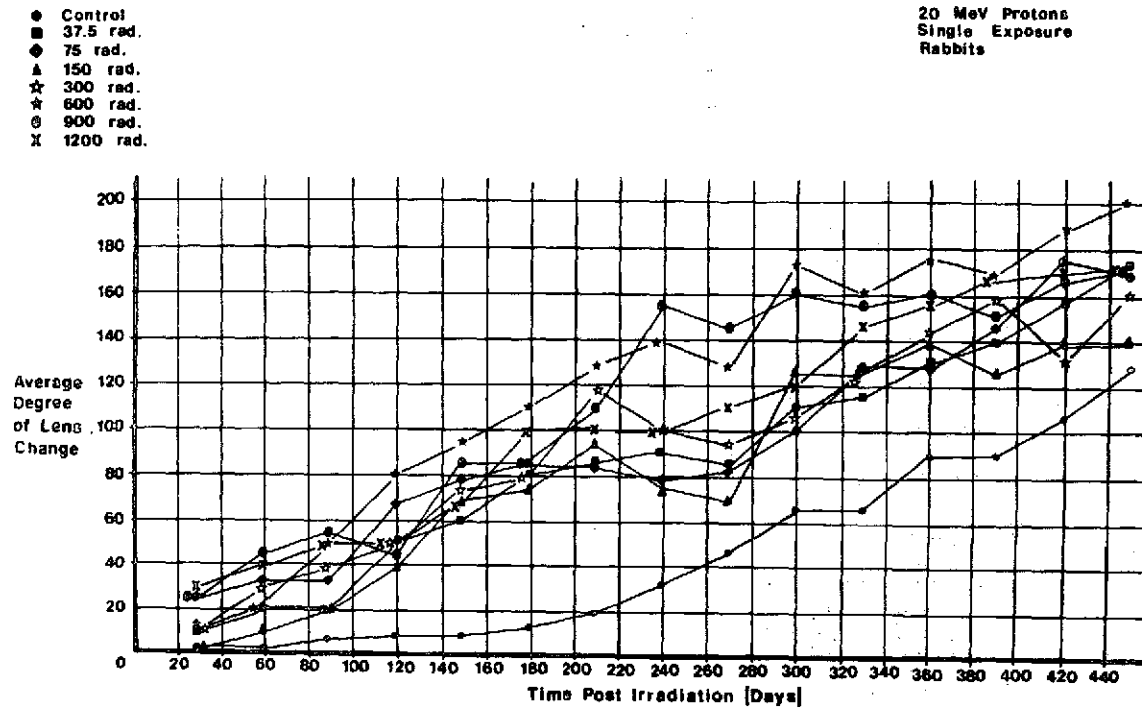


Figure 27

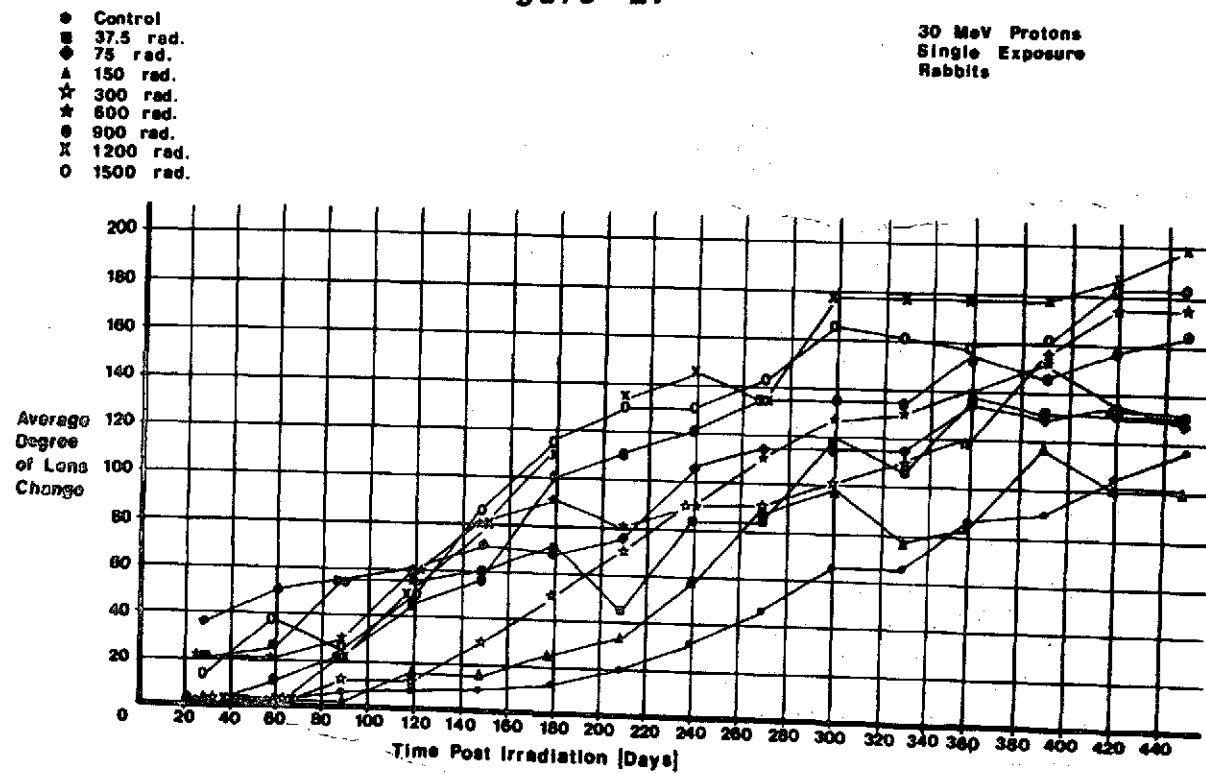


Figure 28

● Control
 ■ 37.5 rad.
 ◆ 75 rad.
 ▲ 150 rad.
 ☆ 300 rad.
 ★ 600 rad.
 ○ 900 rad.
 x 1200 rad.

30 MeV Protons
 5 Daily Exposures
 Rabbits

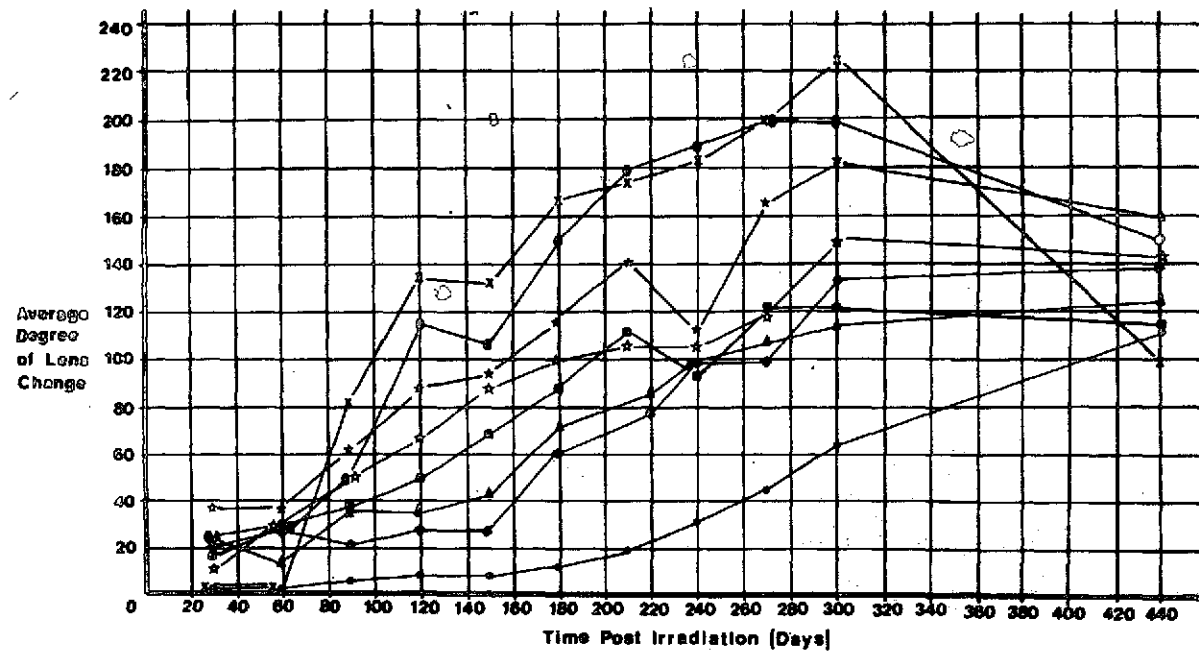
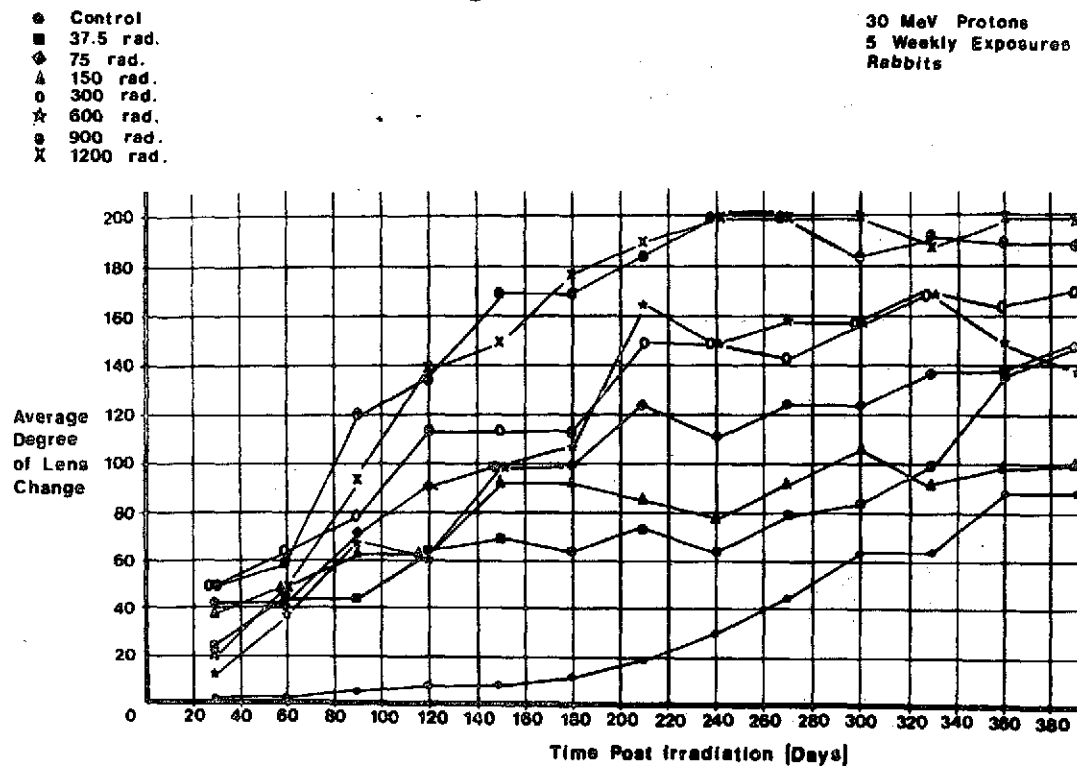


Figure 29



dose dependent response was noted except at the higher total doses received (600.0 to 1500.0 rad) in which the trend of higher dose, greater response was suggested.

Figures 30 thru 33 illustrate ocular data obtained from exposed dogs.

Figure 30 summarizes dogs receiving a single acute exposure to 30 MeV protons in total doses ranging from 62.5 rad to 1000.0 rad. Over the period of study, degree of lens change in the radiates was not significantly greater than that in the control animals.

Figure 31 summarizes data obtained from dogs receiving exposures to 30 MeV proton divided into five equal weekly fractions and total doses ranging from 62.5 rad to 1000.0 rad. Only the radiates in the highest total dose subdivision (1000.0 rad) exhibited lens abnormalities significantly greater than control. This trend began at approximately 600 days post exposure and continued until termination at 1350 days.

Figure 32 exhibits data obtained from dogs receiving a single exposure to 40 MeV protons. Two total dose subdivisions are included, 125.0 rad and 1000.0 rad. Throughout the examination period the 1000.0 rad subdivisions showed a slightly greater incidence of lens abnormalities than control. This greater incidence was of so little magnitude that it might be considered insignificant. With only two exceptions, the 125.0 rad subdivision exhibited less lens abnormalities than control.

Figure 30

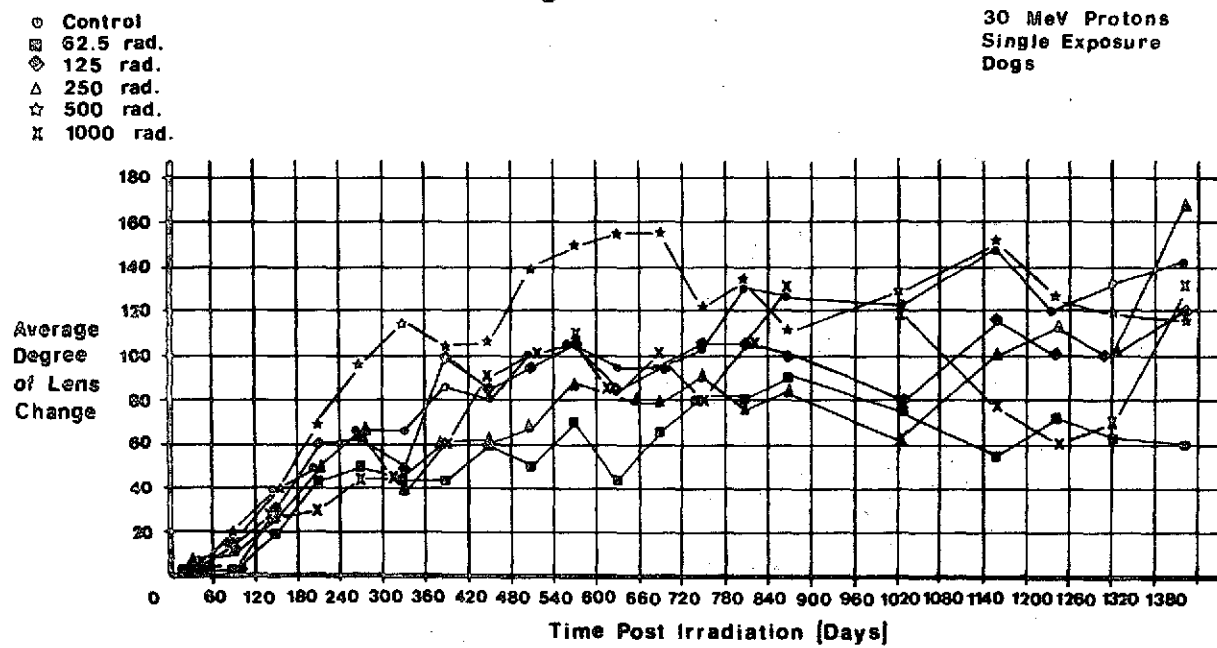


Figure 31

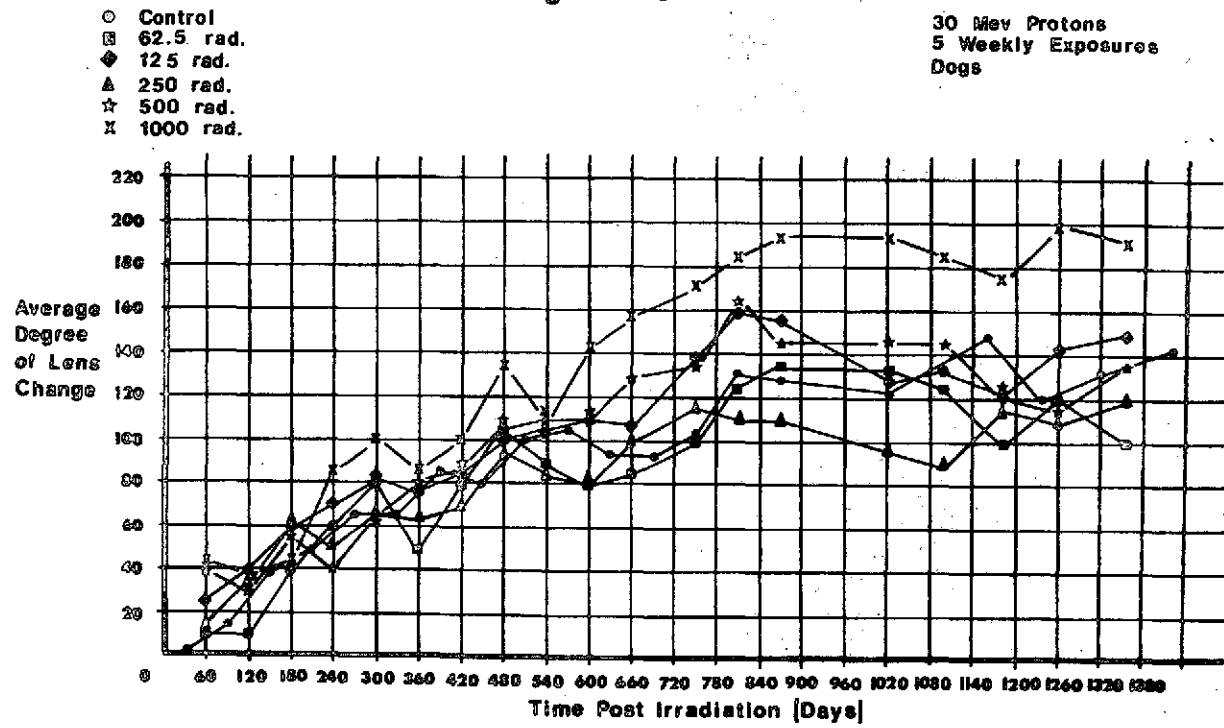


Figure 32

● Control
■ 125 rad.
x 1000 rad.

40 MeV Protons
Single Exposure
Dogs

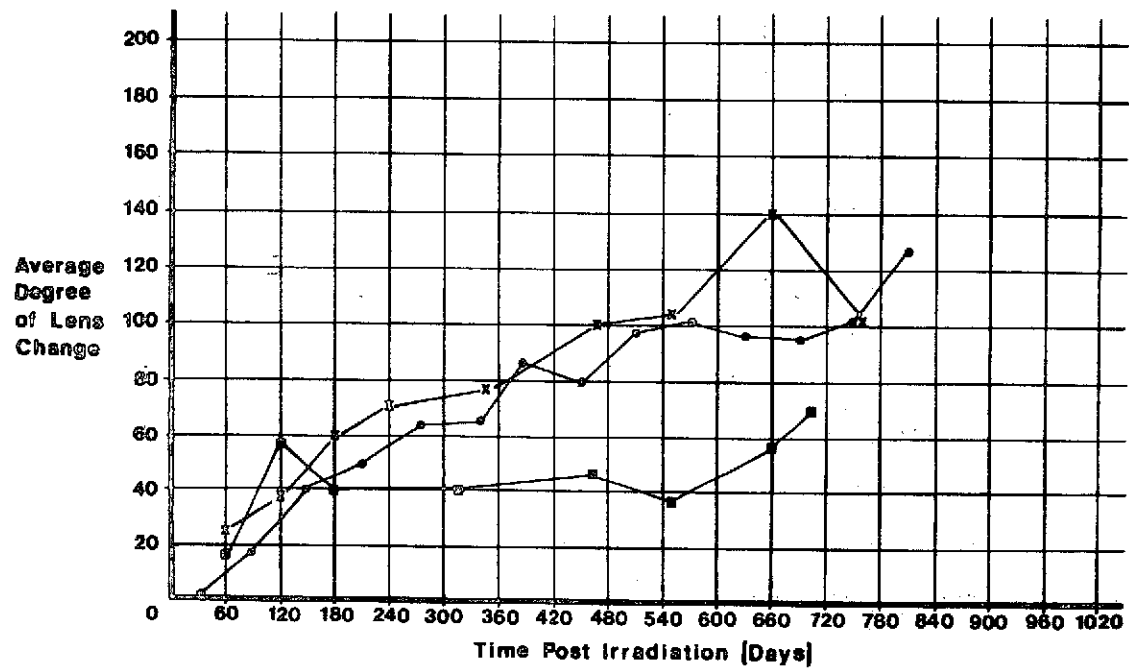


Figure 33 summarizes data from dogs receiving a single exposure to 50 MeV proton in total doses of 125.0 rad and 1000.0 rad. Lens abnormalities in the 1000.0 rad subdivision were significantly greater than control throughout the post exposure examination period. Those animals receiving 125.0 rad did not exhibit ocular changes significantly greater than control.

Throughout the entire study, no animal, rabbit or dog, ever exhibited a fully developed cataract resulting in blindness. Most lens abnormalities progressed no further than a two-plus scoring grade in severity (easily detectable, but not sight impairing) with only a minimal of three-plus opacities (sight impairing but not blind).

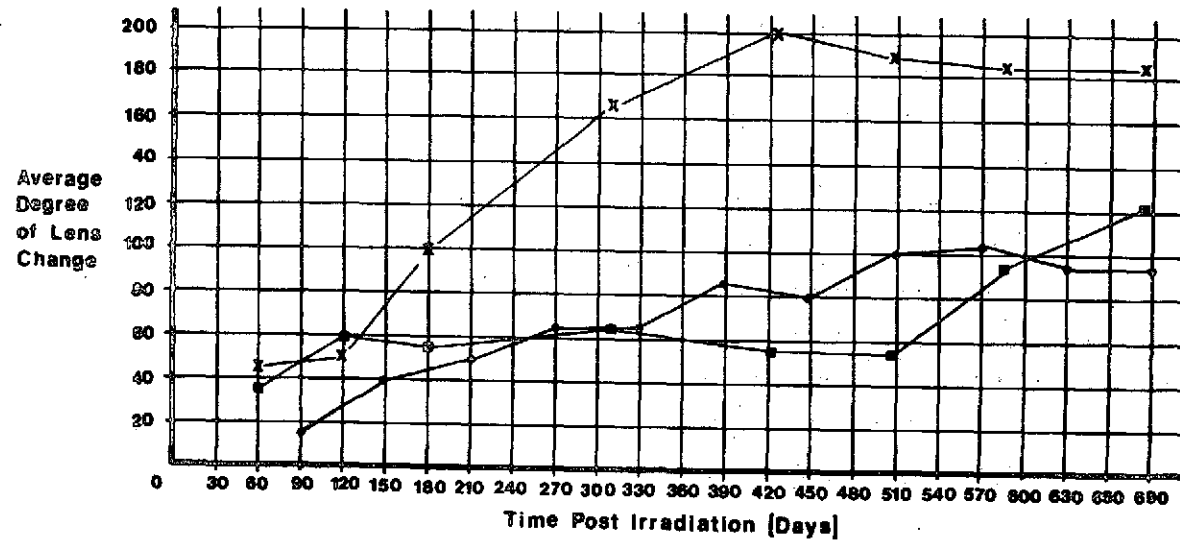
An accidental finding of some interest did occur during the course of investigation. Incident to a proposed study unrelated to this project electroencephalograms (EEG's) were performed on a small number of dogs receiving proton radiation to the eyes. Unexpectedly these animals revealed abnormal EEG wave forms. With this finding, EEG's were performed on dogs from each dosage subdivision, each proton energy group, and each radiation regime. Results were read by two qualified examiners, one of which read them blind.

Certain of the dogs exhibited High Voltage, Slow wave Activity (HVSA) patterns in the EEG which is interpreted to indicate neuronal necrosis and is indicative of abnormal function. The abnormal EEG changes appeared to be radiation dose and energy

Figure 33

○ Control
 □ 125 rad.
 X 1000 rad.

50 MeV Protons
 Single Exposure
 Dogs



related. It was not known whether the observed changes in EEG patterns were regressing or progressing. An attempt to further evaluate these findings was then undertaken.

Twenty additional adult Beagle dogs were added to the study. Ten had their eyes irradiated with 50 MeV protons to a dosage of 1000 rad. Pre-irradiation EEG's in all test animals were interpreted as normal immature patterns as evidenced by mild to moderate High Voltage, Slow Activity (HVSA) in all leads. EEG's performed at 2 weeks and 2, 5, 7 and 10 months post-irradiation revealed no abnormalities. The only change seen in the tracings was a gradual reduction in voltage and concomitant increase in Hertz. Figures 34 thru 39 illustrate this change in one of the irradiated dogs. This is the normal expected change as the EEG matures with age of the animal. A normal mature canine EEG is shown in Figure 40 for comparison.

Control dogs exhibited the same EEG patterns as irradiated dogs and all were considered normal. Figures 41 thru 46 illustrate the EEG changes seen in one of the control dogs.

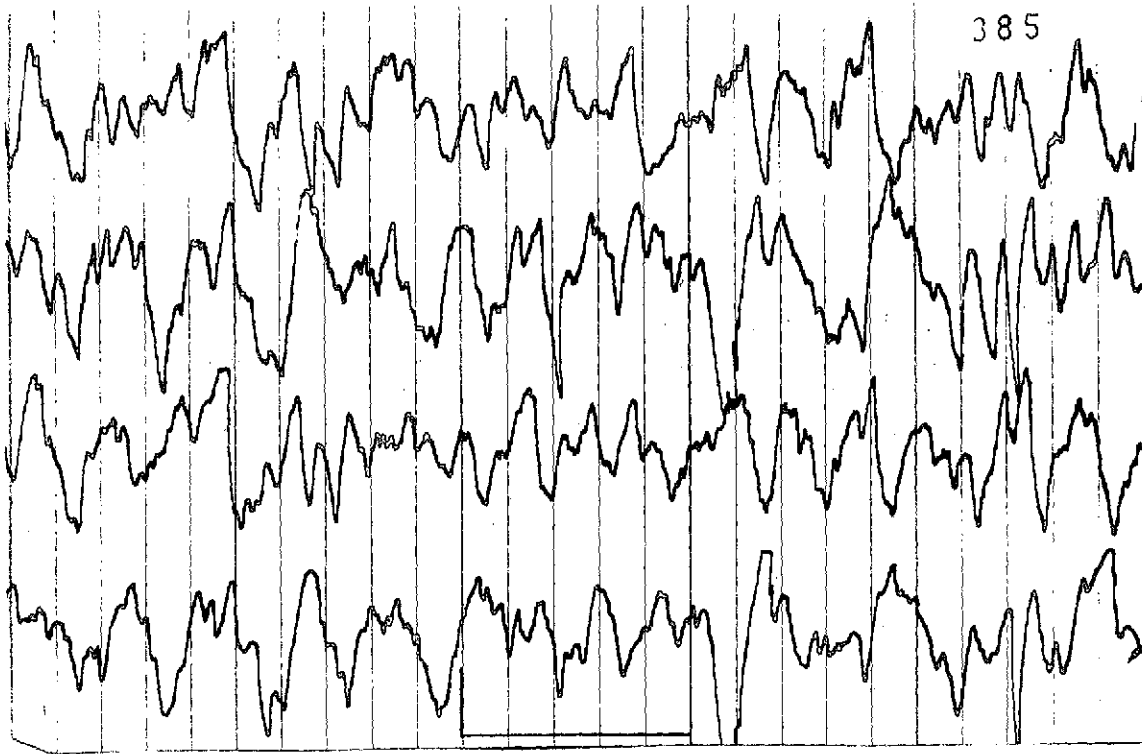


Figure 34 - Pre-irradiation screening EEG (Dog #HHEAS2) under pentothal anesthesia characterized by moderate High Voltage Slow Activity (HVSA) and interpreted as a normal immature pattern. Calibration marks in this and all subsequent figures: 20 μ v and 1 second.

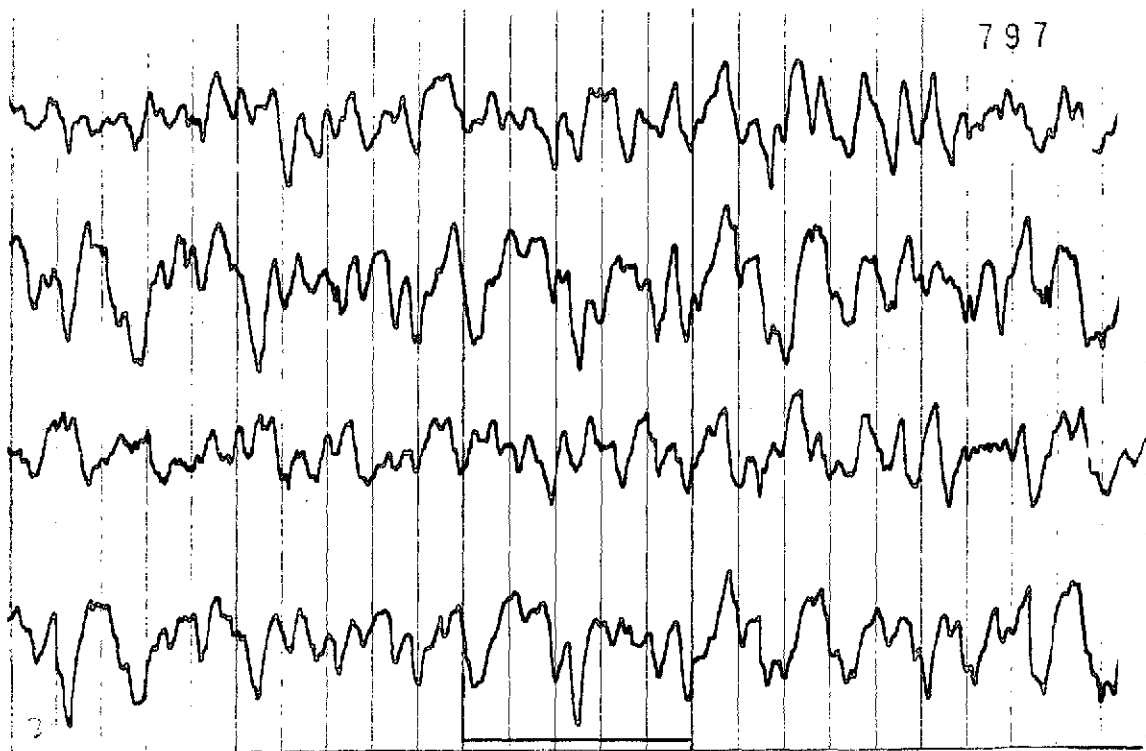


Figure 35 - EEG recording two weeks post-irradiation (Dog #HHEAS2)

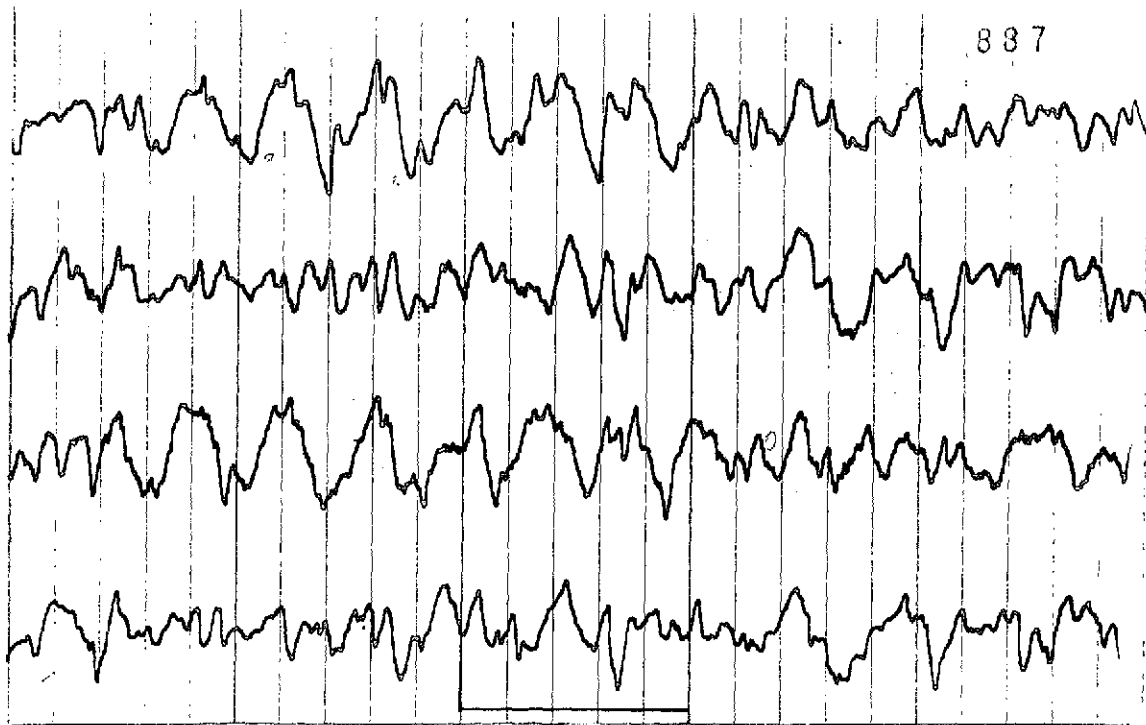


Figure 36 - EEG recording two months post-irradiation (Dog #HHEAS2)

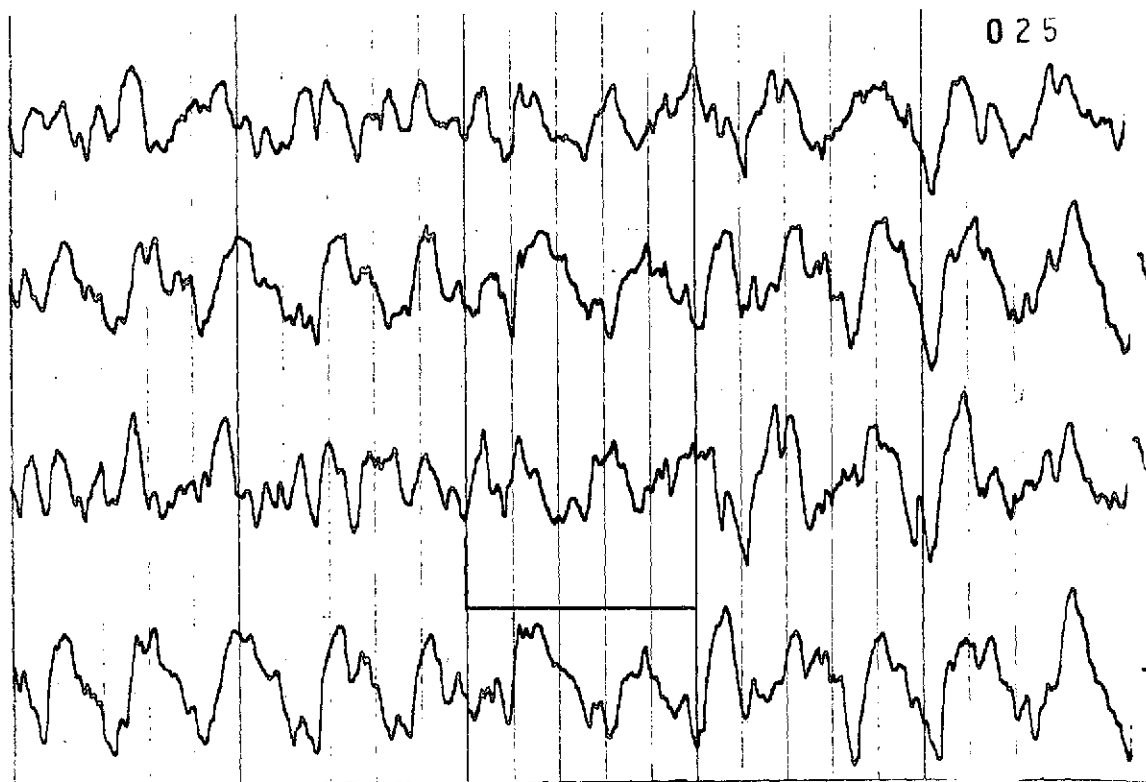


Figure 37 - EEG recording five months post-irradiation
(Dog #HHEAS2)

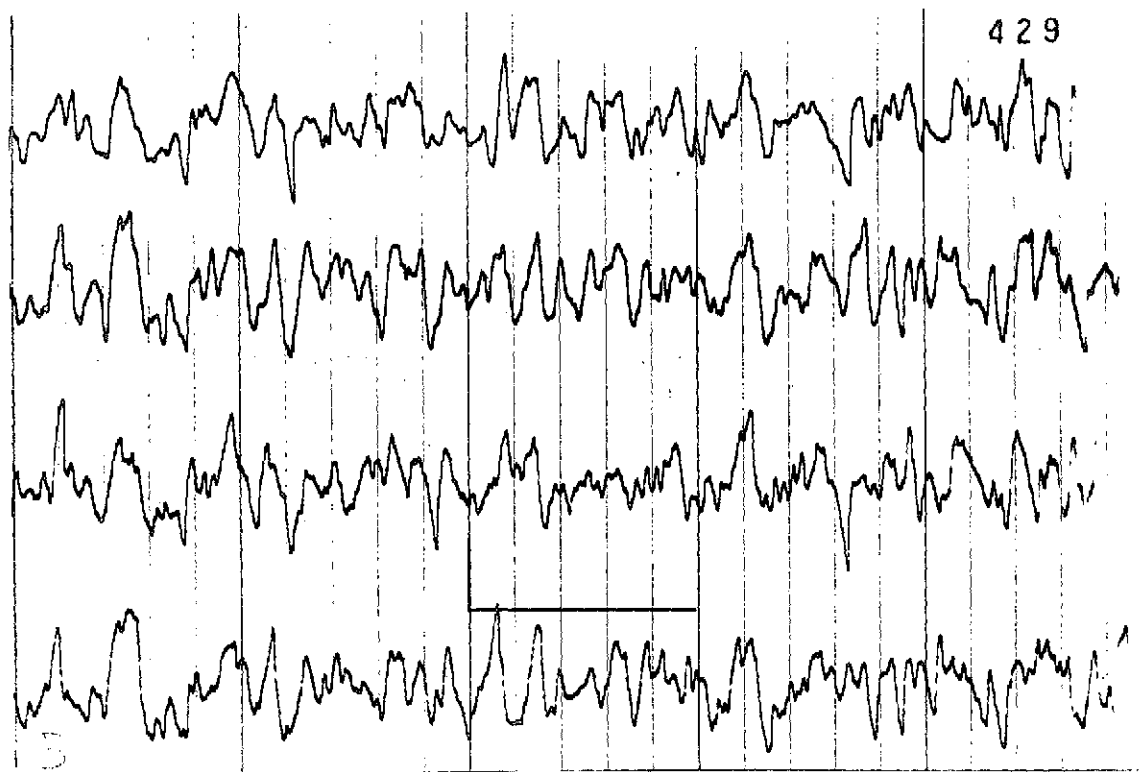


Figure 38 - EEG recording seven months post-irradiation
(Dog #HHEAS2)

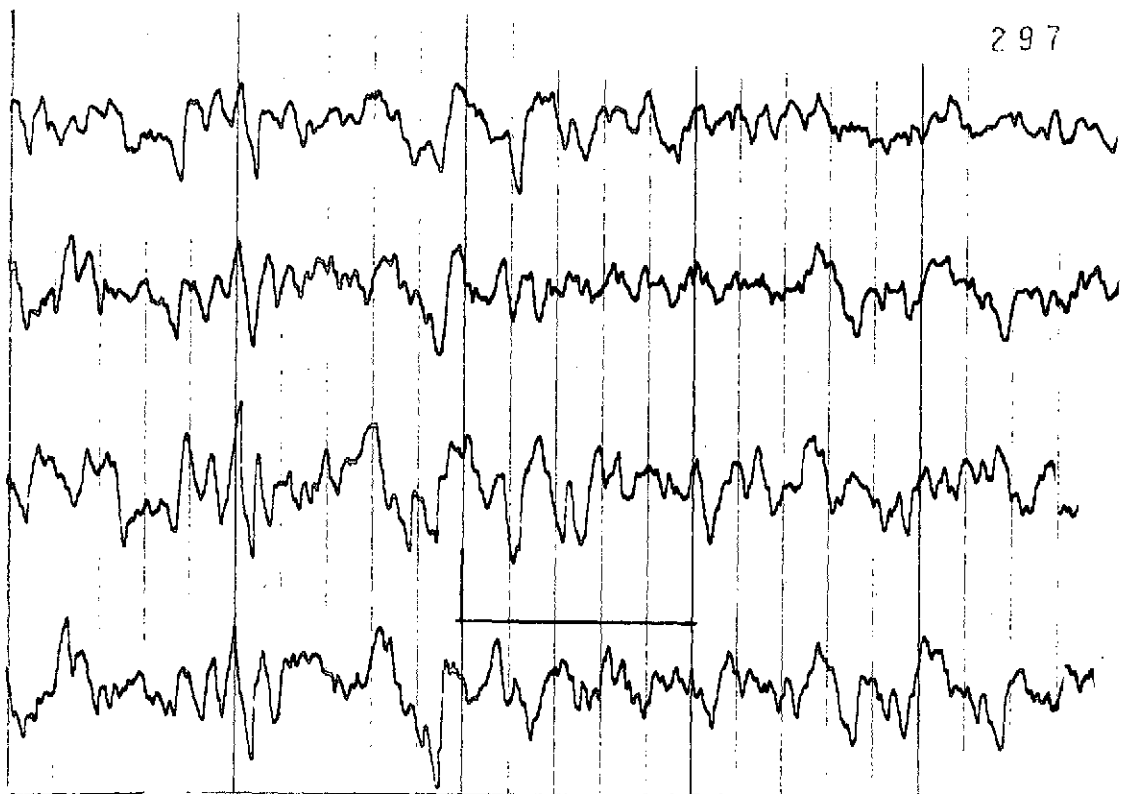


Figure 39 - EEG recording ten months post-irradiation (Dog #HHEAS2)



Figure 40 - Typical intrahemispheric bipolar mature EEG of a normal anesthetized dog.

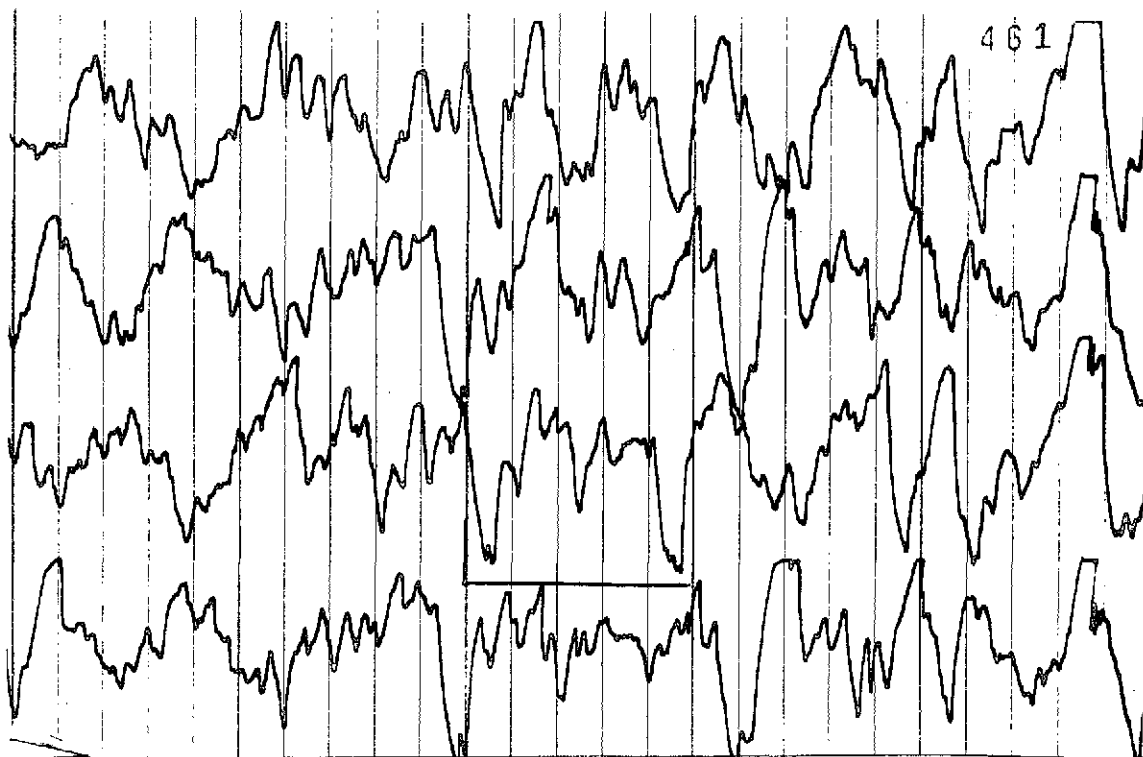


Figure 41 - Initial screening EEG on control dog (Dog #QIZSL6)

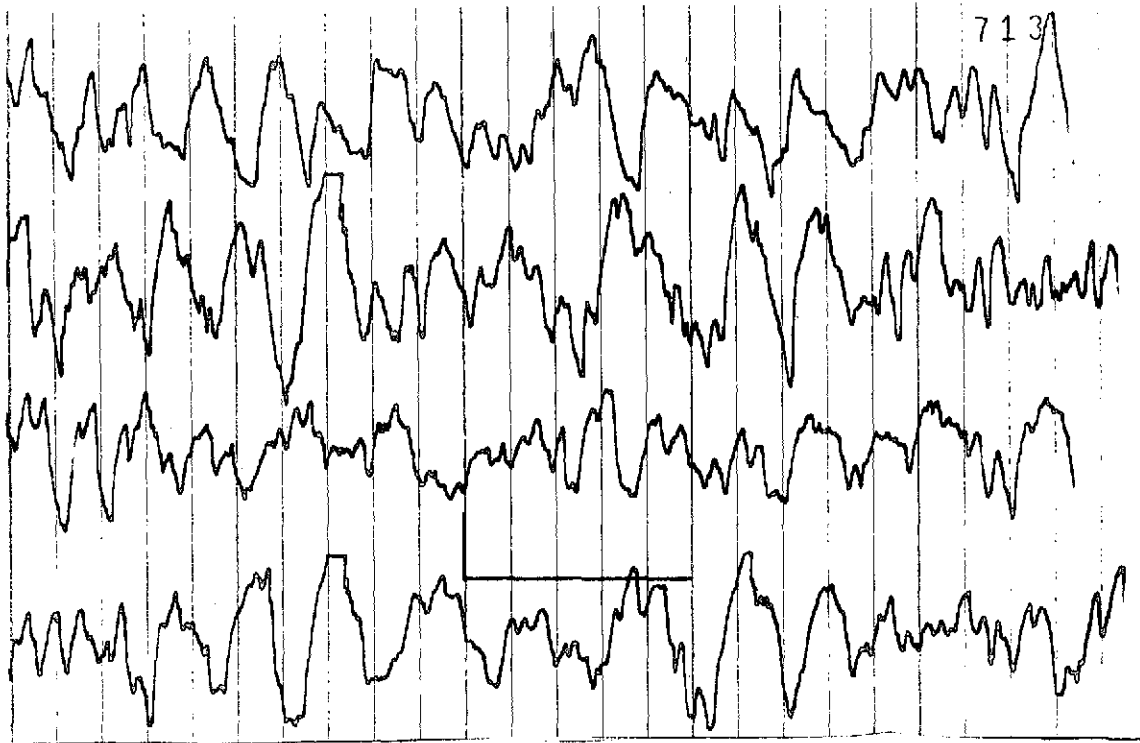


Figure 42 - EEG recording on control dog (Dog #QIZSL6) two weeks post-irradiation

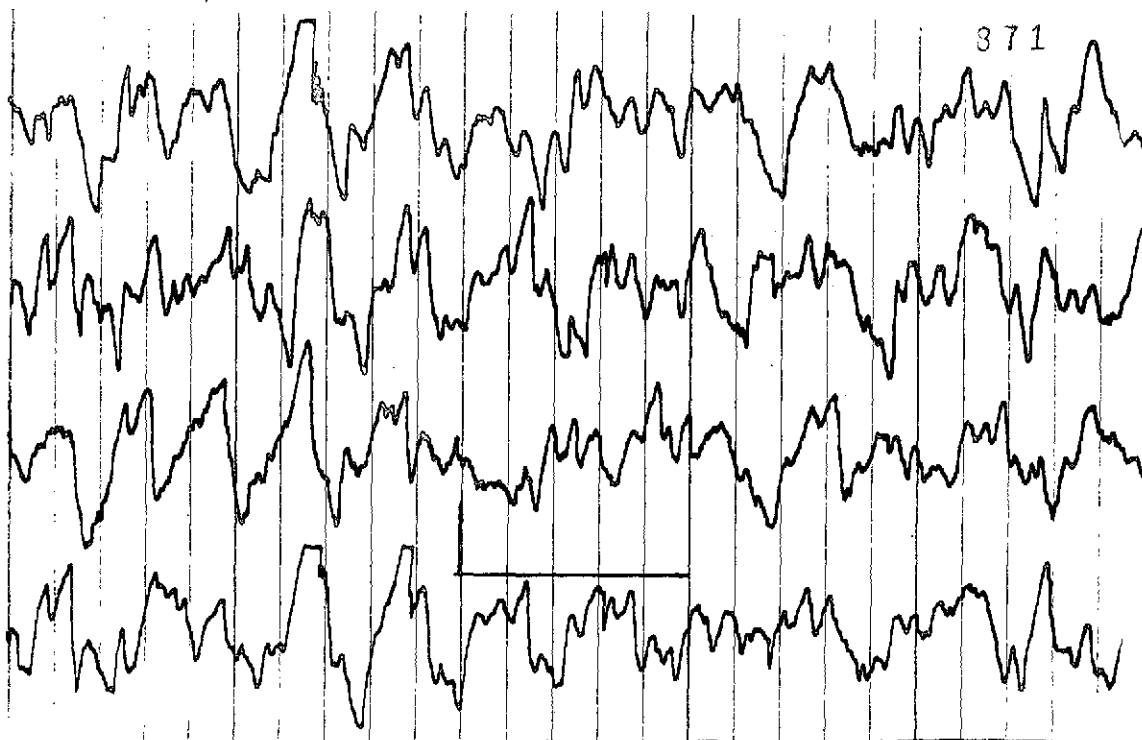


Figure 43 - EEG recording on control dog (Dog #QUIZSL6) two months post-irradiation

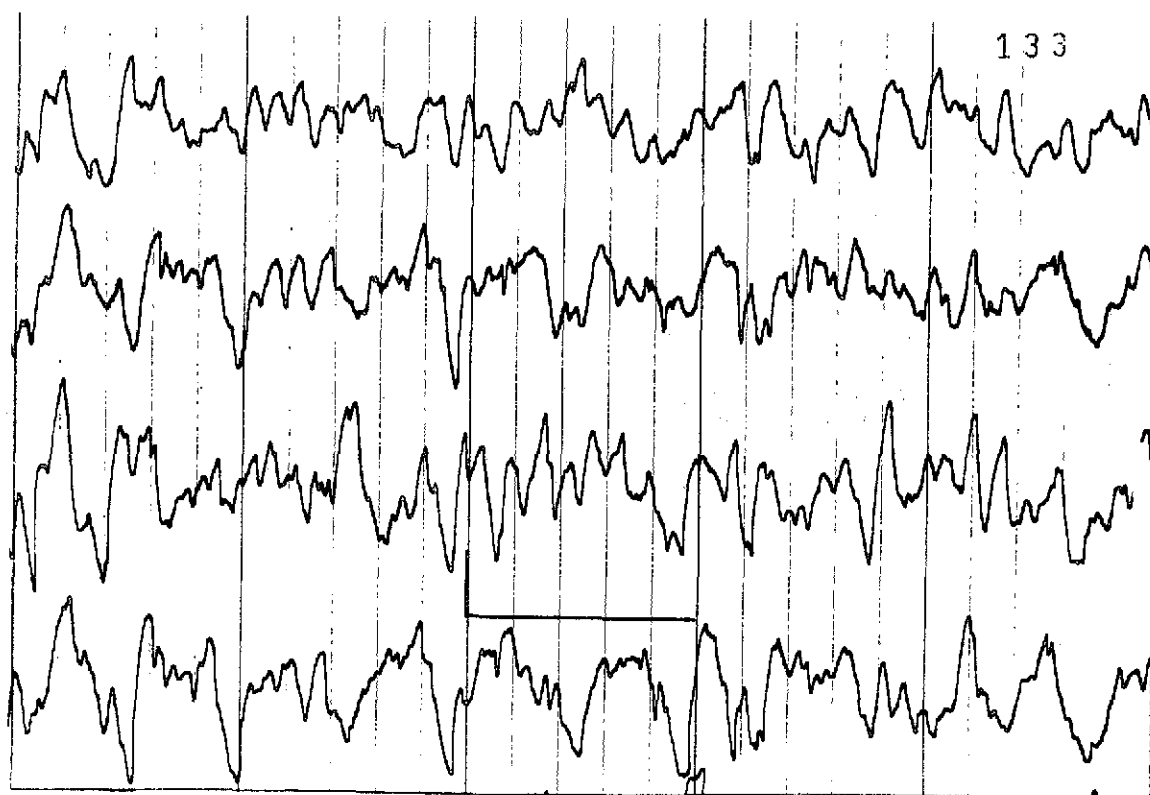


Figure 44 - EEG recording on control dog (Dog #QIZSL6) five months post-irradiation

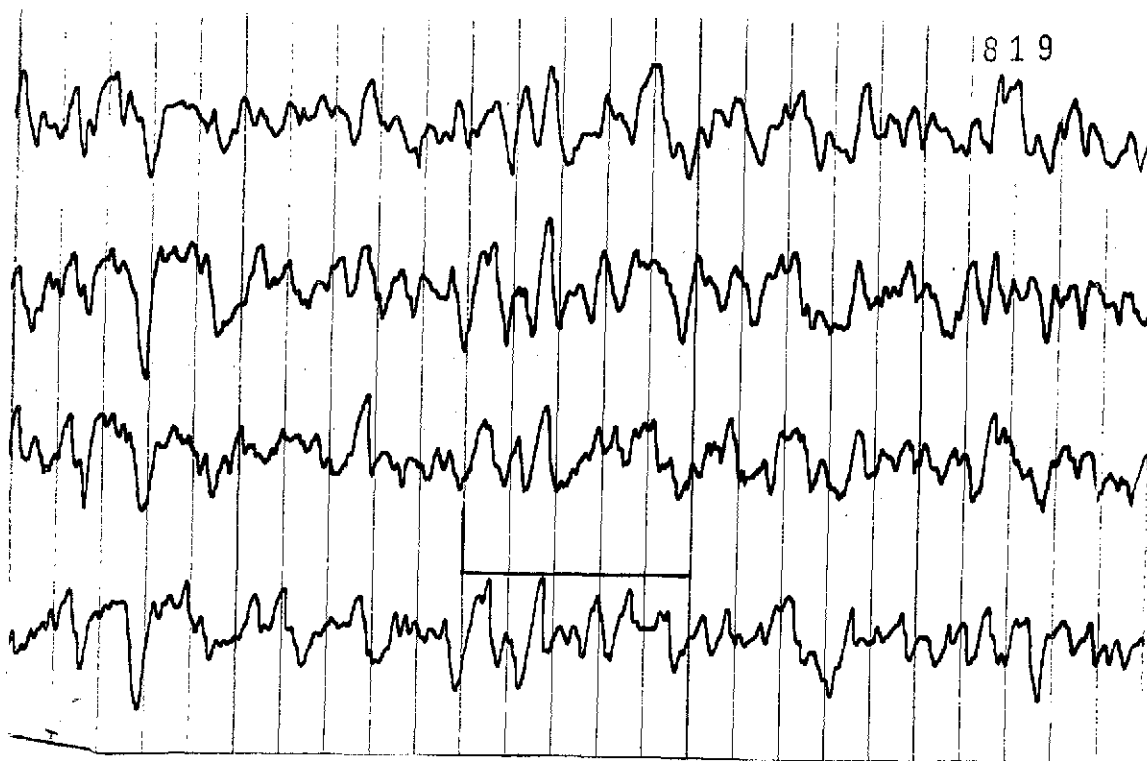


Figure 45 - EEG recording on control dog (Dog #QIZSL6) seven months post-irradiation

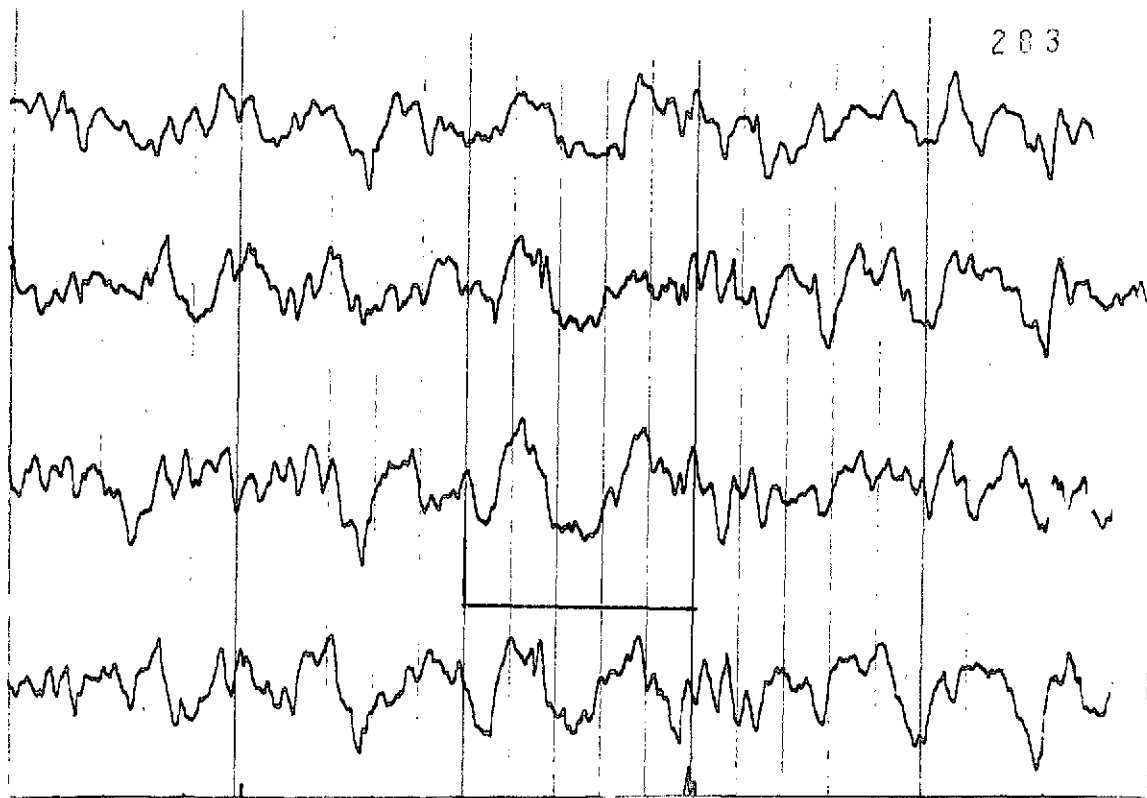


Figure 46 - EEG recording on control dog (Dog #QIZSL6) ten months post-irradiation

V. Conclusions

In summary then, we have measured the spectra, the energy versus depth and the LET versus depth for the proton energies used in the irradiations performed, 10, 20, 30, 40 and 50 MeV. From this data we must conclude that the doses which were quoted are probably accurate to about 5% based on the constants used. The secondary effects of absorption by hair, dose beyond the Bragg peak, beam spread with distance, beam uniformity, were all considered and either found to be insignificant or a method was found in which the effect was corrected for. One concern still remains and that is the quotation of dose. The requirement that the dose at the Bragg peak be the quoted dose and the dose in which all exposures were based, is a bit demanding in that it does require one to make a rather "microscopic" measurement and use it in a rather "macroscopic" way. As the dose varies rapidly in the peak area one can only assume that the dose measured in an infinitesimal thickness indeed exists over a mass as large as a gram. Within our ability to measure, which was 1/1000th of an inch of T.E. plastic, we obtained the curves. This is not to say that the curve did not go higher somewhere in between the area we were able to measure. The results we have quoted would be in error to the extent that the peak height was not properly represented by the experimental measurements made. At the higher energies it is obvious that there are some problems with scattering. On earlier dosimetry runs we had found severe scattering at 40

MeV and for this case the peak entrance ratio was but 2. By requiring the operator to focus the beam a bit more and being selective as to where the beam was defocused, the beam was cleaned up considerably and we were then able to get the data as indicated in the Figure III-22. With the 50 MeV beam, a very difficult beam to achieve with the TAMVEC cyclotron because it pushes the machine to one of its limits of capability, there is still some evidence of low energy proton scatter contaminating the beam proper. One can only say that the measured spectra and the dE/dx curve was that for the beam used to irradiate the animals in the experiment. Thus, while it may not be truly representative of a pure 50 MeV proton beam, it is representative of the proton beam used to irradiate the animals in the experiment.

As with the uncertain method of quoting "rad dose" with protons, one may also question the method of scoring lens abnormalities observed. The types of lesions scored may best be categorized as small refractile bodies in the lens. These are known to be pre-cataractous in congenital cataracts in some breeds of dogs; thus, this was the method chosen. As mentioned above, no animals were observed to have developed a true cataract at any dosage or irradiation schedule used.

If our method of scoring lens abnormalities and our method of quoting proton radiation dosage are acceptable, the radiation dosages now considered acceptable in manned space flight should be satisfactory in so far as results obtained in these animal

models are concerned. Thus, the primary objective of this study has been attained. In addition, no untoward skin reactions were observed in any irradiated animal. When considered in the light of known skin reactions from other types of radiation, this observation is somewhat surprising.

As with all studies of this type, there are unanswered questions as well as factors to be considered in future studies, should they be indicated. First, we would strongly recommend that the dosage problems mentioned above be resolved. There must be a better way. It did not, and still does not, seem appropriate to use the entry dosage. The integral of the specific ionization curve also creates problems for dosage quotations. It was suggested that integration of the specific ionization curve over the body of the lens be used. This, to be accurate, would require measuring the lens thickness and depth in the eye for each animal. Even though the rabbits and dogs used were fairly uniform, there was still a variation in anatomic size.

A question still to be answered concerns the dosage required to cause proton radiation cataracts. Studies at higher dosage levels than those used in this study would be required. Even so, this would be essential for further studies.

It would have been helpful if a standard form of radiation could have been used for comparison purposes. In other words, determination of an RBE would have permitted us to take advantage of a cheaper radiation source as well as data from the published literature.


No information was obtained which might be applicable should radiation modifiers be present. For instance, the high oxygen content in the space craft environment might well affect the radiation response.

Lastly, we must conclude that the observed EEG changes in the dogs whose eyes were irradiated was a chance observation. There are very real and good reasons to doubt this, but in the limited study conducted, cause and effect could not be demonstrated.

APPENDIX 1

dE/dx Computation Program Listing

The program included in the following pages essentially calculates the LET versus depth or the mean range for a given absorber, depending on the option chosen, for protons of energies between 10 - 50 MeV. All of the constants in the theory involved are clearly defined in comment cards in the program. The program has several features which are unique to the experiment at Texas A&M in that the transmission chamber and the air gap space between the end of the transmission chamber and the animal are mocked up in the program. However, this option may or may not be included depending on options selected in setting up the program. The energy loss mechanism is represented by equation 2 of the main report.



```

1  DOUBLE PRECISION AVEXEN,ZBAR,ATMDEN,PPMASS,ELMASS,NORM,ENIN,E,
   *XRARTN,XRARC,M,DLOC,ETA,BETA,SHELL,DEDX,TOTIN,THICK,R,ADD,X,Y,VSQ,
   *SIGMA,Q,QQ,ZINC,SPIONC,FUDFAC,ETA2,ETA4,ETA6,RHO,ATMPLC,EEF,
   *ATWT,ATOMS,ATNO,SUM,AMW,ATOMFR,FXEN,Z,DELXCM,STEPS7,A,EE,TKAIR1,
   *TKAIR2,DINC1,DINC2,STEP1,STEP2,C,PRDIS,H1,H2,H3,H4,H5,H6,
   *ARG?,ZAP,DARS,PP,ADD2
2  DOUBLE PRECISION F,S,G
3  DIMENSION MAX(4), ATWT(25), ATOMS(25), ATNO(25), A(5), QQ(5),
   *EXEN(25),ATOMFR(25)
4  COMMON Q(4,6),ZINC(4,6),AVEXEN(10),ZBAR(10),ATMDEN(10),RHO(10)
5  INTEGER TC, SI, DI

```

NOTE--FOR EASE IN UTILIZING THIS PROGRAM, ALL COMMENT CARDS SHOULD
BE READ. ALL READ STATEMENTS AND THEIR EXPLANATIONS HAVE BEEN
BOUNDED BY ASTERISKS FOR THE USERS CONVENIENCE.

THIS IS A GENERALIZED PROGRAM FOR CALCULATING THE MEAN RANGE OR
FOR GENERATING A DEDX VERSUS DEPTH CURVE FOR VARIABLE ENERGY
PROTONS IN DIFFERENT ABSORBER MATERIALS. NORMALIZATION TO
EXPERIMENTAL DATA IS INCLUDED AS AN OPTION.

IF A MEAN RANGE DETERMINATION IN A PARTICULAR ABSORBER IS DESIRED,
SELECT MI AND SET SI = 0, DI = 0, AND TC = 0. THE MEAN RANGE
WILL BE THE FINAL TOTAL ABSORBER THICKNESS TRAVERSED. THE
TRANSMISSION CHAMBER MAY BE INCLUDED, BUT THE RESULTING MEAN
MEAN RANGE WILL BE FOR THE ENERGY OF THE PROTON LEAVING THE
TRANSMISSION AND NOT FOR THE INITIAL INPUT PROTON ENERGY.

IF A DEDX VERSUS DEPTH CURVE IS DESIRED, SET SI = 1 AND DI = 1.
THE TRANSMISSION CHAMBER CAN BE INCLUDED, DEPENDING ON THE
EXPERIMENTAL SETUP. ACCURATE VALUES OF THE STANDARD DEVIATION
AND MEAN RANGE MUST BE INPUTED. AIR GAPS MAY BE INCLUDED. IF
NORMALIZATION TO EXPERIMENTAL DATA IS DESIRED, SET N1 = 1, N2 = 1,
AND INPUT ACCURATE VALUES FOR NORM, TKAIR1, AND TKAIR2.

NOTE----EXPLANATIONS FOR DI, SI, MI, TC, N1, N2, TKAIR1, TKAIR2,
AND NORM ARE FOUND BELOW.

PPMASS = PROTON MASS IN GRAMS
ELMASS = ELECTRON MASS IN GRAMS
C = SPEED OF LIGHT IN CM/SEC
TOTIN = THE TOTAL ABSORBER THICKNESS IN INCHES.
FUDFAC = FACTOR USED IN NORMALIZING THE THEORETICAL DATA TO
EXPERIMENTAL DATA. IF NO NORMALIZATION IS TO TAKE PLACE,
FUDFAC WILL AUTOMATICALLY BE TAKEN EQUAL TO 1.0
AVEXEN = AVERAGE EXCITATION ENERGY (IN EV) OF THE ABSORBER

ORIGINAL PAGE IS
OF POOR QUALITY

MATERIAL UNDER CONSIDERATION.
 ZBAR = AVERAGE ATOMIC NUMBER OF THE ABSORBER MATERIAL UNDER
 CONSIDERATION.
 ATOMDN = ATOM DENSITY (IN ATOMS/CM³) OF THE ABSORBER MATERIAL
 UNDER CONSIDERATION.

THE SUBSCRIPTED NUMBERS INDICATE THE DIFFERENT MATERIALS TO
 WHICH THE AVERAGE EXCITATION ENERGIES, AVERAGE ATOMIC NUMBERS,
 AND ATOM DENSITIES CORRESPOND.

- 1 = ALUMINUM
- 2 = POLYCARBONATE
- 3 = NITROGEN (N₂)
- 4 = MYLAR
- 5 = TISSUE EQUIVALENT PLASTIC
- 6 = TISSUE EQUIVALENT GAS
- 7 = LUCITE
- 8 = AIR
- 9 = TISSUE

M1 IS THE MATERIAL INDEX. A VALUE OF M1 FROM 1 THROUGH 9 WILL
 DESIGNATE A PARTICULAR ABSORBER TO BE USED IN THE PROGRAM (SEE
 ABOVE). A VALUE OF 10 FOR M1 MEANS THAT A MATERIAL DIFFERENT
 FROM THE MATERIALS LISTED IN THE PROGRAM LIBRARY IS TO BE
 USED. SEE SUBROUTINE 'ABSORB' FOR DETAILS ON NECESSARY INPUT
 DATA TO CALCULATE THE AVERAGE EXCITATION ENERGY, AVERAGE ATOMIC
 NUMBER, AND ATOM DENSITY FOR THE MATERIAL TO BE USED.

PRMSS	= 1.6723D-24
ELMSS	= 9.1072D-28
C	= 2.997925D10
TOTIN	= 0.000000
FUDFAC	= 1.000000
AVEXFN(1)	= 162.958403256621000
AVEXFN(2)	= 71.38440057532959000
AVEXFN(3)	= 80.99999999108352000
AVEXFN(4)	= 75.97310903064134000
AVEXFN(5)	= 73.2950503792450000
AVEXFN(6)	= 67.36988228745409000
AVEXFN(7)	= 69.1955977890327000
AVEXFN(8)	= 94.5657002549337000
AVEXFN(9)	= 73.4426527849192000
ZBAR(1)	= 13.000000000000000
ZBAR(2)	= 4.0606060606060000
ZBAR(3)	= 7.000000000000000
ZBAR(4)	= 4.66666666666667000
ZBAR(5)	= 3.437244759203147000
ZBAR(6)	= 3.643511450381679000
ZBAR(7)	= 3.600000000000000
ZBAR(8)	= 7.262160405843890000
ZBAR(9)	= 3.442549271443593000
ATWGEN(1)	= 6.027198154250901027
ATWGEN(2)	= 9.461113471197259022
ATWGEN(3)	= 5.379524738161022019
ATWGEN(4)	= 1.009999891742072023
ATWGEN(5)	= 1.032287338547449023
ATWGEN(6)	= 1.057384258112627020
ATWGEN(7)	= 1.074185456475064023

ORIGINAL PAGE IS
 OF POOR QUALITY

36 ATMOM(8) = 4.9820897495053847019
 37 ATMOM(9) = 9.625806621452877022
 38 RH0(1) = 2.699 D00
 39 RH0(2) = 1.21 D00
 40 RH0(3) = 1.2504 D-03
 41 RH0(4) = 1.51 D00
 42 RH0(5) = 1.07 D00
 43 RH0(6) = 1.066987 D-03
 44 RH0(7) = 1.19 D00
 45 RH0(8) = 1.29 D-03
 46 RH0(9) = 1.00 D00

 M1 IS THE MATERIAL INDEX. ABSORBER MATERIALS CORRESPONDING
 TO THE INPUT VALUE OF M1 ARE EXPLAINED ABOVE.
 TC IS THE TRANSMISSION CHAMBER INDEX. IF TC = 1, THE
 TRANSMISSION CHAMBER WILL BE INSERTED INTO THE PROGRAM. IF
 TC = 0, THE PROGRAM WILL NEGLECT THE TRANSMISSION CHAMBER.
 S1 IS THE STRAGGLING INDEX. IF S1 = 1, THE PROGRAM WILL
 CALCULATE THE STRAGGLING OF THE PROTONS ABOUT THE MEAN RANGE
 IN THE ABSORBER MATERIAL UNDER CONSIDERATION. IF S1 = 0,
 THE PROGRAM WILL NEGLECT STRAGGLING EFFECTS.
 D1 IS THE DETECTOR INDEX. IF D1 = 1, THE PROGRAM WILL INCLUDE
 DETECTOR EFFECTS. THE DETECTOR WILL BE INSERTED AFTER EACH
 ABSORBER THICKNESS. IF D1 = 0, THE PROGRAM WILL NEGLECT
 DETECTOR EFFECTS.
 N1 AND N2 ARE THE VARIABLES THAT DETERMINE WHETHER OR NOT THE
 THEORETICAL DATA WILL BE NORMALIZED TO EXPERIMENTAL DATA AND
 WHETHER OR NOT AN AIR GAP IS INCLUDED IN THE ENERGY LOSS
 CALCULATIONS. IF N1 = 1 AND N2 = 1, THE PROGRAM WILL CALCULATE
 A FACTOR WHICH WILL NORMALIZE THE THEORETICAL RADS/MIN VERSUS
 DEPTH CURVE TO EXPERIMENTAL DATA. IN THIS CASE, THE VALUE OF
 NORM MUST CORRESPOND TO THE 10% ABSORBER THICKNESS (AIR GAP
 ONLY) EXPERIMENTAL READING. IF N1 = 1 AND N2 = 0, THE PROGRAM
 WILL SIMPLY INCLUDE AN AIR GAP OF SPECIFIED THICKNESS BETWEEN
 THE BEAM TUBE (OR TRANSMISSION CHAMBER, IF USED) AND THE
 ABSORBER HOLDER. NO FACTOR WILL BE CALCULATED, HENCE ANY
 VALUE OF NORM CAN BE INPUT. IF N1 = 0 AND N2 = 0, NO AIR GAPS
 WILL BE INCLUDED AND NO NORMALIZATION FACTOR WILL BE CALCULATED.
 READ, M1, TC, S1, D1, N1, N2, NORM

 ENIN = INITIAL PROTON ENERGY IN MEV.
 XRPAIN = MEAN RANGE (IN INCHES) OF THE ABSORBER MATERIAL
 UNDER CONSIDERATION.
 SIGMA = STANDARD DEVIATION (IN CM) FOR THE STRAGGLING OF THE
 PROTON ABOUT THE MEAN RANGE OF THE MATERIAL UNDER
 CONSIDERATION.

READ, ENIN, XHARIN, SIGMA

THE A'S = NUMBER OF ABSORBERS OF A SPECIFIED THICKNESS TO BE
USED IN THE PROGRAM.

A(1) = NUMBER OF 40 MILL THICKNESSES
A(2) = NUMBER OF 20 MILL THICKNESSES
A(3) = NUMBER OF 10 MILL THICKNESSES
A(4) = NUMBER OF 5 MILL THICKNESS
A(5) = NUMBER OF 1 MILL THICKNESSES

THE QQ'S = NUMBER OF DIVISIONS INTO WHICH EACH ABSORBER SECTION
IS TO BE DIVIDED.

QQ(1) = NUMBER OF DIVISIONS IN 40 MILL SECTION*
QQ(2) = NUMBER OF DIVISIONS IN 20 MILL SECTION*
QQ(3) = NUMBER OF DIVISIONS IN 10 MILL SECTION*
QQ(4) = NUMBER OF DIVISIONS IN 5 MILL SECTION*
QQ(5) = NUMBER OF DIVISIONS IN 1 MILL SECTION*

READ, (A(I), QQ(I), I=1,5)

TKAIR1 = THICKNESS OF THE AIR GAP (IN INCHES) BETWEEN THE
BEAM TUBE (OR TRANSMISSION CHAMBER, IF USED) AND THE
ABSORBER HOLDER.

DINC1 = NUMBER OF DIVISIONS INTO WHICH TKAIR1 IS TO BE DIVIDED.

TKAIR2 = THICKNESS OF THE AIR GAP (IN INCHES) BETWEEN THE
ABSORBER HOLDER AND THE DETECTOR. IT SHOULD BE
MENTIONED THAT AUTOMATIC CORRECTION WILL BE MADE FOR
THE DECREASE IN THE THICKNESS OF THE GAP DUE TO THE
PLACEMENT OF VARIOUS THICKNESSES OF ABSORBER MATERIAL
BETWEEN THE BEAM TUBE (OR TRANSMISSION CHAMBER, IF
USED) AND THE DETECTOR. HENCE, AT NO TIME SHOULD
THE AIR GAP THICKNESS (TKAIR2) BE LESS THAN THE TOTAL
ABSORBER THICKNESS USED.

DINC2 = NUMBER OF DIVISIONS INTO WHICH TKAIR2 IS TO BE DIVIDED.

NOTE-----AN ACCURATE VALUE FOR TKAIR1 MUST BE INPUTED ONLY IF
AN INITIAL AIR GAP IS TO BE INCLUDED IN THE PROGRAM. AN
ACCURATE VALUE FOR TKAIR2 MUST BE INPUTED ONLY WHEN THE
DETECTOR IS BEING UTILIZED.

READ, TKAIR1, DINC1, TKAIR2, DINC2

ORIGINAL PAGE IS
OF POOR QUALITY

```

51 IF (M1.EQ.10) CALL ABSORR(M1)
52 PRINT, AVEXEN(M1), ZBAR(M1), ATMDEN(M1)
53 CALL OUTPUT(M1,ENIN,XBARIN,SIGMA,TC,DI,SI,TKAIR1,TKAIR2,N1,N2)
54 DO 1 I=1,9
55 1 AVEXEN(I) = (AVEXEN(I)*1.60210-19)/1.00-07
56 IF (M1.EQ.10) AVEXEN(10) = (AVEXEN(10)*1.60210-19)/1.00-07
57 ENIN = ENIN*(1.60210-06)
58 XBARCM = XBARIN*2.54000
59 SIGMA = SIGMA/2.54000
60 KKK = 1
61 IF (TC.EQ.1) CALL TRANSIENIN,ELMASS,C,PRMASS)
62 IF (N1.EQ.1) CALL FUDGE(ENIN,TKAIR1,TKAIR2,DINC1,DINC2,NORM,
*N2,FUDFAC,ELMASS,PRMASS,C,TOTIN,KKK)
63 PRINT 103
64 103 FORMAT(IH1)
65 DO 2 I=1,5
66 IF (A(I).EQ.0.0) GO TO 2
67 IF (I.EQ.1) THICK = 0.040000
68 IF (I.EQ.2) THICK = 0.020000
69 IF (I.EQ.3) THICK = 0.010000
70 IF (I.EQ.4) THICK = 0.005000
71 IF (I.EQ.5) THICK = 0.001000
72 NARL = A(I)
73 JAMES = DO(I)
74 STEPS7 = THICK/DO(I)
75 DELXCM = STEPS7*2.54000
76 DO 3 J=1,NARL
77 E = ENIN
78 DO 4 K=1,JAMES
79 R = K
80 ADD = (STEPS7*8)
81 PRDIS = 1.00000
82 VSO = (C**2.0)*(1.0-((PRMASS**2.0)*(C**4.0)))/((ENIN + PRMASS *
*(C**2.0)**2.0))
83 BETA = VSO/(C**2.0)
84 ETA = BETA/((1.0-BETA**2)**0.5)
85 SHELL = S(M1,ETA)
86 DEDX = F(M1,ELMASS,VSO,SHELL,BETA)
87 ENIN = ENIN - DELXCM*DEDX
88 IF ((ENIN=1.00-07/1.60210-13).LE.1.0000) GO TO 5
89 4 CONTINUE
90 IF (SI.EQ.1) PRDIS = 1.0000-G(SIGMA,TOTIN,XBARIN)
91 TOTIN = TOTIN + THICK
92 SPIONC = DEDX*PRDIS/1.60210-06
93 DEDX = DEDX/1.60210-06
94 E = E/1.60210-06
95 EE = ENIN/1.60210-06
96 PRINT 100, THICK, TOTIN, E, EE, PRDIS, DEDX, SPIONC
97 100 FORMAT (6(I),T20,'THE THICKNESS OF THE ABSORBER SECTION =
*,G14.7,' INCHES',/,T20,'THE TOTAL ABSORBER THICKNESS =
*,G14.7,' INCHES',/,T20,'THE PROTON ENERGY ENTERI
*NG THE ABSORBER = ',G14.7,' MEV',/,T20,'THE PROTON ENER
*GY LEAVING THE ABSORBER SECTION = ',G14.7,' MEV',/,T20,'THE PR
*ACTION OF ORIGINAL PARTICLES LEFT = ',G14.7,/,T20,
*DEDX = ',G14.7,' ME
*/CM',/,T20,'THE SPECIFIC IONIZATION IN RADS/MIN =
*,G14.7)
98 IF (DI.EQ.1) CALL DETEC(ENIN,SPIONC,FUDFAC,PRDIS,PRMASS,C,
*ELMASS,TOTIN,TKAIR2,DINC2,KKK)
99 7 CONTINUE

```

ORIGINAL PAGE IS
OF POOR QUALITY

```

100 3 CONTINUE
101 2 CONTINUE
102 PRINT 102
103 102 FORMAT(61//,T20,'THE PROTONS HAVE TRAVERSED ALL ABSORBERS BUT HAVE
*//,T20,'NOT LOST ALL OF THEIR ENERGY. A MEAN RANGE DETERMINATION
*//,T20,'OF DEPTH VERSUS DEPTH CURVE IS NOT COMPLETE. THE//,T20,
*TOTAL ABSORBER THICKNESS SHOULD BE INCREASED.')
104 GO TO 20
105 5 TOTIN = TOTIN + ADD
106 RR = 1.762338D-03 + (2.17368D-04 * ZBAR(MI))
107 E = ENIN/1.6021D-06
108 ADD2 = (RR / (RHO(MI) * 2.54D00)) * E
109 TOTIN = TOTIN + ADD2
110 PRINT 101, THICK, E, TOTIN
111 101 FORMAT (8//,T20,'THE ABSORBER ENERGY FELL BELOW 1 MEV WHILE TRAV
*ERSING THIS ABSORBER',//,T20,'THE THICKNESS OF THIS FINAL ABSORBER
* SECTION = ',G14.7,' INCHES',//,T20,'THE PROTON ENERGY INT
*O THIS FINAL ABSORBER SECTION = ',G14.7,' MEV',//,T20,'THE TOTAL
* DISTANCE TRAVELED BY THE PROTON = ',G14.7,' INCHES')
112 20 PRINT 104
113 104 FORMAT (1H1)
114 STOP
115 END

116 SUBROUTINE TRANS(ENIN,ELMASS,C,PRMASS)
117 DOUBLE PRECISION AVEXEN,ZPAR,ATMDEN,E,ENIN,PRMASS,ELMASS,C,SHELL,
*DETX,F,S,DLOG,BETA,ETA,VSQ,Q,ZINC,EE,STEPSZ
118 COMMON Q(4,6),ZINC(4,6),AVEXEN(10),ZBAR(10),ATMDEN(10),RHO(10)
119 DIMENSION MAX(4)

C
C
C THIS SUBROUTINE INSERTS THE TRANSMISSION CHAMBER IMMEDIATELY
C AFTER THE BEAM TUBE AND CALCULATES THE PROTON ENERGY LOSS
C THROUGH IT. THE ENERGY INTO AND THE ENERGY OUT OF THE CHAMBER
C ARE OUTPUTED.
C
C
120 F = ENIN
121 DO 1 J=1,6
122 Q(1,J) = 1.1D-06
123 1 ZINC(1,J) = 1.00000
124 DO 2 J=1,6
125 Q(2,J) = 8.0D-06
126 2 ZINC(2,J) = 1.00000
127 DO 3 J=1,2
128 Q(3,J) = 1.25D-01
129 3 ZINC(3,J) = 100.0000
130 DO 4 J=3,4
131 Q(3,J) = 1.00000
132 4 ZINC(3,J) = 200.00000
133 Q(3,5) = 0.75000
134 ZINC(2,5) = 150.00000
135 Q(4,1) = 1.0D-03
136 ZINC(4,1) = 100.00000
137 MAX(1) = 6
138 MAX(2) = 6
139 MAX(3) = 5
140 MAX(4) = 1
141 DO 5 I=1,4
142 MI = I

```

```

143      KOOL = MAX(I)
144      DO 6 J=1,KOOL
145      STEPSZ = (Q(I,J)/ZINC(I,J))*2.54D00
146      K=ZINC(I,J)
147      DO 7 L=1,K
148      VSQ = (C**2.0)*(1.0-(((PRMASS**2.0)*(C**4.0)))/((ENIN + PRMASS *
      *(C**2.0)**2.0))
149      BETA = VSQ/(C**2.0)
150      ETA = BETA/((1.0-BETA**2.0)**0.5)
151      SHELL = S(MI,ETA)
152      DEDX = F(MI,ELMASS,VSQ,SHELL,BETA)
153      ENIN = ENIN-DEDX*STEPSZ
154      7 CONTINUE
155      6 CONTINUE
156      5 CONTINUE
157      E = E/1.6021D-06
158      EE = ENIN/1.6021D-06
159      PRINT 100,E,EE
160      100 FORMAT (6//,T20,'THE ENERGY OF THE PROTON ENTERING THE TRANSMISSI
      *ON CHAMBER = ',G14.7,' MEV',/,T20,'THE ENERGY OF THE PROTON LEAVIN
      *G THE TRANSMISSION CHAMBER = ',G14.7,' MEV')

```

```

161      RETURN
162      END

```

WARNING COMMON BLOCK // HAS A DIFFERENT LENGTH THAN WAS SPECIFIED IN A PREVIOUS SUBPROGRAM GREATER LENGTH USED.

```

163      SUBROUTINE DETEC(ENIN,SPIONC,FUDFAC,PRTOIS,PRMASS,C,ELMASS,
      *TOTIN,TKAIR2,DINC2,KKK)
164      DOUBLE PRECISION AVEXEN,ZBAR,ATMDEN,E,ENIN,PRMASS,ELMASS,C,SHELL,
      *DEDX,F,S,DLOG,BETA,ETA,VSQ,Q,ZINC,STEPSZ,SPIONC,TOTIN,TKAIR2,
      *DINC2,EE,EEB,FUDFAC,PRTOIS
165      COMMON D(4,6),ZINC(4,6),AVEXEN(10),ZBAR(10),ATMDEN(10),RHO(10)

```

C
C
C
C
C
C
C

THIS SUBROUTINE MODELS THE DETECTOR USED IN THE EXPERIMENTAL ANALYSIS. THE ROUTINE RETURNS A VALUE FOR THE SPECIFIC IONIZATION IN MEV/SEC THAT CAN BE NORMALIZED TO EXPERIMENTAL DATA, IF DESIRED.

```

166      E = ENIN
167      Q(1,1) = TKA102-TOTIN
168      ZINC(1,1) = DINC2
169      Q(2,1) = 1.0D-06
170      ZINC(2,1) = 1.0D00
171      Q(3,1) = 8.0D-05
172      ZINC(3,1) = 1.0D000
173      Q(4,1) = 0.104D00
174      ZINC(4,1) = 700.00
175      DO 2 I=1,4
176      IF (I.EQ.1) MI = 8
177      IF (I.EQ.2) MI = 1
178      IF (I.EQ.3) MI = 2
179      IF (I.EQ.4) MI = 6
180      STEPSZ = Q(I,1)/ZINC(I,1)*2.54D00
181      K = ZINC(I,1)
182      DO 3 J=1,K
183      VSQ = (C**2.0)*(1.0-(((PRMASS**2.0)*(C**4.0)))/((ENIN + PRMASS *
      *(C**2.0)**2.0))
184      BETA = VSQ/(C**2.0)
185      ETA = BETA/((1.0-BETA**2)**0.5)

```



```

186      SHELL = S(MI,ETA)
187      DEDX = F(MI,ELMASS,VSQ,SHELL,BETA)
188      ENIN = FNIN - DEDX*STEPSZ
189      IF (I.EQ.1) EFE = ENIN
190      2      CONTINUE
191      SPIONC = DEDX*PRDIS*FUDFAC/1.6021D-06
192      EE = ENIN/1.6021D-06
193      ENIN = E
194      E = E/1.6021D-06
195      EEE = EFE/1.6021D-06
196      IF (KKK.EQ.0) GO TO 4
197      PRINT 100, F, EFE, EE, SPIONC
198      100    FORMAT (6(//),T20,'THE PROTON ENERGY INTO THE AIR GAP PRECEEDING TH
          *E DETECTOR = ',G14.7,' MEV',/,T20,'THE ENERGY OF THE PROTON ENTER
          *ING THE DETECTOR = ',G14.7,' MEV',/,T20,'THE ENERGY OF THE PROTON
          *LEAVING THE DETECTOR = ',G14.7,' MEV',/,T20,'THE SPECIFIC IONIZATI
          *ON IN MEV/SEC FOR RADS/MIN, IF NORMALIZATION IS PERFORMED) = ',
          *G14.7)
199      4      CONTINUE
200      RETURN
201      END

```

WARNING COMMON BLOCK // HAS A DIFFERENT LENGTH THAN WAS SPECIFIED IN A PREVIOUS SUBPROGRAM GREATER LENGTH USED

```

202      SUBROUTINE FUDGE(FNIN,TKAIR1,TKAIR2,DINC1,DINC2,NORM,N2,
          *FUDFAC,ELMASS,PRMASS,C,TOTIN,KKK)
203      DOUBLE PRECISION AVEXEN,ZBAR,ATMDEN,E,ENIN,PRMASS,ELMASS,C,SHELL,
          *DEDX,F,S,BLOG,PETA,ETA,VSQ,Q,ZINC,STEPSZ,SPIONC,TKAIR1,DINC1,
          *FUDFAC,STEP1,EE,TKAIR2,DINC2,TOTIN,NORM,PRDIS,EEF
204      COMMON Q(4,6),ZINC(4,6),AVEXEN(10),ZBAR(10),ATMDEN(10),PHO(10)

```

THIS SUBROUTINE WILL INSERT AN AIR GAP OF SPECIFIED THICKNESS
INTO THE PROGRAM AND IS CAPABLE OF CALCULATING A FACTOR WHICH
WILL NORMALIZE THEORETICAL DATA TO EXPERIMENTAL DATA.

```

205      KKK = 0
206      MI = 4
207      STEP1 = TKAIR1/DINC1*2.54000
208      E = FNIN
209      FUDFAC = 1.00000
210      PRDIS = 1.0000
211      K = DINC1
212      DO 1 I=1,K
213      VSQ = ((C**2.0)*(1.0-(((PRMASS**2.0)*(C**4.0)))/((ENIN + PRMASS *
          *(C**2.0))**2.0)))
214      BETA = VSQ/((C**2.0)
215      ETA = BETA/((1.0-BETA**2)**0.5)
216      SHELL = S(MI,ETA)
217      DEDX = F(MI,ELMASS,VSQ,SHELL,BETA)
218      1      ENIN = FNIN - DEDX*STEP1
219      IF (N2.EQ.0) GO TO 2
220      CALL DETEC(ENIN,SPIONC,FUOFAC,PRDIS,PRMASS,C,ELMASS,
          *TOTIN,TKAIR2,DINC2,KKK)
221      FUDFAC = NORM/SPIONC
222      E = F/1.6021D-06
223      EE = ENIN/1.6021D-06
224      PRINT 101, E, EE, NORM, FUDFAC
225      101    FORMAT (5(//),T20,'THE PROTON ENERGY INTO THE AIR GAP BETWEEN THE R
          *EAM PORT AND ABSORBER HOLDER = ',G14.7,' MEV',/,T20,'THE ENERGY OF

```

ORIGINAL PAGE IS
OF POOR QUALITY

```

GO TO 4
CONTINUE
E = E/1.6021D-06
EE = ENIN/1.6021D-06
PRINT 100, E, EE
FORMAT (5(/),T20,'THE PROTON ENERGY INTO THE AIR GAP BETWEEN THE
*BEAM PORT AND ABSORBER HOLDER = ',G14.7,' MEV',/,T20,'THE ENERGY
*OF THE PROTON LEAVING THIS AIR GAP = ',G14.7,' MEV',/,T20,'NO NORM
*ALIZATION IS PERFORMED. ONLY THE INITIAL AIR GAP HAS BEEN CONSIDERED')

```

COMMON BLOCK // HAS A DIFFERENT LENGTH THAN WAS SPECIFIED IN A PREVIOUS SUBPROGRAM GREATER LENGTH USED

THIS SUBROUTINE CALCULATES THE AVERAGE EXCITATION ENERGY (AVEKEN), THE AVERAGE ATOMIC NUMBER (ZBAR), AND THE ATOM DENSITY (ATMDEN) FOR A MATERIAL NOT LISTED IN THE PROGRAM LIBRARY.

 ATPMLC = THE NUMBER OF ATOMS PER MOLECULE OF THE ABSORBER.
 NELEMTS = THE NUMBER OF ELEMENTS IN THE ABSORBER.
 RHO = THE DENSITY OF THE ABSORBER (G/CM3).
 ATWT = THE ATOMIC WEIGHT OF EACH ELEMENT.
 ATOMS = THE NUMBER OF ATOMS OF EACH PARTICULAR ELEMENT PER
 MOLECULE OF THE ABSORBER.
 ATNO = ATOMIC NUMBER OF EACH ELEMENT IN THE ABSORBER

[illegible]

134

```

255 46 FXEN(J) = ATND(J)*(9.76000 + 58.8000/(ATND(J)**1.19))
256 3 X = X + ATDMFR(J)*ATND(J)*DLOG(EXEN(J))
257 2 Y = Y + ATDMFR(J)*ATND(J)
258 Z = X/Y
259 AVEXEN(10) = (2.7182818284)**Z
260 PRINT, AVEXEN(10)
261 RETURN
262 END

```

```

263 FUNCTION S(MI,ETA)

```

C
C
C
C
C

THIS IS A SUBPROGRAM TO CALCULATE THE SHELL CORRECTION TERM

```

264 DOUBLE PRECISION AVEXEN,ZBAR,ATMDEN,ZINC,Q,ETA2,ETA4,ETA6,ETA,S
265 COMMON Q(4,6),ZINC(4,6),AVEXEN(10),ZBAR(10),ATMDEN(10),RHO(10)
266 ETA2 = 1.00090/(ETA**2)
267 ETA4 = ETA2**2
268 ETA6 = ETA2**3
269 S = (0.422377000*ETA2 + 0.0304043000*ETA4 - 0.0038106000*ETA6)*
*(1.00-0.61*(AVEXEN(MI)**2.0) + (3.858019000*ETA2 - 0.1667929000
**ETA4 + 0.00157955000*ETA6)*(1.00-0.91*(AVEXEN(MI)**3.0)

```

```

270 RETURN
271 END

```

WARNING COMMON BLOCK // HAS A DIFFERENT LENGTH THAN WAS SPECIFIED IN A PREVIOUS SUBPROGRAM GREATER LENGTH USED

```

272 FUNCTION F(MI,ELMASS,VSQ,SHELL,BETA)

```

C
C
C
C
C

THIS IS A SUBPROGRAM TO CALCULATE DE/DX

```

273 DOUBLE PRECISION Q,ZINC,AVEXEN,ZBAR,ATMDEN,ELMASS,VSQ,SHELL,
*BETA,F,DLOG
274 COMMON Q(4,6),ZINC(4,6),AVEXEN(10),ZBAR(10),ATMDEN(10),RHO(10)
275 F = (4.0*3.1415927*(14.802980-10)**4.0)*ATMDEN(MI)*ZBAR(MI)*(DLOG
*(2.0000*ELMASS*VSQ/(AVEXEN(MI)*(1.0000-VSQ/(12.997925010)**2.0
*1)))-(BETA**2.0)-SHELL/ZBAR(MI)))/(ELMASS*VSQ)
276 RETURN
277 END

```

WARNING COMMON BLOCK // HAS A DIFFERENT LENGTH THAN WAS SPECIFIED IN A PREVIOUS SUBPROGRAM GREATER LENGTH USED

```

278 FUNCTION G(SIGMA,TOTIN,XBARIN)

```

C
C
C
C
C

THIS IS A SUBPROGRAM FOR THE CALCULATION OF STRAGGLING ABOUT
THE MEAN RANGE XBAR ASSUMING A GAUSSIAN DISTRIBUTION

```

279 DOUBLE PRECISION G,SIGMA,XBARIN,TOTIN,H1,H2,H3,H4,H5,H6,ARG2,ZAP,
*DSQRT,DARS
280 H1 = 0.7052307840-01
281 H2 = 0.4223201230-01
282 H3 = 0.927052720-02
283 H4 = 0.15201430-03
284 H5 = 0.27656720-03
285 H6 = 0.4306380-04
286 ARG2 = (TOTIN-XBARIN)/(DSQRT(2.0000)*SIGMA)
287 IF (DABS(ARG2).LE.1.00-14) ARG2 = 0.0000

```

ORIGINAL PAGE IS
OF POOR QUALITY

```

288      IF(ARG2) 1,2,3
289      1 ARG2 = -ARG2
290      ZAP=(H1*ARG2 + H2*ARG2**2 + H3*ARG2**3 + H4*ARG2**4 + H5*
      *ARG2**5 + H6*ARG2**6)
291      IF (ZAP.GE.50.0) GO TO 6
292      G = 0.5000 + 0.5000*(-1.0000+((1.0000/(1.0000+ZAP)**16.0)))
293      GO TO 5
294      2 G = 0.5
295      GO TO 5
296      3 CONTINUE
297      ZAP=(H1*ARG2 + H2*ARG2**2 + H3*ARG2**3 + H4*ARG2**4 + H5*
      *ARG2**5 + H6*ARG2**6)
298      IF (ZAP.GE.50.0) GO TO 7
299      G = 0.5000 + 0.5000*(1.0000-(1.0000/((1.0000+ZAP)**16.0)))
300      GO TO 5
301      6 G = 0.0
302      GO TO 5
303      7 G = 1.00000
304      5 CONTINUE
305      RETURN
306      END

307      SUBROUTINE OUTPUT(MI,ENIN,XBARIN,SIGMA,TC,DI,SI,TKAIR1,TKAIR2,
      *N1,N2)
308      DOUBLE PRECISION ENIN,XBARIN,SIGMA,TKAIR1,TKAIR2
309      INTEGER TC, DI, SI
310      IF (MI.EQ.1) PRINT 20
311      IF (MI.EQ.2) PRINT 21
312      IF (MI.EQ.3) PRINT 22
313      IF (MI.EQ.4) PRINT 23
314      IF (MI.EQ.5) PRINT 24
315      IF (MI.EQ.6) PRINT 25
316      IF (MI.EQ.7) PRINT 26
317      IF (MI.EQ.8) PRINT 27
318      IF (MI.EQ.9) PRINT 28
319      IF (MI.EQ.10) PRINT 29
320      PRINT 30,ENIN,XBARIN,SIGMA
321      IF (TC.EQ.0) PRINT 34
322      IF (TC.EQ.1) PRINT 35
323      IF (DI.EQ.0) PRINT 36
324      IF (DI.EQ.1) PRINT 37
325      IF (SI.EQ.0) PRINT 38
326      IF (SI.EQ.1) PRINT 39
327      IF (N1.EQ.1.AND.N2.EQ.1) PRINT 31,TKAIR1,TKAIR2
328      IF (N1.EQ.1.AND.N2.EQ.0) PRINT 32,TKAIR1,TKAIR2
329      IF (N1.EQ.0.AND.N2.EQ.0) PRINT 33
330      20 FORMAT (1H1,10(/),T20,'THE ABSORBER MATERIAL UNDER CONSIDERATION I
      *S ALUMINUM')
331      21 FORMAT (1H1,10(/),T20,'THE ABSORBER MATERIAL UNDER CONSIDERATION I
      *S POLYCARBONATE')
332      22 FORMAT (1H1,10(/),T20,'THE ABSORBER MATERIAL UNDER CONSIDERATION I
      *S NITROGEN (N2)')
333      23 FORMAT (1H1,10(/),T20,'THE ABSORBER MATERIAL UNDER CONSIDERATION I
      *S MYLAR')
334      24 FORMAT (1H1,10(/),T20,'THE ABSORBER MATERIAL UNDER CONSIDERATION I
      *S TISSUE EQUIVALENT PLASTIC')
335      25 FORMAT (1H1,10(/),T20,'THE ABSORBER MATERIAL UNDER CONSIDERATION I
      *S TISSUE EQUIVALENT GAS')
336      26 FORMAT (1H1,10(/),T20,'THE ABSORBER MATERIAL UNDER CONSIDERATION I
      *S LUCITE')

```

```

337 27  FORMAT (1H1,10(/),T20,'THE ABSORBER MATERIAL UNDER CONSIDERATION I
      *S AIR')
338 28  FORMAT (1H1,10(/),T20,'THE ABSORBER MATERIAL UNDER CONSIDERATION I
      * TISSUE')
339 29  FORMAT (1H1,10(/),T20,'THE ABSORBER MATERIAL UNDER CONSIDERATION I
      *S NOT IN THE PROGRAM LIBRARY')
340 30  FORMAT ( /,T20,'THE INPUT ENERGY IS = ',G14.7,' MEV',//,T20,
      *'THE MEAN RANGE FOR THE ABSORBER MATERIAL IS = ',G14.7,
      *' INCHES',//,T20,'THE STANDARD DEVIATION FOR THE ABSORBER MATERIAL
      * IS = ',G14.7,' CM',///)
341 31  FORMAT (5(/),T20,'THE AIR GAPS ARE BEING INCLUDED',//,T20,'TKAIR1 =
      * ',G14.7,' INCHES',//,T20,'TKAIR2 = ',G14.7,' INCHES',//,T20,'NORMAL
      *IZATION WILL BE PERFORMED')
342 32  FORMAT(5(/),T20,'THE AIR GAPS ARE BEING INCLUDED',//,T20,
      *'TKAIR1 = ',G14.7,' INCHES',//,T20,'TKAIR2 = ',G14.7,' INCHES',//,
      *T20,'NORMALIZATION WILL NOT BE PERFORMED')
343 33  FORMAT (5(/),T20,'NO AIR GAPS ARE INCLUDED',//,T20,'NO NORMALIZATION
      *N IS PERFORMED')
344 34  FORMAT ( /,T20,'THE TRANSMISSION CHAMBER IS NOT INCLUDED IN THE CA
      *LCULATIONS')
345 35  FORMAT ( /,T20,'THE TRANSMISSION CHAMBER IS INCLUDED IN THE CALCUL
      *ATIONS')
346 36  FORMAT ( /,T20,'THE DETECTOR IS NOT INCLUDED IN THE CALCULATIONS'
      *)
347 37  FORMAT ( /,T20,'THE DETECTOR IS INCLUDED IN THE CALCULATIONS')
348 38  FORMAT ( /,T20,'STRAGGLING EFFECTS ARE NEGLECTED')
349 39  FORMAT ( /,T20,'STRAGGLING EFFECTS ARE INCLUDED IN THE CALCULATIO
      *NS')
350  RETURN
351  END

```

ORIGINAL PAGE IS
OF POOR QUALITY

APPENDIX 2

Comparison with Other Published Results

The comparison of the proton dosimetry results of the Davis group with our results has indicated several areas of difference. Initially the mean ranges based on their published data were compared with our calculations and significant differences of up to 95% were found. For instance, the 20 MeV proton range was calculated to be 141 mills of Lucite whereas a published value of 275 mills is given. For 35 MeV protons a calculated range of 389 mills was found and a published range of 373, reasonably well in agreement. For the 45 MeV protons a calculated range of 612 mills was found and an experimental value given in a publication as 708 mills - again a significant error. We then questioned ourselves whether our program was calculating the ranges in Lucite properly. To verify the program accuracy, the values of ranges for 22, 34 and 46 MeV protons in Lucite were calculated and compared to those listed in the Tables of Energy Loss and Ranges of heavy charged particles by Barkus and Berger, which was prepared under contract for NASA by NBS. We agreed with the published values of Barkus and Berger within 7 tenths of a percent, in all cases. We therefore came to the conclusion that the ranges in Lucite for two of the cases are erroneous.

Using the computer program we next determined the entrance and the exit dE/dx in lithium fluoride chips positioned in Lucite for 20, 35 and 45 MeV protons. Using the thickness of 35 mills - essentially one millimeter - for the lithium fluoride crystals, which closely approximated the thickness of the crystals used by the Davis group; the crystals were centered at different depths in Lucite that approximated the positions chosen by the Davis group as indicated in their paper. The computer runs were then made for one chip at a time. This was done to eliminate the possible large energy degradation which would occur if many crystals were lined up in a single row. The dE/dx of the protons at the entrance and the exit of the crystals was computed and the results plotted in Figures A1 thru A3. As can be seen from the 20 MeV results, Figure A1, the variation in dE/dx across the crystals is relatively small until the mean range is approached at which point the variation becomes considerable. As is plainly visible, the variation in dE/dx across the crystals centered at 80 mills is relatively large while the dE/dx variation for the crystal centered at 100 mills is so large that it is difficult to see how a specific value of dE/dx for that single position can be obtained. The same results are observed for the 35, and 45 MeV data, Figures A2 and A3. In all cases, the energy of the protons went to zero before completely traversing the last crystal. The size of the lithium fluoride crystals used was so large it appears to us that there is no way to generate an accurate dE/dx

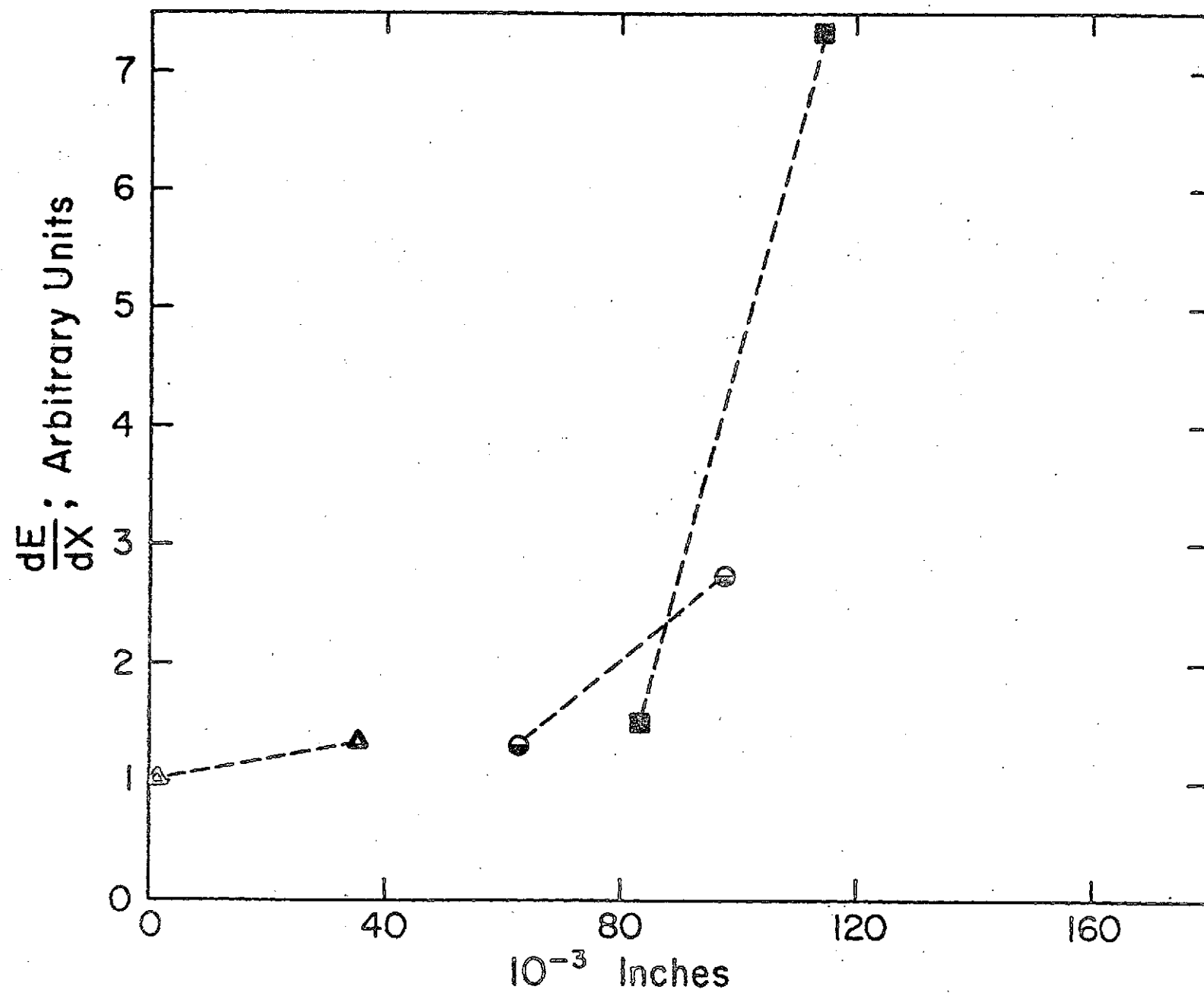


Figure A1
 dE/dx vs Depth in Lucite for
LiF Crystals - 20 MeV Protons

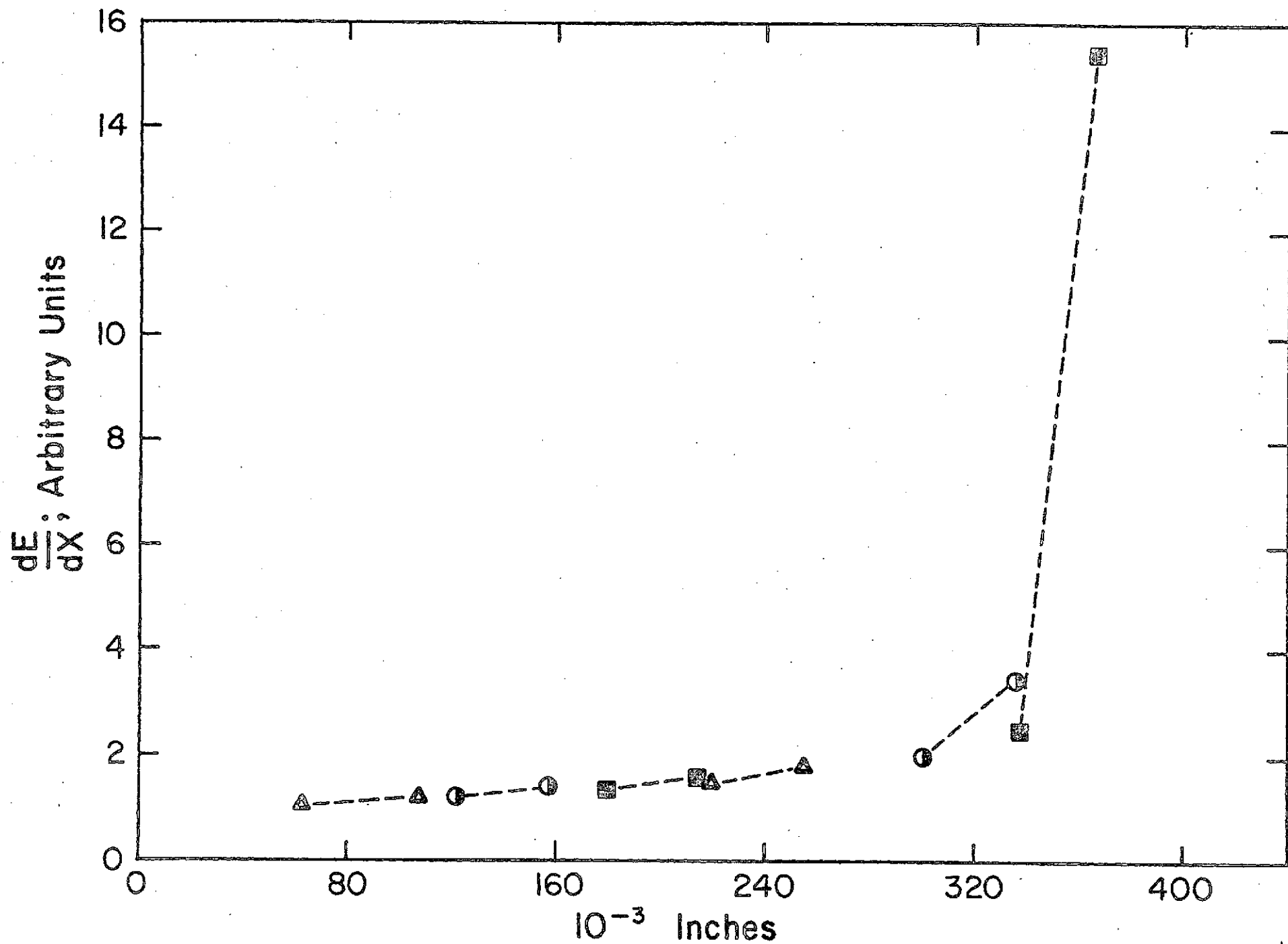


Figure A2
 dE/dx vs Depth in Lucite for
LiF Crystals - 35 MeV Protons

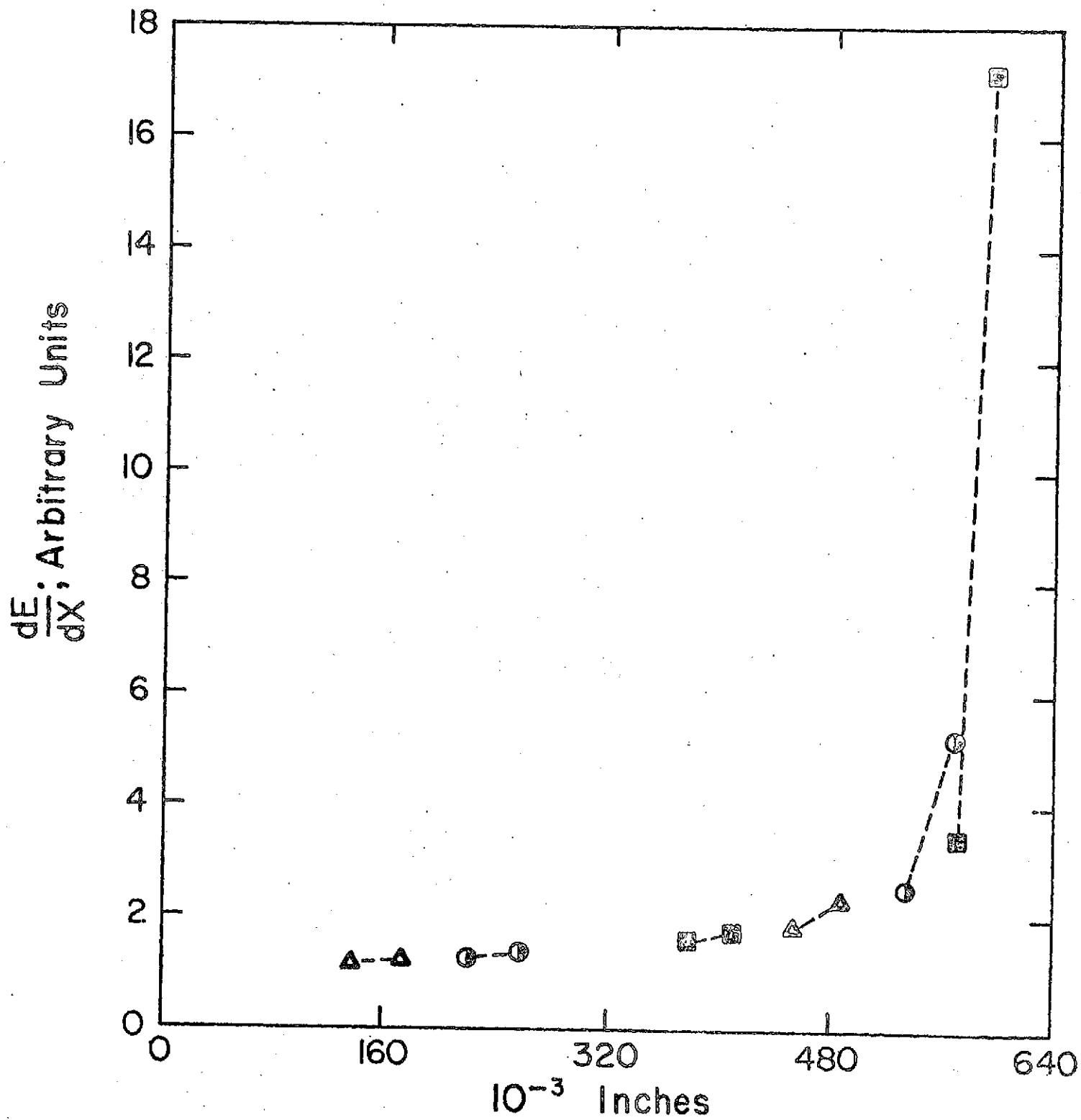


Figure A3
 $\frac{dE}{dx}$ vs Depth in Lucite for
LiF Crystals - 45 MeV Protons

curve in the Bragg peak region using this technique. The Bragg peak measurement discrepancy is further illustrated by comparison of the depth dose peak full width at half maximum versus proton energy in Table A1. The differences here are obvious and are consistent with the results one would expect due to the size problem of the lithium fluoride. The net result of this Bragg peak measurement discrepancy is reflected in the Bragg peak doses quoted for the animals irradiated. With the broadening of the peaks, a larger fluence of protons are required to give a stated Bragg peak dose. Thus, the total energy deposited per unit of dose quoted is greater for the peaks which are broadened due to contamination by scattered protons. Different biological results per given dose would therefore not be surprising.

TABLE A1 - dE/dx Full Width at Half Maximum

	TAMU	DAVIS	RUSSIAN
10 MeV	.13 mm	--	--
20 MeV	.57 mm	2.3 mm	--
30 MeV	.9 mm	--	--
35 MeV	--	2.2 mm	--
40 MeV	1.0 mm	--	--
45 MeV	--	7 mm	--
70 MeV	--	--	6 mm